

**Astrocyte-specific gene recombination *in vivo* -  
Tamoxifen-induced and -independent recombination**

**Dissertation**

zur Erlangung des akademischen Grades des Doktors  
der Naturwissenschaften (Dr. rer. nat.)  
der Medizinischen Fakultät, Institut für Physiologie,  
der Universität des Saarlandes

vorgelegt von  
Carmen Vanessa Kasakow  
geb. Bohn  
geboren in Heppenheim

Homburg, September 2018

The experimental work depicted in this thesis has been carried out at the Center for Integrative Physiology and Molecular Medicine in the Department of Molecular Physiology at the University of Saarland, Germany. The work was done independently from November 2013 until September 2018 with no other sources than stated by me.

1. Referee:

Prof. Dr. Frank Kirchhoff

University of Saarland

Center for Integrative Physiology and Molecular Medicine

Department of Molecular Physiology

Building 48

66421 Homburg

2. Referee:

Prof. Dr. Carola Meier

University of Saarland

Institute of Anatomy and Cell biology

Building 61

66421 Homburg

Day of defense: \_\_\_\_\_

**FÜR MEINE FAMILIE**

# CONTENT

Abbreviations.....	VIII
List of Figures.....	X
List of Tables.....	XII
<b>1. Summary.....</b>	<b>1</b>
<b>2. Zusammenfassung.....</b>	<b>3</b>
<b>3. Introduction .....</b>	<b>5</b>
3.1. Multiple astrocytic functions in the mouse central nervous system .....	5
3.2. Expression of astrocytic metabotropic and ionotropic ion channels .....	7
3.3. ATP induced Ca <sup>2+</sup> signaling in astrocytes .....	11
3.4. Tamoxifen metabolism .....	12
<b>4. Aim .....</b>	<b>15</b>
4.1. Astrocyte-specific gene recombination and the influence of tamoxifen- induced recombination .....	15
<b>5. Materials and Methods.....</b>	<b>16</b>
5.1. Materials .....	16
5.1.1. Reagents .....	16
5.1.2. Consumables and kits .....	16
5.1.3. Devices.....	16
5.1.4. Buffers, aqueous solutions and media .....	17
5.1.5. Purchased buffers .....	18
5.1.6. Enzymes.....	19
5.1.7. Drugs.....	19
5.1.8. Antibodies.....	19
5.1.9. Primers .....	20
5.1.10. Animals .....	22
5.1.11. Hard- und Software .....	24
5.1.12. Mouse administration .....	28
5.1.13. Statistical analysis.....	29
5.1.14. Cell and receptor schemes of the introduction.....	29
5.2. Methods .....	30
5.2.1. Tail biopsies .....	30
5.2.2. Mouse perfusion .....	30



5.2.3. Tamoxifen treatment.....	30
5.3. Sample preparation for LC-HR-MS/MS analysis .....	31
5.4. LC-HR-MS/MS analysis .....	31
5.4.1. Isolation and analysis of genomic DNA.....	32
5.4.2. Immunohistochemical analysis .....	33
5.4.3. Processing of DNA and RNA samples .....	33
5.5. Cell sorting.....	39
5.5.1. Magnetic activated cell sorting (MACS) .....	39
5.6. Injury models .....	39
5.6.1. Anesthesia and mouse preparation for injury models.....	39
5.6.2. Cortical stab wound injury.....	40
5.6.3. Cranial window .....	40
5.6.4. Microscopy .....	41
5.7. Next generation sequencing (NGS) .....	43
5.7.1. Laboratory and animal handling.....	44
<b>6. Results .....</b>	<b>45</b>
6.1. Refined protocols of tamoxifen application for DNA recombination in mouse astrocytes.....	45
6.1.1. Fast uptake and clearance of tamoxifen and its bioactive metabolite 4-OH- TAM.....	45
6.1.2. Maximal recombination levels are reached by three or five days of TAM injections in cortex or cerebellum, respectively .....	49
6.1.3. GLAST-Cre <sup>ERT2</sup> mediated DNA recombination to quantify astroglial cell numbers .....	54
6.2. Tamoxifen-independent recombination .....	58
6.2.1. IHC analysis and quantification of different astrocyte-specific Cre <sup>ERT2</sup> driver lines crossbred to the reporter mouse lines GCaMP3 and tdTomato .....	58
6.2.2. Quantitative real time PCR analysis of the same mouse lines confirm results of Orbit image quantification.....	69
6.2.3. Pathological conditions can trigger tamoxifen-independent recombination in GFAP-Cre <sup>ERT2</sup> mice.....	75
6.3. P2Y1 receptor cKO mice.....	76
6.3.1. High reduction of P2Y1R mRNA on astrocytes .....	76

6.3.2. DNA data of MACS isolated astrocytes and mRNA expression data from NGS confirm observations of total homogenates .....	78
6.3.3. Differentially expressed genes after P2Y1R ablation .....	81
6.4. Astroglial P2Y1 receptor knockout had no impact on acute injuries .....	83
6.4.1. Loss of astroglial P2Y1 receptors without impact on acute brain injury .....	83
6.4.2. GCaMP3 reporter expression led to an increase in GFAP expression upon astroglial P2Y1R ablation .....	86
6.5. Ca <sup>2+</sup> signaling in astrocytes.....	89
6.5.1. Smaller and shorter Ca <sup>2+</sup> signals in cKO mice under anesthetized and awake conditions .....	89
<b>7. Discussion.....</b>	<b>97</b>
7.1. Tamoxifen-induced recombination .....	97
7.1.1. Pharmacokinetic profile of tamoxifen and its metabolites revealed fast accumulation and clearance of all metabolites in the brain .....	97
7.1.2. TAM injections for three or five consecutive days revealed highest recombination efficiencies dependent on brain region and floxed allele .....	99
7.1.3. GLAST-Cre <sup>ERT2</sup> -driven recombination to determine the percentage of astrocytes in different brain regions .....	101
7.2. Tamoxifen-independent recombination had no effect on floxed receptor alleles in the cortex .....	101
7.3. P2Y1 receptor ablation and its impact on astrocytes .....	105
7.4. Ca <sup>2+</sup> signaling of astrocytes <i>in vivo</i> .....	108
7.4.1. Differences in astrocytic Ca <sup>2+</sup> signaling after P2Y1 receptor ablation in gliapil and soma.....	108
<b>8. Outlook .....</b>	<b>111</b>
<b>9. References.....</b>	<b>112</b>
<b>10. Appendix I.....</b>	<b>119</b>
10.1. No tamoxifen-independent recombination of non-astrocytic Cre <sup>ERT2</sup> driver lines .....	119
10.2. Heatmaps of <i>in vivo</i> Ca <sup>2+</sup> imaging .....	120
10.3. Detailed procedure of Ca <sup>2+</sup> imaging analysis using MSparkles.....	127
10.4. Comparison of anesthetized and awake Ca <sup>2+</sup> signals revealed higher signal amplitudes in gliapil and soma .....	130
10.5. Raw data of <i>in vivo</i> Ca <sup>2+</sup> imaging .....	132

<b>11. Appendix II.....</b>	<b>134</b>
11.1. List of Publication.....	134
11.1.1. Publication .....	134
11.1.2. Posters/ Oral presentations.....	134
<b>12. Acknowledgement .....</b>	<b>135</b>

## ABBREVIATIONS

AMPA	$\alpha$ -amino-3-hydroxy-5-methyl-4-isoxazolepropionic acid
ATP	Adenosine triphosphate
bp	base pairs
BSA	bovine serum albumin
cKO	conditional knockout
cl	contralateral
CLSM	confocal laser-scanning microscopy
CNS	central nervous system
con	control
DAPI	4',6-diamidino-2-phenylindole
DNA	desoxyribonucleic acid
dNTP	2'-Desoxyribonucleosid-5'-triphosphate
dpi	days post injection
dpw	days post window
EDTA	ethylenediaminetetraacetic acid
EGFP	enhanced green fluorescent Protein
END	endoxifen
ER	estradiol receptor
EYFP	enhanced yellow fluorescent Protein
GFAP	glial fibrillary acidic protein
GFP	green fluorescent protein
GLAST	glutamate aspartate transporter
GLT1	glutamate transporter 1
hpi	hours post injection
HRP	horse radish peroxidase
HS	horse serum
HSP	heat shock protein
il	ipsilateral
kb	kilobase pairs
LC-HR-MS/MS	liquid chromatography-high resolution-mass spectrometry
loxP	Locus of crossover x
mc	monoclonal

MIP	maximum intensity projection
mRNA	messenger ribonucleic acid
n	number
NDM-TAM	N-desmethyl-tamoxifen
NGS	next generation sequencing
NMDA	N-methyl-D-aspartate
ns	non significant
4-OH-TAM	4-hydroxytamoxifen
o.n.	over night
2P-LSM	two-photon laser-scanning microscopy
PBS	phosphate buffered saline
PCR	polymerase chain reaction
P2Y1R	P2Y purinoceptor 1
PFA	paraformaldehyde
pc	polyclonal
pi	post injury
RT	room temperature
RT-PCR	real time polymerase chain reaction
SDS	sodium dodecyl sulfate
SEM	standard error of the mean
SD	standard deviation
SWI	stab wound injury
tg	transgene
Taq	Thermophilus Aquaticus
TAM	tamoxifen
TgH	transgenic mouse, generated by homologous recombination
TgN	transgenic mouse, generated by non-homologous recombination
Tris	tris(hydroxymethyl)aminomethane
UV	ultraviolet light
w	week
wt	wild type

The dimensions of this thesis are consistent with the International System of Units (SI).

## LIST OF FIGURES

Figure 1.	Multiple tasks of astrocytes.....	6
Figure 2.	Distribution and function of diverse metabotropic and ionotropic ion channels at the tripartite synapse .....	8
Figure 3.	Purinergic signaling in the CNS .....	10
Figure 4.	P2Y and P2X receptor mRNA expression of glial cells .....	11
Figure 5.	Tamoxifen metabolism in mice .....	13
Figure 6.	Expression of Cre <sup>ERT2</sup> in astrocytes of the GLAST locus .....	14
Figure 7.	Analysis of SWI experiments of cKO and control animals with the ImageJ plugin LRoi.....	25
Figure 8.	2P-LSM imaging of awake mice and data processing of Ca <sup>2+</sup> signals via MSparkles .....	27
Figure 9.	Treatment protocols for LC-HR-MS/MS analysis .....	31
Figure 10.	Primer efficiencies to amplify various gene loci.....	38
Figure 11.	TAM injection protocol, surgery and imaging preparation .....	43
Figure 12.	Brain concentrations of TAM and its derivatives peaked between 8 and 24 hpi and showed clearance within 7 dpi.....	46
Figure 13.	Serum concentrations of TAM and its metabolites .....	49
Figure 14.	Three to five daily TAM injections give maximal DNA recombination depending on the brain region .....	51
Figure 15.	Interval injections every second day or every 8 h revealed differences in recombination efficiencies of floxed loci .....	53
Figure 16.	Recombination efficiencies were constant for target and reporter genes .....	56
Figure 17.	Inducible DNA recombination in mouse astroglia.....	58
Figure 18.	Tamoxifen-independent recombination of the GLAST-Cre <sup>ERT2</sup> line indicated by high GCaMP3 reporter expression.....	60
Figure 19.	Tamoxifen-independent recombination of GLAST-Cre <sup>ERT2</sup> x Rosa26-tdTomato mice .....	62
Figure 20.	Quantification of tamoxifen-independent recombination of the GLAST-Cre <sup>ERT2</sup> driver line revealed high reporter expression .....	63
Figure 21.	Negligible non-tamoxifen-induced recombination of GCaMP3 in GFAP-Cre <sup>ERT2</sup> mice.....	65

Figure 22.	Fewer cells expressed tdTomato in GFAP-Cre <sup>ERT2</sup> mice.....	66
Figure 23.	Quantification of low reporter expression after tamoxifen-independent recombination in GFAP-Cre <sup>ERT2</sup> mice.....	67
Figure 24.	Primarily GLAST-Cre <sup>ERT2</sup> driven tamoxifen-independent recombination of the reporter GCaMP3 in the cerebellum .....	70
Figure 25.	Tamoxifen-independent recombination of the floxed reporter .....	73
Figure 26.	Tamoxifen-independent recombination after GFAP upregulation under pathological conditions .....	76
Figure 27.	Reduction of P2Y1R mRNA in homogenates of various brain regions.....	77
Figure 28.	Reduction of floxed <i>p2ry1</i> alleles at the DNA and mRNA level of MACS isolated astrocytes.....	79
Figure 29.	Contamination of astrocytic population after MACS with microglia, neurons, NG2 glia and oligodendrocytes .....	80
Figure 30.	Next generation sequencing revealed 50 % reduction of <i>p2ry1</i> alleles in the cKO and an upregulation of <i>p2rx6</i> .....	81
Figure 31.	No difference between cKO and control mice after SWI on glial activation .....	85
Figure 32.	Quantification of astroglial and microglial activation after acute injury revealed no differences between cKO and control mice .....	86
Figure 33.	Differences between cKO and control mice after SWI on glial activation when GCaMP3 is expressed .....	88
Figure 34.	GFAP upregulation ipsilaterally and contralaterally of P2Y1R cKO mice.....	89
Figure 35.	Anesthetized P2Y1 cKO mice had smaller and shorter Ca <sup>2+</sup> signals in gliapil and soma.....	92
Figure 36.	Smaller and shorter Ca <sup>2+</sup> signals of awake P2Y1R cKO mice in gliapil and soma .....	94
Figure 37.	Stronger and shorter Ca <sup>2+</sup> signals in gliapil and soma.....	96
Figure 38.	Overview and conclusion of the tamoxifen study .....	99
Figure 39.	Length of floxed sequence influences tamoxifen-independent recombination.....	103
Figure 40.	Negligible tamoxifen-independent recombination of the PLP- and NG2-Cre <sup>ERT2</sup> driver line.....	119

Figure 41.	Heatmaps of <i>in vivo</i> Ca <sup>2+</sup> data revealed no pattern changes in Ca <sup>2+</sup> signals .....	127
Figure 42.	Composition of Ca <sup>2+</sup> data representing each imaging session, animal and Ca <sup>2+</sup> signal of the gliapil .....	128
Figure 43.	Composition of Ca <sup>2+</sup> data representig each animal, imaging session and Ca <sup>2+</sup> signal of the soma .....	129
Figure 44.	Differences of Ca <sup>2+</sup> signals in gliapil and soma between anesthetized and awake mice.....	131

## LIST OF TABLES

Table 1.	Devices .....	16
Table 2.	Primary antibodies.....	19
Table 3.	Secondary Antibodies.....	19
Table 4.	Genotyping primers .....	20
Table 5.	mRNA expression primers.....	21
Table 6.	DNA recombination primers.....	21
Table 7.	Mouse lines .....	24
Table 8.	Setup for reverse transcriptase PCR .....	35
Table 9.	Components for qRT-PCR for gene expression and DNA recombination .....	36
Table 10.	qRT-PCR program for the light cyclcr .....	36
Table 11.	qRT-PCR program of tdTomato, <i>p2ry1</i> , <i>gria1</i> and GCaMP3 for the light cyclcr .....	37
Table 12.	Brain and serum concentrations of TAM and its metabolites.....	49
Table 13.	Different tamoxifen injection protocols for recombination of the <i>p2ry1</i> and <i>gria1</i> locus .....	54
Table 14.	Percentage of fluorescence intensities of the GLAST-Cre <sup>ERT2</sup> and GFAP-Cre <sup>ERT2</sup> mouse lines (median; standardized to ct2/wt/+TAM) .....	68
Table 15.	Statistical comparison of the different mouse lines and Cre <sup>ERT2</sup> genotypes .....	68
Table 16.	GLAST-Cre <sup>ERT2</sup> and GFAP-Cre <sup>ERT2</sup> driven recombination of <i>gcamp3</i> alleles .....	71
Table 17.	Recombination of floxed <i>p2ry1</i> , <i>gria1</i> and <i>gcamp3</i> alleles in ctx and cb .....	74



Table 18.	Statistical comparison of the floxed alleles with different GLAST genotype .....	74
Table 19.	Data of Figure 35.....	132
Table 20.	Data of Figure 36.....	132
Table 21.	Data of Figure 37.....	133

## 1. SUMMARY

Astrocytes express a plethora of neurotransmitter receptors that form “microdomains” for signaling pathways along their processes. The purinergic P2Y1 receptor (P2Y1R) is involved in long-range intercellular signaling of astrocytes involving gliotransmitter release. In neuropathological situations, blocking of P2Y1R can provide neuroprotection against glutamatergic excitotoxicity as occurring in stroke models.

To investigate and temporally control the expression of the main purinergic receptor P2Y1 in cortical astrocytes, we took advantage of GLAST-Cre<sup>ERT2</sup> x P2Y1<sup>fl/fl</sup> receptor mice. For precise temporal control of gene recombination, we explored the pharmacokinetic properties of tamoxifen after intraperitoneal injections using mass spectrometry (HPLC-MS). In addition, successful astroglial recombination was determined by quantitative real time PCR (qRT-PCR) of genomic DNA and mRNA in conditional knockout (cKO) mice. Our HPLC-MS analysis showed a fast uptake of TAM and its most active metabolite 4-hydroxytamoxifen (4-OH-TAM) in the brain peaking already at eight hours post injection. The clearance of TAM and 4-OH-TAM was similarly fast. Both were almost completely excreted 48 hours after injection. The efficiency of TAM-induced recombination was also determined by qRT-PCR of genomic DNA purified from brain homogenates of cKO mice, and in addition, by quantifying reporter-positive cells in GLAST-Cre<sup>ERT2</sup> x tdTomato mice, revealing the percentage of astrocytes among all neural cells. In the cortex 20 % of all cells were GLAST-positive, whereas in the cerebellum only 6 % account for astrocytes. The astroglial *p2ry1* gene deletion resulted in mRNA reductions of 43 % in the cortex and 61 % in the cerebellum, revealing a high amount of astrocytic P2Y1R among all neural cells.

MACS isolated astrocytes showed a higher percentage of receptor ablation compared to total brain homogenates but did not reach 100 % reduction. A reduction of about 60 % in the cortex and about 30 % in the cerebellum was detected, indicating that not all sorted cells were recombined. Next generation sequencing results revealed about 50 % reduction of P2Y1R mRNA in cKOs in cortex and cerebellum.

To investigate the impact of P2Y1R under pathological conditions, we performed the stab wound injury model to cKO and control mice. Staining of the glial fibrillary acidic protein (GFAP) of coronal sections revealed no impact of the P2Y1R on lesion size and astrocytic activation.

The characterization and comparison of spontaneous-evoked  $\text{Ca}^{2+}$  signals was performed in anesthetized and awake P2Y1R control and cKO mice. We demonstrated a burst of  $\text{Ca}^{2+}$  signals upon ATP application on control astrocytes with enhanced and shortened signals in gliapil and soma. In contrast,  $\text{Ca}^{2+}$  signals of the P2Y1R cKO were smaller and shorter compared to controls, reflecting the reduction of purinergic signaling in astrocytes. We observed changes in  $\text{Ca}^{2+}$  signaling in the gliapil of the cKO, indicating alterations of  $\text{Ca}^{2+}$  signals in astrocytic microdomains.  $\text{Ca}^{2+}$  signals were even shorter and smaller in awake mice, revealing the influence of anesthesia on astrocytic  $\text{Ca}^{2+}$  signaling.

In summary, ablation of the P2Y1R could be demonstrated at the molecular level. A functional analysis of cKO mice revealed changes in the *in vivo*  $\text{Ca}^{2+}$  signals, indicating an important role of this receptor for astrocytic function.

## 2. ZUSAMMENFASSUNG

Astrozyten exprimieren eine Reihe von Neurotransmitter-Rezeptoren, die Mikrodomänen für die intrazelluläre Signaltransduktion entlang ihrer Fortsätze ausbilden. Der purinerge P2Y1-Rezeptor (P2Y1R) ist an raumgreifenden astrozytären Signalen beteiligt und schützt Neurone vor glutamaterger Überstimulation, wie sie bei Infarkten vorkommt.

Zur Untersuchung und zeitlichen Kontrolle der P2Y1-Rezeptor-Expression, wurden Tamoxifen-induzierbare GLAST-Cre<sup>ERT2</sup> x P2Y1<sup>fl/fl</sup> Mäuse verwendet. Für die präzise zeitliche Induktion der Genrekombination, wurden die pharmakokinetischen Eigenschaften von Tamoxifen nach einer intraperitonealen Injektion mittels Massenspektrometrie (HPLC-MS) ermittelt. Zusätzlich wurde die erfolgreiche astrogliale Rekombination mittels quantitativer Real-time PCR (qRT-PCR) mit genomische DNA und mRNA in konditionalen Knockout-Mäusen (cKO) ermittelt.

Die HPLC-MS-Analyse zeigte eine schnelle Aufnahme von Tamoxifen und dessen Hauptmetabolit 4-Hydroxy-Tamoxifen (4-OH-TAM) in das Gehirn, mit erreichten Höchstwerten schon acht Stunden nach der Injektion. Ähnlich schnell sanken die Werte von TAM und 4-OH-TAM auch wieder und waren 48 h nach der Injektion kaum noch detektierbar. Die TAM-induzierte Rekombinationseffizienz wurde auch in Gehirnhomogenaten von cKOs durch qRT-PCR Analyse genomischer DNA ermittelt. Zudem wurden Reporter-positive Zellen in GLAST-Cre<sup>ERT2</sup> x tdTomato Mäusen zur Quantifizierung des Astrozytenanteils im Vergleich zu allen anderen neuronalen Zellen verwendet. Im Kortex wurden 20 % GLAST-positive Zellen (= Astrozyten) über qRT-PCR rekombinierter Allele sowie Auszählung Reporter-positiver Zellen ermittelt, wohingegen im Zerebellum nur 6 % Astrozyten detektiert werden konnten. Im cKO wurde die Reduktion der P2Y1R mRNA mittels qRT-PCR überprüft. In Kortex und Zerebellum resultierte die astrogliale Deletion des *p2ry1* Gens in einer Reduktion der P2Y1R mRNA um 43 % in Kortex- und 61 % in Zerebellum-Homogenaten.

In MACS isolierten Astrozyten konnte, im Vergleich zu den Gehirnhomogenaten, eine stärkere Deletion des Rezeptors nachgewiesen werden, jedoch wurde auch hier keine 100 %ige Reduktion erreicht. Auf DNA Ebene konnte eine Reduktion um 60 % im Kortex und 30 % im Zerebellum detektiert werden. Dies weist darauf hin, dass nicht alle isolierten Zellen rekombiniert waren. Next Generation Sequencing (NGS) Daten

bestätigen für Kortex und Zerebellum eine Reduktion der P2Y1R mRNA in den cKOs (50 %).

Der Einfluss des P2Y1R unter pathologischen Bedingungen wurde mittels einer akuten Verletzung (Stichverletzung) von cKOs und Kontrollen analysiert. Das Anfärben koronaler Hirnschnitte mit dem sauren Gliafaserprotein Marker (glial fibrillary acidic protein, GFAP) zeigte keinen Einfluss des P2Y1R auf die Läsionsgröße und astrozytäre Aktivierung.

Ein weiterer Punkt in dieser Studie stellte die Charakterisierung und der Vergleich von spontan-auftretenden  $\text{Ca}^{2+}$  Signalen in anästhesierten und wachen P2Y1R Kontroll- und cKO Mäusen dar. Die Applikation von ATP zeigte eine deutliche Veränderung der  $\text{Ca}^{2+}$  Signale von Kontroll-Astrozyten mit verstärkten aber kürzeren Signalen von Gliapil und Soma. Im Gegensatz dazu, waren die  $\text{Ca}^{2+}$  Signale des P2Y1R cKOs schwächer aber ebenfalls kürzer als die Signale der Kontrollen, was auf einen Verlust des purinergen Signalwegs in Astrozyten hinweist. Veränderungen der  $\text{Ca}^{2+}$  Signale im Gliapil des cKOs weisen auf veränderte  $\text{Ca}^{2+}$  Signale in den astrozytären Mikrodomänen in den Fortsätzen hin. Die  $\text{Ca}^{2+}$  Signale von wachen cKO Mäusen waren noch schwächer und stärker verkürzt, was den starken Einfluss der Anästhesie auf die  $\text{Ca}^{2+}$  Signale zeigt.

Zusammenfassend konnten wir die Deletion des P2Y1R auf molekularer Ebene nachweisen. Die funktionelle Analyse des cKOs zeigte Veränderungen der  $\text{Ca}^{2+}$  Signale, was auf eine wichtige Rolle des Rezeptors für die astrozytäre Funktion hinweist.

### 3. INTRODUCTION

#### 3.1. Multiple astrocytic functions in the mouse central nervous system

Astrocytes are the main macroglia in the central nervous system with several unique functions. They enwrap blood vessels with their endfeet to take up nutrients from the blood and provide them for neurons (Faulkner *et al.*, 2004, Liu *et al.*, 2018). Astrocytes are actively involved in the regulation of cerebral blood flow. The release of glutamate from synapses can activate metabotropic glutamate receptors (mGluR) on astrocytes and can induce intracellular  $\text{Ca}^{2+}$  elevations. This increase induces the generation of arachidonic acid (AA). Metabolites of AA are released from astrocytes and cause either vasodilation or vasoconstriction in adjacent arterioles. Which pathway is activated by the increase of  $\text{Ca}^{2+}$ , depends on the level of  $\text{pO}_2$  and lactate in the tissue (Attwell *et al.*, 2010, Gordon *et al.*, 2011, MacVicar & Newman, 2015).

Astrocytes enwrap the pre- and postsynapses of neurons with their processes to form tripartite synapses (Araque *et al.*, 1999). In these microdomains, they clear the extracellular space from substances and ions like glutamate and potassium. By uptake of neurotransmitters, they prevent neurotoxicity caused by prolonged activation of receptors (Danbolt, 2001, Becerra-Calixto & Cardona-Gómez, 2017). This structure also enables the direct communication between neurons and astrocytes. The neuronal presynapse releases transmitters which can activate several neurotransmitter receptors located on astroglial processes. Activation of these receptors leads to a  $\text{Ca}^{2+}$  influx and intracellular  $\text{Ca}^{2+}$  increase (Araque *et al.*, 1999, Araque, 2008, Perea & Araque, 2005, Guerra-Gomes *et al.*, 2017). These  $\text{Ca}^{2+}$  signals cause the release of gliotransmitters (e.g. glutamate, ATP, D-serine) that can influence neuronal activity and plasticity (Kirchhoff *et al.*, 2001, Ricci *et al.*, 2009, Harada *et al.*, 2015).  $\text{Ca}^{2+}$  elevations that originate from one astrocyte can propagate to neighboring astrocytes. This  $\text{Ca}^{2+}$  wave can spread over the astrocytic syncytium as a long-range intercellular communication between astrocytes (Alberdi *et al.*, 2005, Cornell-Bell & Finkbeiner, 1991, Charles *et al.*, 1991, Cornell-Bell *et al.*, 1990, Scemes & Giaume, 2006, Bazargani & Attwell, 2016). Mechanisms responsible for cell-to-cell signal transduction are either activated gap junctions or the vesicular release of gliotransmitters like ATP.

These agonists induce a  $\text{Ca}^{2+}$  increase in neighboring cells (Scemes & Giaume, 2006, Koizumi, 2010, Bazargani & Attwell, 2016).

Changes in intracellular  $\text{Ca}^{2+}$  concentrations can activate diverse transcription factors acting on gene expression, leading to long-term changes in protein expression. Intracellular  $\text{Ca}^{2+}$  oscillations can induce e.g. morphological changes or alterations in gap junction coupling thereby modulating astrocytic plasticity (Pirttimäki & Parri, 2013, Papouin *et al.*, 2017).

To analyze protein functions on a cellular level the inducible Cre recombinase represents a reliable tool. The  $\text{Cre}^{\text{ERT2}}$  system leads to changes on the DNA level upon tamoxifen treatment. With this tool it is possible to knockout target genes and/or to express fluorescent proteins in a cell type and time specific manner, to analyze and influence  $\text{Ca}^{2+}$  signals, modulate transcription factors or glial signaling cascade (Fig. 1).

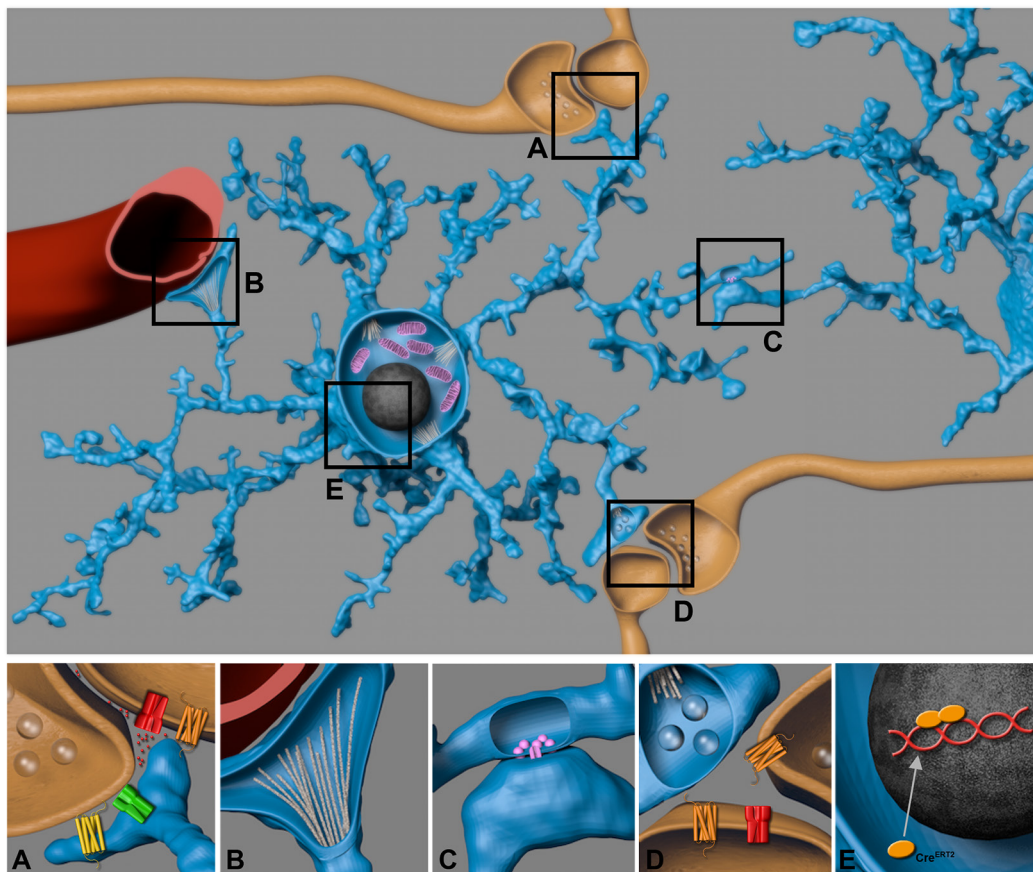


**Figure 1. Multiple tasks of astrocytes**

Astrocytes have multiple functions in the central nervous system (CNS): (A) Astrocytic processes with contact to neuronal synapses form the tripartite synapse. Glial glutamate uptake from the synaptic cleft prevents neuronal excitotoxicity. Glutamate binding to various receptors (AMPA and NMDA) induces modulation of intrinsic

signaling cascades. (B) Astrocytes with contact to blood vessels take up nutrients and provide them for neurons. They modify the blood vessel diameter via release of metabolites of arachidonic acid. (C) Astrocytes build cell-to-cell contacts with other astrocytes forming the astrocytic syncytium. They are connected via gap junctions to exchange ions, metabolites and water.  $\text{Ca}^{2+}$  signals can spread over wide distances via this network to transfer information. (D) Astrocytes modify neuronal plasticity and sensitivity by the release of gliotransmitters like ATP, D-serine and glutamate. Subsequently, they control and support synaptic transmission. (E)  $\text{Cre}^{\text{ERT2}}$  induces changes on the DNA level upon tamoxifen treatment, leading to excision of floxed alleles or expression of transgenic proteins. Neuronal signals lead to changes in DNA transcription due to activation of various transcription factors.

### **3.2. Expression of astrocytic metabotropic and ionotropic ion channels**

Astrocytes express various types of ionotropic and metabotropic receptors. The ionotropic glutamate receptors are subdivided in receptors of the NMDA-(N-methyl-D-aspartate), AMPA-( $\alpha$ -amino-3-hydroxy-5-methyl-4-isoxazolepropionic acid) and KA-type (kainic acid) (Matthias *et al.*, 2003, Grass *et al.*, 2004, Schipke *et al.*, 2001, Mayer, 2005). These subtypes are permeable for different cations. AMPA and KA receptors are mainly permeable for  $\text{Na}^+$  and  $\text{K}^+$  while NMDA receptors are also permeable for  $\text{Ca}^{2+}$  ions (Mayer & Westbrook, 1987, Hollmann *et al.*, 1991, Karakas & Furukawa, 2014, Wright & Vissel, 2012). AMPA receptors are commonly expressed in glia and in many brain regions like the cerebellum, cortex, hippocampus and brainstem. They can be assembled out of four different subunits: GluA1-4. Depending on the brain region the receptor composition can vary which also leads to distinct receptor function (Verkhratsky & Kirchhoff, 2007, Seifert & Steinhäuser, 2001, Bowie, 2012) (Fig. 2).



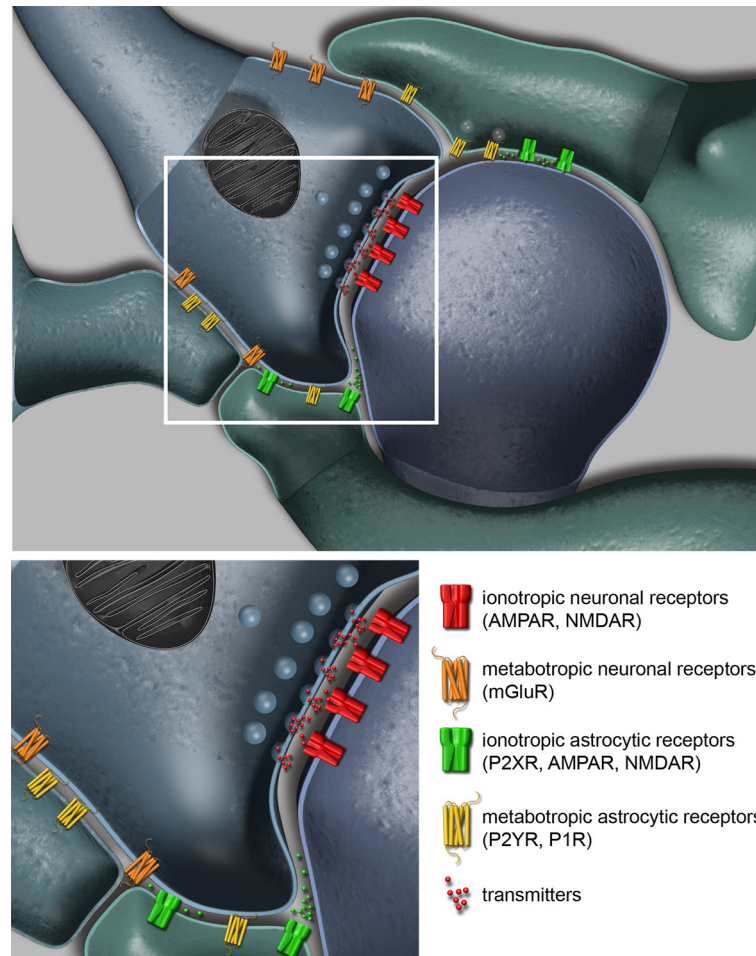


**Figure 2. Distribution and function of diverse metabotropic and ionotropic ion channels at the tripartite synapse**

The tripartite synapse consists of the neuronal pre- and postsynapse and the astrocytic processes. Perisynaptic activation leads to the release of transmitters (e.g. glutamate) from synaptic vesicles into the synaptic cleft. These transmitters activate diverse ionotropic or metabotropic neuronal receptors located on the postsynapse (e.g. AMPAR, NMDAR, mGluR). Astrocytes also express a plethora of purinergic metabotropic and ionotropic receptors like P2Y (P2Y<sub>1</sub>R), P1 adenosine (A1R, A2AR, A2BR, A3R), P2X (P2X<sub>6</sub>R, P2X<sub>7</sub>R) and AMPA receptors (Abbracchio *et al.*, 2009, Verkhratsky & Kirchhoff, 2007). Astrocytes release gliotransmitters, like ATP or D-serine to activate ionotropic P2X or NMDA receptors located at the postsynapse (Gordon & Bains, 2006).

Purinergic receptor types such as the metabotropic P1 adenosine and P2Y receptors as well as the ionotropic P2X purinoceptors are expressed by astrocytes.

P2X receptors are trimeric ion channels that open within milliseconds upon ATP binding, causing a conformational change so that Ca<sup>2+</sup> and Na<sup>+</sup> enter the cell in exchange for K<sup>+</sup> (Browne *et al.*, 2010, North, 2016). P2X receptors are divided in seven

subtypes (P2X<sub>1-7</sub>) involved in several functions like synaptic transmission and secretion of transmitters (Hattori & Gouaux, 2012) (Fig. 3).

Adenosine receptors (P1R) consist of seven transmembrane domains and are classified in four different receptor types: A<sub>1</sub>, A<sub>2A</sub>, A<sub>2B</sub> and A<sub>3</sub>. These G protein coupled receptors mediate adenosine controlled modulation of neuronal and glial function and neuron-glia signaling (Abbracchio *et al.*, 2009, Sheth *et al.*, 2014) (Fig. 3).

G protein coupled P2Y receptors are divided in two groups: P2Y<sub>1,2,4,6,11</sub>, and P2Y<sub>12,13,14</sub> based on their G protein subfamily. P2Y<sub>1</sub>R are broadly distributed on glial cells. They are expressed by astrocytes, oligodendrocytes and microglia (Butt, 2011). The binding of their ligand adenosine diphosphate (ADP) activates P2Y<sub>1</sub>R (Kirischuk *et al.*, 1995, Franke *et al.*, 2012). The receptors are G<sub>q/11</sub> coupled and lead to the activation of phospholipases (PLA<sub>2</sub>, PLC) and protein kinase C (PKC). PLC activity results in the cleavage of phosphatidylinositol 4,5-bisphosphate (PIP<sub>2</sub>) into inositoltriphosphate (Ins-P<sub>3</sub>) and diacylglycerol (DAG). DAG activates PKC whereas Ins-P<sub>3</sub> binds to the Ins-P<sub>3</sub> receptor on the surface of the endoplasmatic reticulum mediating Ca<sup>2+</sup> release into the cytoplasm (Verkhratsky *et al.*, 2009, Franke *et al.*, 2012). The increase of intracellular Ca<sup>2+</sup> influences the bi-directional communication between neurons and astrocytes by release of gliotransmitters. Astrocytes itself are capable of releasing ATP as response to neuronal ATP release thereby modulating synaptic transmission (Lalo *et al.*, 2011, Pascual *et al.*, 2005). P2Y<sub>1</sub> also activates signal transduction mechanisms like the mitogen-activated protein (MAP) kinase or the phosphoinositide-3-kinase (PI3K) pathway (Franke *et al.*, 2012) (Fig 3).

The exact function of astrocytic P2Y<sub>1</sub> receptors under pathological conditions, like brain injury or cytotoxic edema, is a matter of debate in literature. Some studies claim the beneficial role of P2Y<sub>1</sub> receptors during pathological circumstances, whereas others describe a neuroprotective effect after receptor downregulation (Shinozaki *et al.*, 2017, Zheng *et al.*, 2010).

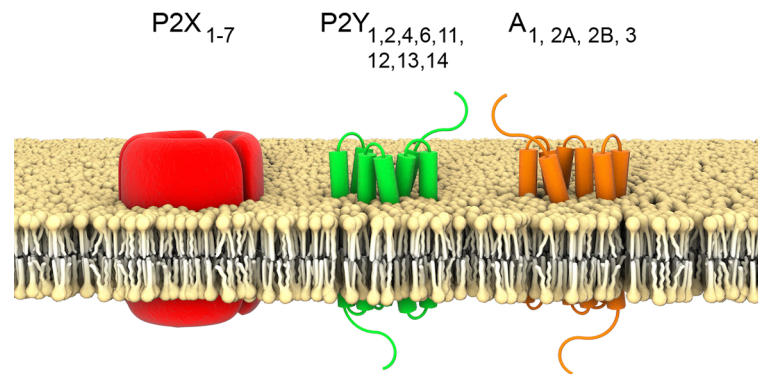


**Figure 3. Purinergic signaling in the CNS**

Purinergic receptors are divided in two main classes: ionotropic and metabotropic purinoceptors. The ionotropic P2X receptors consist of three subunits that undergo a conformational change upon ATP binding which leads to the influx of  $\text{Na}^+$  and  $\text{Ca}^{2+}$  and  $\text{K}^+$  efflux. The metabotropic receptors are further classified into P2Y and adenosine receptors. They consist of seven transmembrane domains and are G protein coupled. Upon ligand binding an intracellular signaling cascade is induced.

Astrocytes, neurons and myelinating oligodendrocytes express *p2ry1* mRNA ([www.brainrnaseq.com](http://www.brainrnaseq.com) of the Ben Barres laboratory (Zhang *et al.*, 2014)). Astrocytes express about 9 % of the *p2ry1* mRNA compared to neurons and oligodendrocytes. The ionotropic receptors P2X6 and P2X7 are highly expressed in astrocytes whereas P2X7 is mainly expressed in OPCs and microglia/macrophages but only low expression was found in neurons (Fig. 4 A). During development and aging *p2ry1* mRNA expression in mouse cortical astrocytes starts to be detectable at P7 and then remains on same levels until two years of age ( $0.8 \pm 0.6$  -  $0.3 \pm 0.04$  fragments per kilobase million, FPKM) (Fig. 4 B).

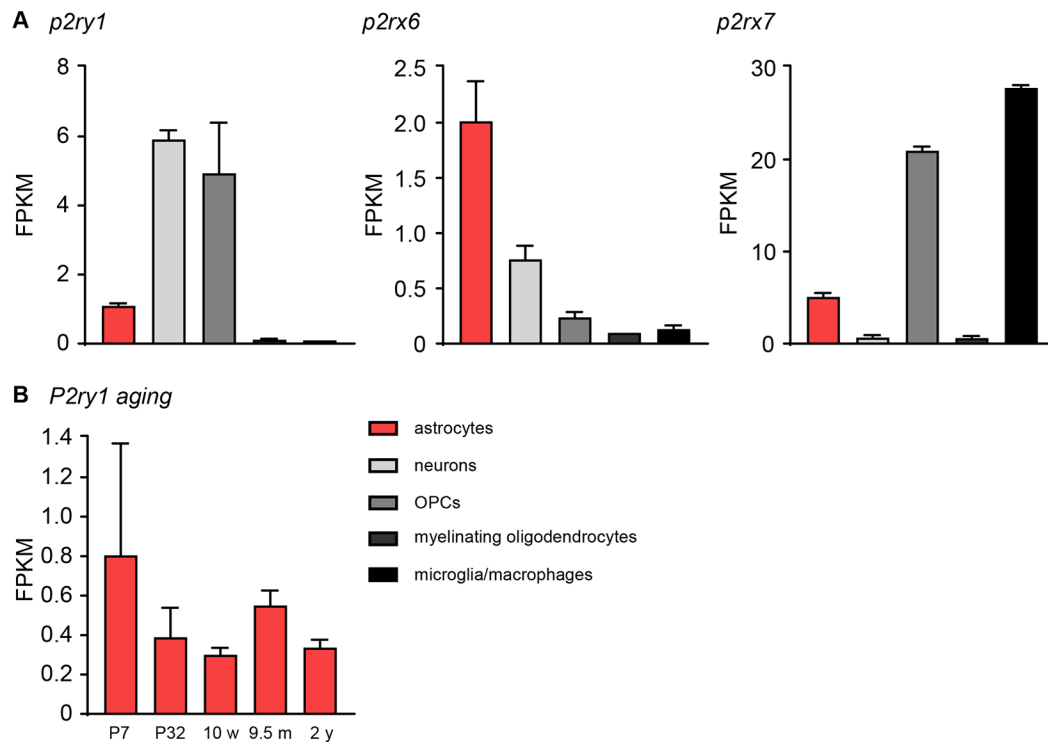


**Figure 4. P2Y and P2X receptor mRNA expression of glial cells**

(A) P2Y1R mRNA is mainly expressed by neurons ( $5.9 \pm 0.3$  FPKM) and myelinating oligodendrocytes ( $4.9 \pm 1.5$ ) but also by astrocytes ( $1.1 \pm 0.06$  FPKM). Higher expressed in astrocytes are the ionotropic receptors P2X6 ( $2.0 \pm 0.4$  FPKM) and P2X7 ( $5.1 \pm 0.4$  FPKM). P2X7R is mainly expressed in OPCs ( $21.0 \pm 0.4$  FPKM) and microglia/macrophages ( $27.8 \pm 0.3$  FPKM) but only low expressed in neurons ( $0.7 \pm 0.3$  FPKM). (B) *P2ry1* mRNA expression in mouse cortical astrocytes varies slightly between P7 and 2 years of age (P7:  $0.8 \pm 0.6$ ; P32:  $0.4 \pm 0.1$ ; 10 w:  $0.3 \pm 0.003$ ; 9.5 m:  $0.6 \pm 0.007$  and 2 y:  $0.3 \pm 0.04$  FPKM). Data modified after (Zhang *et al.*, 2014, Clarke *et al.*, 2018).

### 3.3. ATP induced $\text{Ca}^{2+}$ signaling in astrocytes

Astrocytes are involved in the generation and maintenance of  $\text{Ca}^{2+}$  waves. Extracellularly induced astrocytic  $\text{Ca}^{2+}$  signals are mediated by ATP released by adjacent neurons, leading to the activation of purinergic receptors, like P2Y1. Binding of the ligand to the purinergic receptor triggers an internal signaling cascade leading to the release of  $\text{Ca}^{2+}$  from the endoplasmic reticulum (ER) (Fields & Burnstock, 2006, Abbracchio *et al.*, 2009, Cotrina *et al.*, 2000).

Astrocytes are able to generate spontaneous  $\text{Ca}^{2+}$  signals as well as  $\text{Ca}^{2+}$  signals induced by neuronal activity. Spontaneous  $\text{Ca}^{2+}$  signals mainly depend on the vesicular release of adrenaline and noradrenaline, leading to the activation of adrenergic  $\alpha$ 1-

receptors (Ding *et al.*, 2013). These  $\text{Ca}^{2+}$  signals originate in astroglial processes and propagate to the soma. The main  $\text{Ca}^{2+}$  activity was found in astroglial processes and not in the soma. In general,  $\text{Ca}^{2+}$  signals are very diverse, depending on the astrocytic subpopulations or the different microdomains of astrocytic processes. *In vivo*, astrocytic  $\text{Ca}^{2+}$  elevations are triggered by external stimuli, like whisker stimulation, visual stimuli or locomotion of the animal (Nimmerjahn *et al.*, 2004, Wang *et al.*, 2006, Agulhon *et al.*, 2008). Different types of  $\text{Ca}^{2+}$  signals were characterized in cerebellar Bergmann glia as well as the influence of anesthesia on these signals (Nimmerjahn *et al.*, 2009). Astrocytic  $\text{Ca}^{2+}$  signals of awake mice can be divided in three signal types. First,  $\text{Ca}^{2+}$  sparkles as smaller, localized signals, second  $\text{Ca}^{2+}$  bursts including signals of around 40 cells and third  $\text{Ca}^{2+}$  flares involving large networks of astrocytes and appearing only under locomotion. Under anesthesia, flares are completely absent and sparkles mainly abolished.  $\text{Ca}^{2+}$  bursts require purinergic signaling whereas flares and sparkles either need activation of  $\text{Na}^+$  channels or glutamatergic transmission (Nimmerjahn *et al.*, 2009).

### 3.4. Tamoxifen metabolism

Tamoxifen (TAM), used for more than 30 years in the therapy of hormone-dependent breast cancer, has become an important component of the Cre<sup>ERT2</sup>/loxP system, for the analysis of gene functions in inducible conditional mouse mutants. TAM as a prodrug is oxidized in the liver by cytochrome P450 isoenzymes (CYPs) to several primary and secondary metabolites: N-desmethyl-tamoxifen (NDM-TAM), 4-hydroxytamoxifen (4-OH-TAM) and endoxifen (END) (Caldas & Tannock, 2013, Goetz *et al.*, 2008, Stearns & Rae, 2008) (Fig. 5). TAM and its metabolites bind to estrogen receptors (ER) with different affinities. In human, suppression of the estrogen-dependent cell proliferation by 4-OH-TAM is 30- to 100-fold higher compared to TAM (Borgna & Rochefort, 1981, Jordan *et al.*, 1977, Robertson *et al.*, 1982), although it represents less than 10 % of all primary oxidation products of TAM (Desta *et al.*, 2004). END shares identical properties but is present in concentrations up to 10-fold higher than 4-OH-TAM (Johnson *et al.*, 2004, Stearns *et al.*, 2003).

In mice, the pharmacokinetic profile of TAM appears significantly different, mainly due to the lower expression and activity levels of cytochrome P450 isoenzymes (CYP) (Reid *et al.*, 2014, McLaughlin *et al.*, 2008). TAM is mainly metabolized to NDM-TAM by CYP3A and to a significant lower amount to 4-OH-TAM by CYP2D6. NDM-TAM can

be further metabolized to END by CYP2D6, whereas 4-OH-TAM is converted into END by CYP3A (Chang *et al.*, 2016) (Fig. 5).

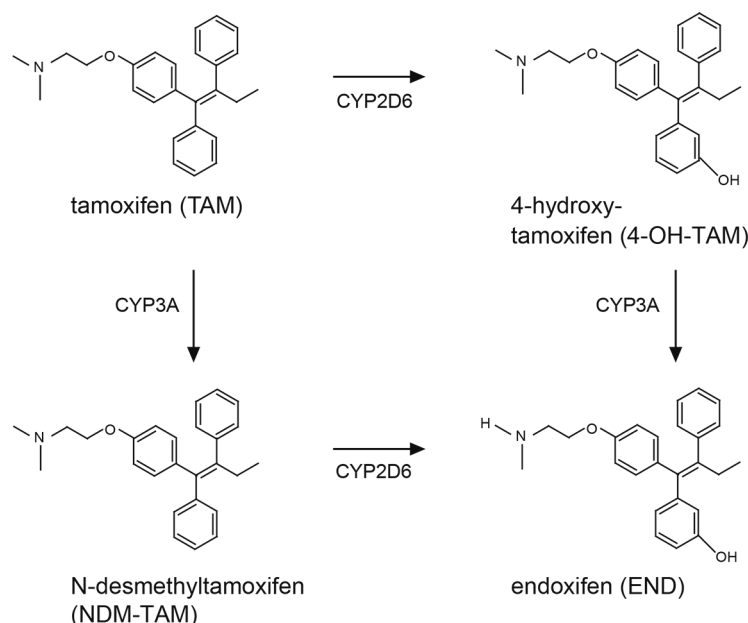


**Figure 5. Tamoxifen metabolism in mice**

TAM is converted by CYP3A to NDM-TAM, which is one major primary TAM metabolite. This metabolite undergoes multiple oxidation steps including 4-hydroxylation to END by CYP2D6. 4-Hydroxylation of TAM to 4-OH-TAM by CYP2D6 represents another primary metabolic route, with significant importance for experimental biology in mice. A small proportion of endoxifen appears to result from N-demethylation of 4-OH-TAM by CYP3A (modified after (Jahn, Kasakow *et al.*, 2018).

The Cre DNA recombinase mediates site-specific recombination between two loxP sites ("floxed" sequence). Advantage of the Cre/loxP system is the independency of any co-factors or other sequence elements for efficient recombination (Nagy, 2000). Therefore, this system is well adapted for a foreign environment e.g. the mouse cell (Lewandoski, 2001).

An improved version of Cre recombination is the Cre<sup>ERT2</sup>/loxP system to achieve not only spatially but also temporally controlled gene recombination. Cre<sup>ERT2</sup> is a fusion protein consistent of the mutant ligand binding domain of the estradiol receptor (ER) and the Cre DNA recombinase. Mutation of the estradiol receptor inhibits the binding of its natural ligand  $\beta$ -estradiol, but enables binding of the synthetic ligand 4-hydroxy-tamoxifen (4-OH-TAM) (Leone *et al.*, 2003, Metzger & Chambon, 2001). The translocation of Cre<sup>ERT2</sup> into the nucleus is induced by TAM. In absence of the ligand the heat shock protein HSP90 is bound to Cre<sup>ERT2</sup> inhibiting its transfer from the cytosol

into the nucleus. Upon TAM treatment HSP90 dissociates from the complex, Cre<sup>ERT2</sup> translocates and mediates recombination between loxP sites (Feil *et al.*, 1997, Metzger & Chambon, 2001, Weber *et al.*, 2001, Hirrlinger *et al.*, 2006). The advantage of the inducible Cre<sup>ERT2</sup>/loxP is the temporal determination of the recombination event. Many astrocytic promoters, e.g. the regulatory elements of the glutamate aspartate transporter (GLAST), are already active in embryonic progenitors leading to recombinant oligodendrocytes and neurons in the adult mouse brain (Regan *et al.*, 2007).

Since its introduction, the inducible Cre/loxP system was used either for the generation of conditional gene-deficient mice or for the induction of cell type-specific reporter expression (www.jax.org, www.networkglia.eu/en/animal\_models) (Fig. 6).

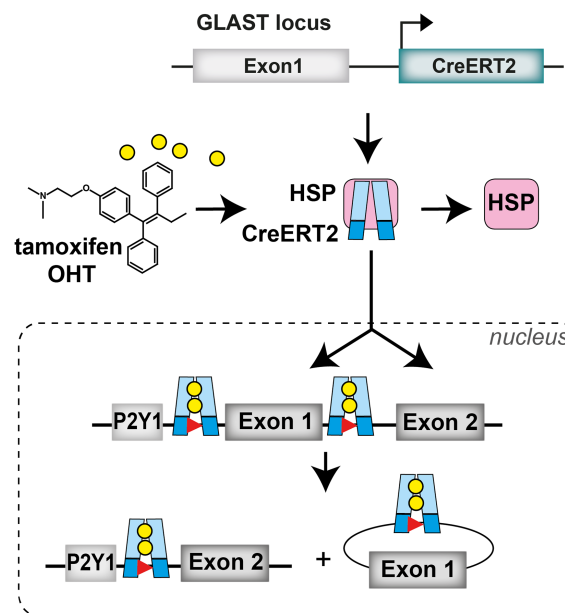


**Figure 6. Expression of Cre<sup>ERT2</sup> in astrocytes of the GLAST locus**

A mutant ligand binding domain of the estradiol receptor was fused to the Cre DNA recombinase. Activation can be induced by application of the synthetic ligand TAM. In absence of this ligand the heat shock protein HSP90 keeps the Cre<sup>ERT2</sup> fusion protein in the cytoplasm. Through TAM application HSP90 dissociates from the complex and induces the translocation of Cre<sup>ERT2</sup> into the nucleus, where recombination between two loxP sites, which flank a region of interest („floxed“) can start. Schematic illustration of the recombination strategy, representative for the P2Y1R knockout, where Cre<sup>ERT2</sup> was knocked into the locus of the astrocyte-specific locus of GLAST (Mori *et al.*, 2006).

## 4. AIM

### 4.1. Astrocyte-specific gene recombination and the influence of tamoxifen-induced recombination

Astrocytes are the main glial cell type in the brain. They express a range of neurotransmitter receptors localized along their processes that cover synapses, blood vessels and constitute “microdomains” for signaling pathways.

First, to identify the optimal tamoxifen-injection protocol for maximal recombination efficiency, the pharmacokinetic profile of TAM and its metabolites was determined. Diverse injection protocols were tested for different gene loci. In this context, the extent of tamoxifen-independent recombination, caused by adverse Cre<sup>ERT2</sup> activity, was evaluated. Therefore, various Cre<sup>ERT2</sup> driver lines were analyzed at the DNA and protein level.

Second, the influence of astroglial purinergic P2Y1 receptors was investigated by taking advantage of conditional knockout mice (cKO), where gene recombination of floxed P2Y1 receptors was controlled by an astrocyte-specific and tamoxifen-inducible Cre DNA recombinase (GLAST-Cre<sup>ERT2</sup>). The effect of P2Y1R ablation was evaluated by the analysis of *in vivo* Ca<sup>2+</sup> signals. Therefore, changes in signal amplitudes and duration of anesthetized and awake animals were investigated. Characterization of cKO mice and its consequences was additionally analyzed by next generation sequencing to identify changes in mRNA expression pattern. P2Y1 receptor ablation was also examined under pathological conditions by utilizing the established cortical stab wound injury (SWI) model.



## 5. MATERIALS AND METHODS

### 5.1. Materials

#### 5.1.1. Reagents

Standard chemicals were purchased from customary companies like Sigma Aldrich (Taufkirchen), Eppendorf (Hamburg), Merck (Darmstadt), BioRad (München), Invitrogen (Karlsruhe), Roche (Penzberg), Carl Roth (Karlsruhe), Amersham Biosciences (Freiburg), Serva (Heidelberg), Thermo Fisher Scientific (Karlsruhe) and BD Falcon (Heidelberg).

#### 5.1.2. Consumables and kits

Pipette tips, Sarstedt (Nümbrecht); glas pipettes, VWR International (Darmstadt); Falcontubes, Greiner Bio-One (Frickenhausen); Eppendorf reaction tubes, Eppendorf (Hamburg); Venomix canulas, Braun (Melsungen); 96-well-PCR-reaction-tubes, 4titude (Berlin); 24-well-culture-plates, Sarstedt (Nümbrecht); object slides and cover slips, Menzel-Gläser (Braunschweig); RT-PCR 96-well plates, Axon (Kaiserslautern); REDExtract-N-Amp™ Tissue PCR Kit, Sigma-Aldrich (Taufkirchen); All prep DNA/RNA Mini Kit, Qiagen (Hilden); All prep DNA/RNA Micro Kit, Qiagen (Hilden), Invisorb Spin Tissue Mini Kit, Invitex (Berlin); Precellys homogeneizing tubes, Precellys-Keramik-Kit, peqlab (Erlangen); Super Signal West Pico Chemiluminescent Substrate and Pierce BCA Protein Assay Kit, Thermo Scientific (Rockford); Adult Brain Dissociation Kit, Anti-ACSA-2 MicroBead Kit, Miltenyi (Bergisch Gladbach).

#### 5.1.3. Devices

**Table 1. Devices**

Device	Producer
Gel chambers, combs and casting trays for agarose gels	Workshop of the institute
Confocal microscope LSM 710	Zeiss
AxioScan.Z1	Zeiss
Precellys 24 (Homogenizer)	peqlab Biotechnologie GmbH
Thermomixer comfort	Eppendorf
Vibrotom VT1000S/VT1200S	Leica
Centrifuges	Eppendorf

Device	Producer
Scales (CPA 8201/CPA 2245)	Sartorius
Infinite PRO 200 microplate reader	Tecan
Preparations- and perfusion instruments	F.S.T., Pharmacia
peqSTAR Thermo Cycler	peqlab Biotechnologie GMBH
Quantum gel documentation system	peqlab Biotechnologie GMBH
BioSpectrometer	Eppendorf
CFX96 Real-Time PCR Detection System	BioRad
Device	Producer
Vacuum pump	Integra Biosciences
Pipettes	Brand
Shaker DRS-12	neoLab
Water facility Milli-Q or GenPure	Merck/Thermo Scientific
Intelli Mixer	neoLab
IKA C MAG HS 7 digital (magnetic mixer)	ChemLabz
Spectrophotometer	Eppendorf
NanoPhotometer	DeNovix
Electrophoresis Power Supply	Consort
gentleMACS Octo Dissociator with heaters	Miltenyi

#### 5.1.4. Buffers, aqueous solutions and media

All buffers and aqueous solutions were prepared with deionized water (dH<sub>2</sub>O) (Milli-Q (Merck) or GenPure (Thermo Scientific)). All concentrations are final concentrations.

##### 5.1.4.1. General buffers

###### PBS (Phosphate-buffered saline, 10x; pH 7.4)

NaCl	1.37	M
KCl	27	mM
Na <sub>2</sub> HPO <sub>4</sub>	100	mM
KH <sub>2</sub> PO <sub>4</sub>	18	mM

(pH was adjusted with HCl solution (37 %))

###### 4 % PFA in 1x PBS (pH 7.4)

Paraformaldehyde	4 %	(w/v)
NaOH	10	M

(added until PFA is dissolved)

Tris-Acetate-EDTA-Buffer (TAE 50 x)

Tris-Base Tris(hydroxymethylaminomethan)	2	M
Acetic acid (100 %)	1	mM
EDTA (Ethylenediaminetetraacetate, 0.5 M, pH 8)	1	mM

**5.1.4.2. Immunohistochemistry (IHC)**Standard protocol

Permeabilization-/blocking buffer and buffer for primary antibodies

4 % horse serum (HS), 0.3 % Triton-X-100 in 1x PBS

Buffer for secondary antibodies

2 % HS in 1x PBS

**5.1.4.3. Induction of recombination**Tamoxifen

Tamoxifen in Miglyol (Caesar & Loretz)	10	mg/ml
--	----	-------

**5.1.4.4. Perfusion for qRT-PCR samples/ cortical window surgery**ACSF (artificial cerebrospinal fluid)/ cortex buffer (pH 7.4)

NaCl	124	mM
KCl	3	mM
NaH <sub>2</sub> PO <sub>4</sub>	1.2	mM
NaHCO <sub>3</sub>	26	mM
MgCl <sub>2</sub>	2	mM
CaCl <sub>2</sub>	2	mM

Carbogen gas

Oxygen	95 %
Carbon dioxide	5 %

**5.1.5. Purchased buffers**

Hanks' Balanced Salt Solution (HBSS, w/o Ca<sup>2+</sup> and Mg<sup>2+</sup>, Sigma-Aldrich)

Dulbecco's Phosphate Buffered Saline (1x D-PBS, Sigma-Aldrich)

For MACS 0.5 % Bovine Serum Albumin (BSA, Sigma-Aldrich) was added to the D-PBS buffer (1x D-PBS-BSA buffer).

### 5.1.6. Enzymes

REDTaq™ DNA Polymerase (Sigma-Aldrich Co.)

5x Hot Start Taq Eva Green® (Axon)

Omniscript (Qiagen)

### 5.1.7. Drugs

Tetrodotoxin (TTX) (Alemone Labs)	1	μM
ATP (Na <sup>+</sup> ) (Sigma Aldrich)	10	μM

### 5.1.8. Antibodies

#### 5.1.8.1. Primary antibodies

**Table 2. Primary antibodies**

Antibody	Producer	Clonality	Species	Dilution
GFAP	DakoCytomation	pc	rabbit	1:1000
GFAP	Abcam	pc	goat	1:1000
GFAP	Novocastra	mc	mouse	1:1000
Iba1	Wako	pc	rabbit	1:500
DsRed	Clontech	pc	rabbit	1:500
GFP	Abcam	mc	mouse	1:1000
GFP	Rockland	pc	goat	1:1000

#### 5.1.8.2. Secondary antibodies

Secondary antibodies for immunohistochemistry were purchased from Invitrogen (Molecular Probes)/Abcam and used in a dilution 1:1000 or 1:500.

**Table 3. Secondary Antibodies**

Antibody	Producer	Dilution
Donkey α-rabbit Alexa 488-conjugated	Invitrogen	1:1000
Donkey α-mouse Alexa 555 conjugated	Invitrogen	1:1000
Donkey α-goat Alexa 488conjugated	Invitrogen	1:1000
Donkey α-goat Alexa 546 conjugated	Invitrogen	1:1000
Donkey α.goat Alexa 647conjugated	Invitrogen	1:1000
Donkey α-rabbit Cy5	Abcam	1:500

### 5.1.8.3. Dyes

Ethidiumbromide (Sigma)

TO-PRO 3 (Invitrogen)

DAPI (Roche)

EvaGreen (Axon)

Texas Red-dextran (70 kDa, Invitrogen)

### 5.1.9. Primers

#### 5.1.9.1. Primers for genotyping

**Table 4. Genotyping primers**

Name	Number	Sequence	PCR product
GLAST forward	11984	5'-GAGGCACTTGGCTAGGCTCTGAGGA-3'	KI 400 bp WT 700 bp
GLAST reverse	11985	5'-GAGGAGATCCTGACCGATCAGTTGG-3'	
Cre <sup>ERT2</sup> reverse	11986	5'-GGTGTACGGTCAGTAAATTGGACAT-3'	
GFAP-Cre <sup>ERT2</sup> forward	4750	5'-CAGGTTGGAGAGGAGACGCATCA-3'	TG 500 bp WT 700 bp
GFAP-Cre <sup>ERT2</sup> reverse	7963	5'-CGTTGCATCGACCGGTAATGCAGGC-3'	
GLAST forward	11984	5'-GAGGCACTTGGCTAGGCTCTGAGGA-3'	
GLAST reverse	11985	5'-GAGGAGATCCTGACCGATCAGTTGG-3'	
P2Y1 forward	23992	5'-CAAGTTCAGGTGGCCAGTTTTCTTGG-3'	KI 304 bp WT 228 bp
P2Y1 reverse	23993	5'-AGTTGCCCGCACGTCCTTCAGC-3'	
tdTomato KI forward	27490	5'-GGCATTAAAGCAGCGTATCC-3'	KI 196 bp WT 297 bp
tdTomato KI reverse	27491	5'-CTGTTCTGTACGGCATGG-3'	
tdTomato WT forward	27488	5'-AAGGGAGCTGCAGTGGAGTA-3'	
tdTomato WT reverse	27489	5'-CCGAAAATCTGTGGGAAGTC-3'	
GCaMP3 KI forward	27632	5'-CACGTGATGACAAACCTTGG-3'	KI 245 bp WT 327 bp
GCaMP3 KI reverse	27496	5'-GGCATTAAAGCAGCGTATCC-3'	
GCaMP3 WT forward	14025	5'-CTCTGCTGCCTCCTGGCTTCT-3'	
GCaMP3 WT reverse	14026	5'-CGAGGCGGATCACAAGCAATA-3'	
Gria1 forward	7975	5'-CACTCACAGCAATGAAGCAGGAC-3'	KI 250 bp WT 200 bp
Gria1 reverse	7976	5'-CTGCCTGGGTAAAGTGAAGTGG-3'	

### 5.1.9.2. Primers for quantification of mRNA expression

**Table 5. mRNA expression primers**

Name	Number	Sequence	PCR product
b-actin forward	9146	5'-CTTCCTCCCTGGAGAAGAGC-3'	124 bp
b-actin reverse	9147	5'-ATGCCACAGGATTCCATACC-3'	
P2Y1 forward	24001	5'-CACGAGTTTGTGAAGGCACG-3'	69 bp
P2Y1 reverse	24003	5'-GCTTCTTCTTGACCTGTGTATGCA-3'	
Aquaporin 4 forward	30574	5'-TGGAGGATTGGGAGTCACC-3'	92 bp
Aquaporin 4 reverse	30575	5'-TGAACACCAACTGGAAAGTGA-3'	
Aldh1l1 forward	29513	5'-GAGGAAGCAGCCACCTATGA-3'	66 bp
Aldh1l1 reverse	30582	5'-TGGCTGGTCCCAGTTGAT-3'	
Itgam forward	30576	5'-CAATAGCCAGCCTCAGTGC-3'	65 bp
Itgam reverse	30577	5'-GAGCCCAGGGGAGAAGTG-3'	
NeuN forward	29474	5'-GAAGAGAATGGCGAGACACTG-3'	67 bp
NeuN reverse	30580	5'-GGCCCATAGACTGTTCTACC-3'	
PDGFR $\alpha$ forward	30525	5'-AAGACCTGGGCAAGAGGAAC-3'	67 bp
PDGFR $\alpha$ reverse	30526	5'-GAACCTGTCTCGATGGCACT-3'	
MBP forward	30529	5'-CCTCAGAGGACAGTGATGTGTTT-3'	62 bp
MBP reverse	30530	5'-AGCCGACGTCCCATTGTT-3'	
GS forward	30531	<b>5'-CTCGCTCTCCTGACCTGTTT-3'</b>	94 bp
GS reverse	30532	<b>5'-TTCAAGTGGGAACCTTGCTGA-3'</b>	
GLT1	29519	<b>5'-GATGCCTTCCTGGATCTCATT-3'</b>	93 bp
GLT1	30583	<b>5'-CAGAACTTTCTTTGTCACTGTCTGA-3'</b>	

### 5.1.9.3. Primers for quantification of DNA recombination

**Table 6. DNA recombination primers**

Name	Number	Sequence	PCR product
b-actin forward	29472	5'-CTGCTCTTTCCCAGACGAGG-3'	137 bp
b-actin reverse	29473	5'-AAGGCCACTTATCACCAGCC-3'	
NrgIII forward	4767	5'-GTGTGCGGAGAAGGAGAAAAC-3'	120 bp
NrgIII reverse	4805	5'-AGGCACAGAGAGGAATTCATTTCTTA-3'	
P2Y1 rec. forward	23996	5'-CTTAGATCGGTCGCAGCTCC-3'	127 bp
P2Y1 rec. reverse	23997	5'-GCGCTTTTGTGCGTTAATTA-3'	
P2Y1 gain forward	23998	5'-CTTAGATCGGTCGCAGCTCC-3'	154 bp
P2Y1 gain reverse	24000	5'-TGGCCAGTTTCTTGAGACA-3'	
Gria1 gain forward	10466	5'-GTTTCAGACAGGGACCCTCTCA-3'	129 bp
Gria1 gain reverse	10467	5'-GCCTGCCTGGGTAAAGTGACT-3'	

Name	Number	Sequence	PCR product
GCaMP3 loss forward	35304	5'-TCTGGATCTGTGACCTGC-3	197 bp
GCaMP3 loss reverse	35305	5'-TGGTGGCGAGATCCTTATCG-3	
GCaMP3 gain forward	35302	5'-GGCAACGTGCTGGTTATTGTG-3'	237 bp
GCaMP3 gain reverse	35303	5'-TCGTACAGATCCCGACCCA-3'	
tdTomato forward	STO1357782	5'-ATCATGTCTGGATCCCCATC-3'	218 bp
tdTomato reverse	STO1357783	5'-CGTGGCCGTTTCATGGAGCCCC-3'	

## 5.1.10. Animals

### 5.1.10.1. Transgenic mice

#### TgH (GLAST-Cre<sup>ERT2</sup>)<sub>GLAC</sub>

The GLAST-Cre<sup>ERT2</sup> mouse line expresses an inducible Cre DNA recombinase variant (Cre<sup>ERT2</sup>), where the mutant ligand binding domain of the estradiol receptor is fused to the Cre DNA recombinase. The Cre<sup>ERT2</sup> fusion protein was inserted into exon 2 of the GLAST (glutamate aspartate transporter) locus (*slc1a3*) leading to an astrocyte specific expression (Mori *et al.*, 2006). This mouse line was kindly provided by Magdalena Götz (München).

#### TgN (hGFAP-Cre<sup>ERT2</sup>)<sub>GCTF</sub>

A fragment of the human GFAP promoter controls the expression of the Cre<sup>ERT2</sup> fusion protein to achieve a tamoxifen-inducible Cre driver line (Cre<sup>ERT2</sup>) in astrocytes (Hirrlinger *et al.*, 2006). This mouse line was generated via non-homologous recombination (oocyte injection).

#### TgH (P2Y1<sup>fl/fl</sup>)<sub>P2Y1</sub>

The P2Y1 mouse line carries a floxed exon 1 of the *p2ry1* gene (Leon *et al.*, 1999, Rudolph *et al.*, 2016). The conditional P2Y1 receptor knockout is achieved by crossbreeding this line with GLAST-Cre<sup>ERT2</sup> mice and induction of recombination by tamoxifen treatment. Investigated animals were distinguished in controls (con) (*slc1a3* wt/ fl/fl P2Y1) and knockouts (cKO) (*slc1a3* ct2/wt/ fl/fl P2Y1). This mouse line was kindly provided by Christian Gachet (Strasbourg).

**TgH (Gria1<sup>fl/fl</sup>)<sub>Gria1</sub>**

The Gria1 mouse line carries a floxed exon 11 of the *gria1* gene, the subunit 1 of the AMPA receptors (Fuchs *et al.*, 2007). This mouse line is crossbred to the GLAST-Cre<sup>ERT2</sup> mice to achieve a conditional knockout when tamoxifen is applied. Analyzed animals were distinguished in controls (*slc1a3* wt/ fl/fl Gria1) and cKO (*slc1a3* ct2/wt/ fl/fl Gria1). This mouse was kindly provided by Rolf Sprengel (Heidelberg).

**TgH (Rosa26-GCaMP3)<sub>GCaMP3</sub>**

The Ca<sup>2+</sup> indicator mouse line Rosa26-GCaMP3 shows an enhanced green fluorescent protein (EGFP) signal after the binding of Ca<sup>2+</sup> to calmodulin. This mouse line was crossbred to the GLAST-Cre<sup>ERT2</sup> mouse line and upon tamoxifen application the Cre recombinase leads to the deletion of a floxed STOP cassette ahead of the GCaMP3 sequence (Paukert *et al.*, 2014). Investigated animals were distinguished in controls (*slc1a3* wt/ fl/fl GCaMP3) and reporter expressing (*slc1a3* ct2/wt/ fl/fl GCaMP3) mice. The mouse line was kindly provided by Amit Agarwal (Heidelberg) and Dwight Bergles (Baltimore).

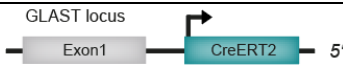
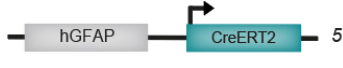
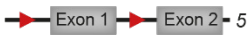



**TgH (Rosa26-tdTomato)<sub>tdTomato</sub>**

The reporter mouse line Rosa26-tdTomato expresses the red fluorescent reporter tdTomato when crossbred to the GLAST-Cre<sup>ERT2</sup> mouse line and tamoxifen application. Cre<sup>ERT2</sup> leads to the deletion of a floxed STOP cassette positioned ahead of the fluorescent protein sequence (Madisen *et al.*, 2010). Investigated animals were distinguished in controls (*slc1a3* wt/ fl/fl tdTomato) and reporter expressing (*slc1a3* ct2/wt/ fl/fl tdTomato) mice. The mouse line was kindly provided by Hongkui Zeng (Seattle).

(GLAC, GCTF, P2Y1, Gria1, GCaMP3 and tdTomato are laboratory internal abbreviations).



**Table 7. Mouse lines**

Mouse line	Costruit	Reference
TgH(GLAST-Cre <sup>ERT2</sup> ) <sub>GLAC</sub>		(Mori <i>et al.</i> , 2006)
TgN(hGFAP-Cre <sup>ERT2</sup> ) <sub>GCTF</sub>		(Hirrlinger <i>et al.</i> , 2006)
TgH(P2Y1 <sup>fl/fl</sup> ) <sub>P2Y1</sub>		(Leon <i>et al.</i> , 1999)
TgH(Gria1 <sup>fl/fl</sup> ) <sub>Gria1</sub>		(Fuchs <i>et al.</i> , 2007)
TgH(Rosa26-GCaMP3) <sub>GCaMP3</sub>		(Paukert <i>et al.</i> , 2014)
TgH(Rosa26-tdTomato) <sub>tdTomato</sub>		(Madisen <i>et al.</i> , 2010)

### 5.1.11. Hard- und Software

The depicted confocal or AxioScan images of this thesis were made with the Zeiss Software Zen (Zeiss). Images were then processed with ImageJ, Adobe Photoshop CS7, Adobe Illustrator CS7, Adobe InDesign CS7 (Adobe), Orbit Image Analysis (Idorsia Pharmaceuticals Ltd) and Zen lite (Zeiss).

Quantitative real time PCR results were analyzed with the CFX-Manager software 3.0 (BioRad). The results ( $\pm$  SD/SEM) were depicted as charts generated with GraphPad Prism 7 and processed with Adobe Illustrator. The analysis for statistical significance (e.g. unpaired t-test, two tailed), was also performed using GraphPad Prism 7.

Data base research was done with help of the internet service PubMed of the National Center for Biotechnology Information (NCBI; <http://www.ncbi.nlm.nih.gov/pubmed>).

#### 5.1.11.1. ImageJ plugin LRoi

LRoi is a custom made ImageJ plugin (<http://imagej.net/User:CIPMM-MolPhys>), designed to create uniform regions-of-interest (ROIs) with a specific width and height. LRoi creates a set of neighboring, non-overlapping ROIs, along a user-drawn guidance line (Fig. 7). It allows the user to specify a set of constraints, e.g. the number of ROIs and the ROI width. The ROI height is determined by dividing the length of the guidance line by the number of ROIs to create. For this reason, the exact length of the guidance line is also user-adjustable. ROIs are then created based on the user-defined constraints, taking the center-point of the guidance line as reference. This allows to create a set of ROIs with a defined and uniform area, facilitating analysis and comparability.

Additionally, LRoi provides the ability to create ROIs perpendicular to the user-drawn guidance line, to create two perpendiculars, cross shaped, sets of ROIs as well as ROI grids. LRoi was designed by Gebhard Stopper (Department of Molecular Physiology).

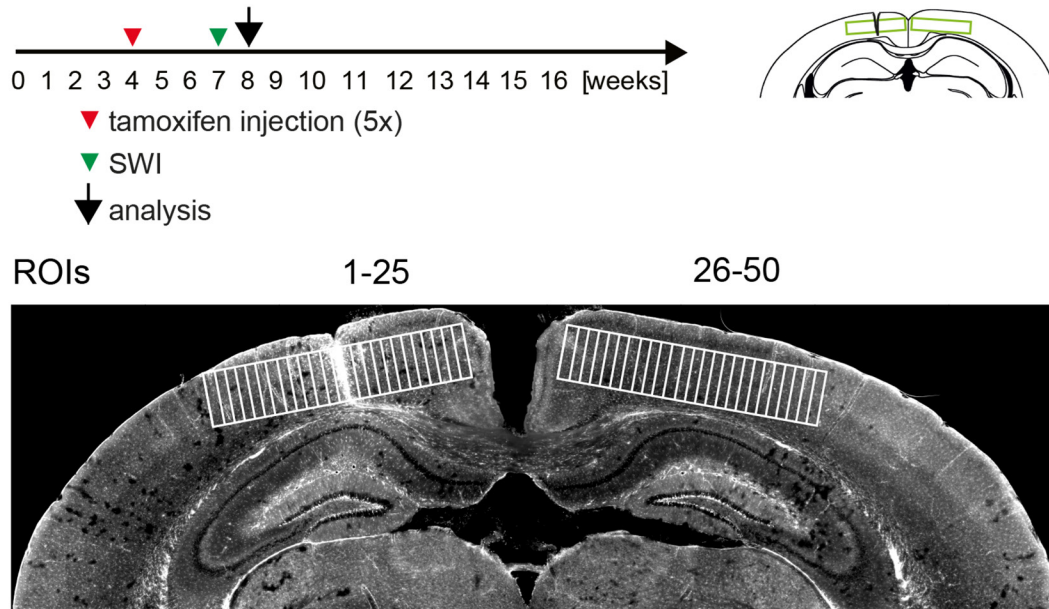


**Figure 7. Analysis of SWI experiments of cKO and control animals with the ImageJ plugin LRoi**

(A) For SWI experiments P2Y1 cKO and con mice were crossbred with two reporter strains (GCaMP3 and tdTomato) and injected with TAM at the age of four weeks and SWI was performed 21 dpi (days post injection). After seven days post lesion (dpl) mice were perfused, brains cut frontally and slices immunohistochemically stained and scanned with the epifluorescence microscope AxioScan.Z1 (Zeiss). Images were exported and further processed in ImageJ, with the custom made plugin LRoi. Regions of interest (ROIs, 1-25) were created perpendicular to the lesion and another 25 ROIs (26-50) were created on the contralateral side. In total these 25 ROIs analyzed an area of  $2500 \mu\text{m} \times 500 \mu\text{m} \times 5 \mu\text{m}$  (L x H x W). Via multi-measurement application LRoi quantifies the fluorescence intensities of all stainings at once. Data were converted in ‰ to simplify the numeric values.

#### 5.1.11.2. MATLAB-app MSparkles

MSparkles is a custom made MATLAB-app. It is specifically designed for the analysis of  $\text{Ca}^{2+}$  signals and provides two analysis modes, classical ROI analysis as well as morphological  $\text{Ca}^{2+}$ -transient analysis. The ROI analysis itself provides four modes of operation. Automatic ROI detection, based on temporal derivatives, ROI grid analysis, global ROI analysis and analysis of hand-drawn ROIs. For each ROI, the signal trace is computed as the mean value per time-step. Then, for each trace a peak detection and classification algorithm is executed, which returns the full width at half maximum

(FWHM) and signal-peaks (amplitude), grouped by their deviation from the mean ( $\mu$ ) in orders of one, two and three standard deviations (1 SD, 2SD and 3 SD). Signals of the 1 SD represent small signals, 2 SD medium sized signals and 3 SD large signals. The same signals of the respective groups are additionally analyzed for their signal duration.

In addition to classical ROI analysis, MSparkles offers morphological signal analysis. Here, the dynamic expansion and contraction of  $\text{Ca}^{2+}$  waves are computed using morphological operators such as opening, closing, erosion and dilation. Thereafter, the 2D time-dependent image space is treated as a 3D space in which groups of three dimensionally connected objects are computed. Each group represents a spatially and temporally isolated  $\text{Ca}^{2+}$  signal. For purposes of visualization, each signal is assigned a unique color, which is scaled in its intensity by the corresponding signal's peak value. Prior to any of these two analysis approaches, images are run through a pre-processing pipeline. This pipeline performs de-noising using the PURE-LET (Luisier *et al.*, 2010) algorithm, drift correction based on cross-correlation, and automatic background estimation and de-trended by fitting a low order polynomial in a least squares sense. The fitted polynomial is then used as approximation for basal  $\text{Ca}^{2+}$  level,  $F_0$ , which is then used for data normalization  $\Delta F/F_0$ . The app was programmed by Gebhard Stopper (Department of Molecular Physiology) (Fig. 8).

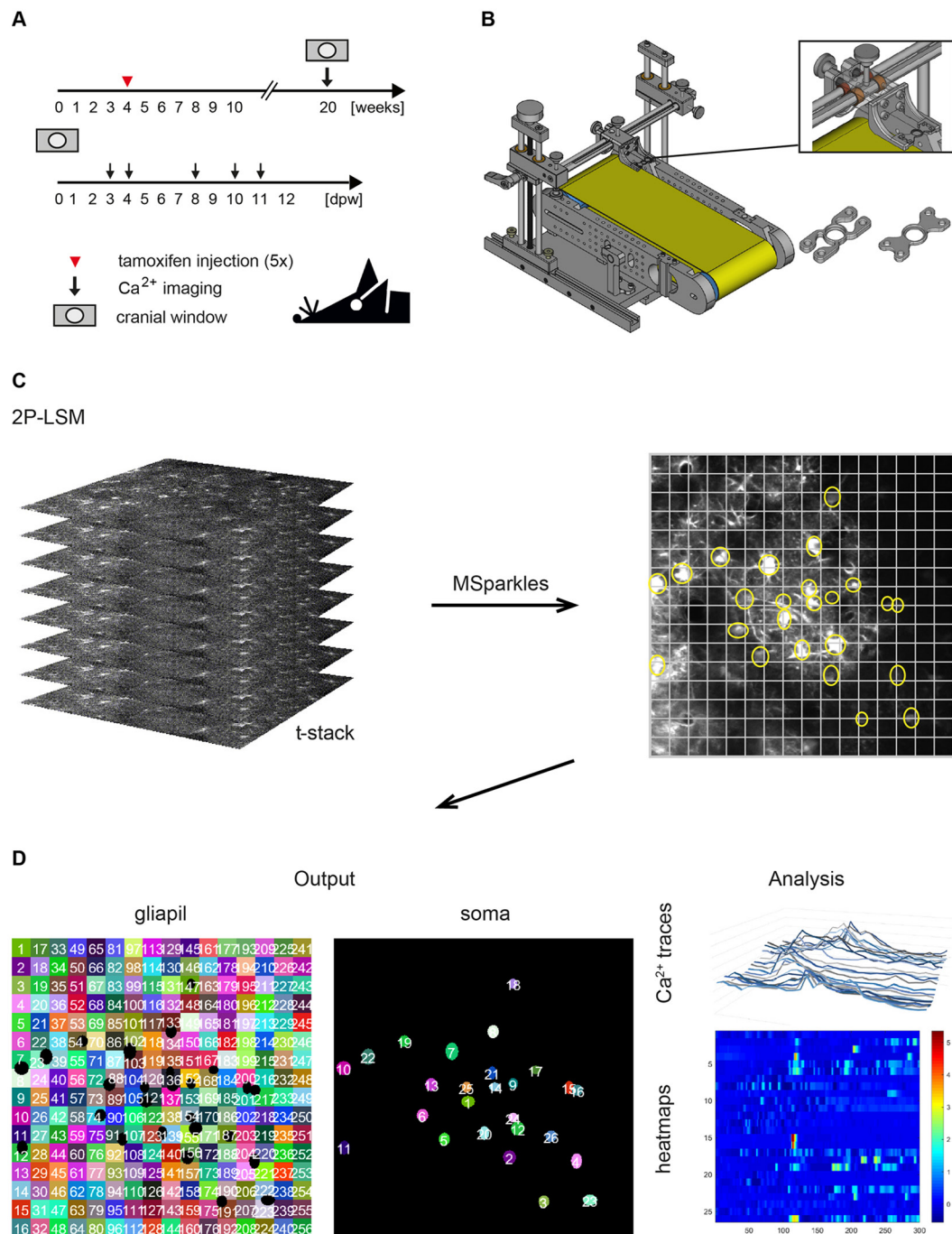


**Figure 8. 2P-LSM imaging of awake mice and data processing of Ca<sup>2+</sup> signals via MSparkles**

(A) Mice were injected with TAM at the age of four weeks and the cranial window surgery was performed at the age of 20 w. After three days of recovery mice were imaged under the 2P-LSM at day 3, 4, 8, 10 and 11. (B) Mice were able to move freely on a treadmill with only the head restrained. Therefore special custom-made head holders were designed and also the treadmill itself was designed by Gebhard Stopper (Department of Molecular Physiology). (C) After the imaging session data were

combined to a t-stack via ImageJ and denoised. Movies were uploaded in MSparkles (MATLAB-app) and ROIs around cell bodies were drawn manually (yellow circles). (D) Automatic ROI detection, ROI grid analysis, global ROI analysis and analysis of manually defined ROIs were processed by the software. Here we focused on the ROI grid analysis that analysis  $\text{Ca}^{2+}$  signals of fine processes (gliapil) and on manual ROIs detecting somatic  $\text{Ca}^{2+}$  signals. MSparkles generates also individual  $\text{Ca}^{2+}$  traces and compressed heatmaps of all signals.

#### 5.1.11.3. Orbit Image Analysis

The Orbit Image Analysis software is an open source software developed by Manuel Stritt, Isabelle Giraud and Ledia Lilaj at Actelion Pharmaceuticals Ltd, now Idorsia Pharmaceuticals (Seger *et al.*, 2016, Seger *et al.*, 2018). A major advantage of the software is its ability to process large image files having multiple scenes and containing several gigabytes of data. Orbit provides many built-in image processing algorithms and uses machine learning techniques for tissue quantification as well as object segmentation and classification. Therefore, the system needs to be trained for individual tasks. For the analysis of the tamoxifen-independent recombination, whole slices derived from the AxioScan.Z1 (Zeiss) were processed with Orbit. Individual models like an exclusion/inclusion model to distinguish tissue from background were created. To measure the fluorescence intensity of recombined cells and DAPI, an analysis, building up on the exclusion/inclusion model was used. Different models were created for the mouse lines expressing either the reporter tdTomato or GCaMP3. The output of Orbit after processing the slices is a fluorescence intensity ratio of the recombined reporter expressing cells and DAPI. The results of the fluorescence intensities were normalized to animals that express Cre<sup>ERT2</sup> and were injected with TAM for three consecutive days of the respective mouse lines (slc1a3 ct2/wt; gctf ct2/wt; cspg4 ct2/wt, pcet ct2/wt +TAM) and were further processed using GraphPad Prism7 and Adobe Illustrator 7.

#### 5.1.12. Mouse administration

For mouse administration, the database PyRAT (Python based Relational Animal Tracking) from Scionics Computer Innovation GmbH was used. PyRAT is a web based "Lab Animal Colony Management Software" which enables comprehensive and transparent handling of animal facility data. All relevant informations of the mouse and each mouse line are accessible (mouse number (earmark), date of birth, sex, genotype, pedigree, license and the current project).

### 5.1.13. Statistical analysis

The number of analyzed mice for each experiment is stated in the caption. All data were tested for normal distribution by the Shapiro-Wilk test and statistical analysis was chosen accordingly. For analysis of  $\text{Ca}^{2+}$  signals all data were tested for outliers by the ROUT-test. Identified outliers were removed from data sets.

Inter-group comparisons of qRT-PCR data were performed by two-tailed Student *t* test using the GraphPad Prism 7 software (GraphPad Software Inc.). Data are represented as means  $\pm$  SD or  $\pm$  SEM of natural replicates (mice) with \*  $P < 0.05$ ; \*\*  $P < 0.01$ ; \*\*\*  $P < 0.001$ ; \*\*\*\*  $P < 0.0001$ . Significant outliers were not included into calculations.

$\text{Ca}^{2+}$  data showed non-normal distribution and were therefore analyzed via Mann-Whitney test with GraphPad Prism 7. Data are represented as median (minimum 25 %, maximum 75 % percentile) of  $\text{Ca}^{2+}$  signals (amplitude/ duration) with \*  $P 0.01-0.05$ ; \*\*  $P 0.001-0.01$ ; \*\*\*  $P 0.0001-0.001$ ; \*\*\*\*  $P > 0.00001$ . Significant outliers were not included into calculations.

For analysis of the stab wound injury data AxioScan images (at least  $n = 6$ ) of frontal slices were analyzed with LRoi. At least three animals per condition ( $n=3-7$ ; cKO vs. con) were processed and further analysis was performed by two-way Anova. Data are represented as means  $\pm$  SD of measured fluorescence intensities (25 ROIs ipsilateral and contralateral) with \*  $P < 0.05$ ; \*\*  $P < 0.01$ ; \*\*\*  $P < 0.001$ ; \*\*\*\*  $P < 0.0001$ .

Data of the the Orbit image analysis showed non-normal distribution and were therefore analyzed by Mann-Whitney test. Data are represented as median  $\pm$  interquartile range of measured fluorescence intensities (ct2/wt/+TAM, wt/wt/ $\pm$ TAM; ct2/wt/-TAM; ct2/ct2/-TAM) with \*  $P 0.01-0.05$ ; \*\*  $P 0.001-0.01$ ; \*\*\*  $P 0.0001-0.001$ ; \*\*\*\*  $P > 0.00001$ .

### 5.1.14. Cell and receptor schemes of the introduction

Effigos AG (Leipzig) drew figure 1, 2 and 3 of the introductory part.

## **5.2. Methods**

### **5.2.1. Tail biopsies**

Mouse tail biopsies were taken at the age of three till four weeks by the animal caretakers of the animal facility at the Center for Integrative Physiology and Molecular Medicine (CIPMM) in Homburg. The extracted genomic DNA was used for genotyping of transgenic mice by PCR analysis. Until further usage the 0.5 cm mouse tail biopsies were stored at -20°C.

### **5.2.2. Mouse perfusion**

Mice were anesthetized with (ketamine/xylazine; 140 mg/kg and 10 mg/kg body weight). The abdomen was opened to reach the diaphragm. Intersection of the diaphragm led to a pulmonary collapse. The ribs were loosened to the collarbone and the thorax was removed. A vein canula was placed into the left ventricle and perfusion with a peristaltic pump was started. Mice were perfused with ice cold ACSF (artificial cerebrospinal fluid) or HBSS (Hank's balanced salt solution w/o  $\text{Ca}^{2+}$  or  $\text{Mg}^{2+}$ ; Sigma) for 2-3 min. Simultaneously, an incision of the vena cava superior was made to drain the blood from the body. After perfusion brains were dissected and used for further experiments. Brains were either directly separated in several brain regions, frozen on dry ice and stored at -80 °C until isolation of DNA, mRNA and protein, directly homogenized in 0.9 % NaCl for LC-HR-MS/MS analysis or postfixed over night in 4 % paraformaldehyde (PFA) in PBS for vibratome sections. For pharmacokinetic analysis blood was withdrawn from the right auricle (400–600 µl) before perfusion and centrifuged at 3000 min<sup>-1</sup> for 10 min to obtain the serum. Samples were kept in light-protected 2 ml tubes at -80 °C till further analysis.

### **5.2.3. Tamoxifen treatment**

Tamoxifen (TAM) was dissolved in Miglyol (medium-chain triglycerides, Caesar & Loretz) at concentration of 10 mg/ml, aliquoted and stored at 4°C. The intraperitoneal application of TAM was done by the animal caretakers of the CIPMM. Mice were either injected once a day at the age of four weeks for one, two, three or five consecutive days or at different intervals: 3x TAM all 8 h or all 48 h. The daily TAM volume was dependent on the weight of each mouse (100 mg/kg body weight). Mice were analyzed

8 h and 48 h post injection (hpi) or 21 d, 200 d after the first injection (dpi). Pharmacokinetic analysis was performed on C57BL/6NRj mice that received a single dose of TAM for one or three consecutive days. Brain and serum samples were collected at 1 hpi, 4 hpi, 8 hpi, 24 hpi, 2 dpi, 5 dpi, 7 dpi, 14 dpi, 21 dpi or after 3 d, 4 d, 7 d, 21 d post injection, respectively (Jahn, Kasakow *et al.*, 2018).

### 5.3. Sample preparation for LC-HR-MS/MS analysis

C57BL/6NRj mice were injected with TAM as described before and samples of serum and brain homogenates were isolated and further processed by LC-HR-MS/MS (Fig. 9).

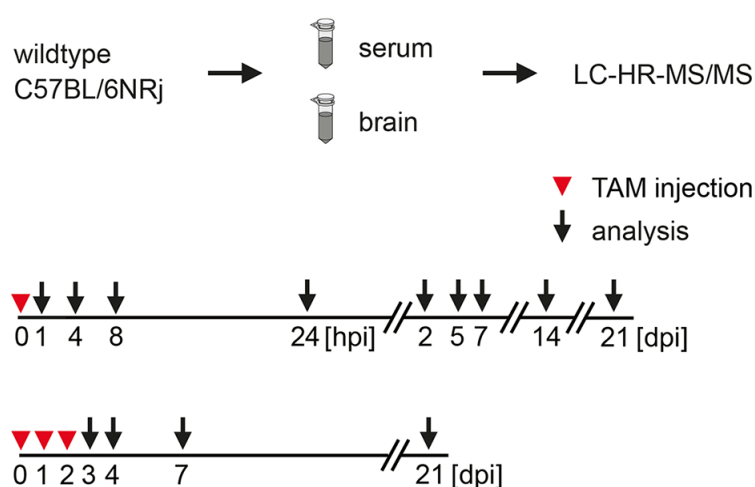


**Figure 9. Treatment protocols for LC-HR-MS/MS analysis**

(A) Samples (serum/brain) of treated C57BL/6NRj wild type (wt) mice were collected and were analyzed by LC-HR-MS/MS. (B, C) Mice were injected at an age of 28 d with TAM (100 mg/kg) once (B) or for three consecutive days (C, red triangles). Brain and blood samples were collected at different time points (indicated with black arrows). After processing, samples were analyzed by LC-HR-MS/MS for TAM and its derivatives NDM-TAM, 4-OH-TAM and END.

### 5.4. LC-HR-MS/MS analysis

Homogenized brain and serum samples were processed for LC-HR-MS/MS as established before (Helfer *et al.*, 2017): brain or serum samples were mixed with an internal standard (risperidone) and zinc sulfate ( $\text{ZnSO}_4$ ) solution. Samples were vortexed, stored shortly at  $-20^\circ\text{C}$  and subsequently centrifuged. The supernatant was transferred into brown glass vials for LC-HR-MS/MS analysis. The extracts were analyzed using an Accela LC system, controlled by the Aria software and coupled to a



high resolution Q-Exactive system. Mass calibration was performed according to the manufacturer's recommendations every 72 h using external mass calibration. Quantifications were performed with homogenized brain or serum sample calibrators spiked with defined concentrations of TAM, as well as its metabolites NDM-TAM, 4-OH-TAM and END. The spiked concentrations ranked between 0.1 and 1,000 ng/ml and were divided into three separate calibration ranges (five calibrators each) from 0.1 to 10, 10 to 100, and 100 to 1,000 ng/ml with equidistant concentrations, respectively. The measurements were performed by Andreas Helfer and Julian Michely (Department of Experimental and Clinical Pharmacology and Toxicology, Prof. Dr. Hans H. Maurer University of Saarland, Homburg)

#### **5.4.1. Isolation and analysis of genomic DNA**

##### **5.4.1.1. Isolation of genomic DNA from mouse tails**

The REDExtract-N-Amp<sup>TM</sup> Tissue PCR Kit (Sigma-Aldrich) was used to extract genomic DNA from mouse tail biopsies. Initially the working solution was prepared by mixing tissue preparation solution and extraction solution in a ratio 4:1. The mouse tail biopsies (0.5 cm) were incubated with 62.5 µl of the working solution for 10 min at room temperature (RT) under shaking conditions (Thermomixer comfort, Eppendorf, 700 min<sup>-1</sup>). In the next step the samples were heated to 95°C for 20 min in the water bath. After adding the neutralization solution B, the extract is ready for PCR. The extracted DNA can be used directly or stored at 4°C for a longer period.

##### **5.4.1.2. Polymerase chain reaction**

The polymerase chain reaction (PCR) is based on specific DNA amplification by certain thermal cycling steps (Mullis and Faloona, 1987). The reactions for genotyping were executed in 96-well PCR reaction tubes in a peqSTAR Thermo Cycler (peqlab Biotechnologie GMBH).

##### **5.4.1.3. Agarose gel electrophoreses**

For DNA separation, 1.5-2.0 % agarose gels, stained with ethidium bromide (0.015 %), were documented with the Quantum gel documentation system (peqlab Biotechnologie GMBH).

## **5.4.2. Immunohistochemical analysis**

### **5.4.2.1. Preparation of vibratome sections**

For preparation of vibratome sections a Leica VT1000S Vibratome (Leica) was used. The fixed brains (4 % PFA) were cut sagittally or frontally in 40  $\mu$ m sections and transferred in 24-well culture plates with 1x PBS. After preparation, the slices were stored at 4°C or immediately processed for immunohistochemical stainings.

### **5.4.2.2. Immunohistochemical staining of vibratome sections**

Slices were treated according to the standard protocol as previously described (Huang *et al.*, 2014). Vibratome sections were simultaneously permeabilized and blocked for 1 h at RT with the permeabilization-and blocking buffer. Primary antibodies were diluted (primary antibody solution) and incubated over night at 4°C. The next day sections were rinsed 3 x 10 min in 1 x PBS and incubated for 2 h at RT with secondary antibodies (diluted in secondary antibody solution). Subsequently, sections were rinsed again 3 x 10 min in 1x PBS. Additionally, DAPI (f.c. 1  $\mu$ g/ml), a specific dye for nucleic acids, was added to the secondary antibody incubation. Finally, slices were transferred into a water bath and mounted in Aquapoly mount (Polysciences) or Immu-Mount (Thermo Scientific).

## **5.4.3. Processing of DNA and RNA samples**

### **5.4.3.1. Isolation of DNA and RNA from mouse tissue or cells**

For isolation of DNA and RNA the AllPrep DNA/RNA Mini Kit or the AllPrep DNA/RNA Micro Kit from Qiagen were used (Qiagen). Isolation of genomic DNA was done with the Invisorb Spin Tissue Mini Kit (Stratec Biomedical AG). AllPrep DNA/RNA Mini and Micro Kits were designed to purify genomic DNA and total RNA simultaneously from tissue samples or MACS isolated cells, respectively. The prepared samples from mouse brain, including brainstem (bs), cerebellum (cb), cortex (ctx) and hippocampus (hc), were stored at -80°C until homogenization (Precellys 24, peqlab Biotechnologie GmbH). The frozen tissue was transferred into a Precellys tube filled with an appropriate volume sucrose buffer (600  $\mu$ l for bs, cb and ctx; 300  $\mu$ l for hc) and immediately placed into the Precellys 24. The tissue was homogenized for 2 x 10 s at 5500 min<sup>-1</sup> with 10 s pause in between and then centrifuged for a few seconds at 10.000 min<sup>-1</sup> to reduce the foam. MACS samples were treated equally but

homogenized in only 100 µl sucrose buffer. All homogenates were further processed with the appropriate kits following manufacturers' instructions. Purified DNA and RNA were stored at -20°C until further processing. DNA from the optic nerve was isolated with the Invisorb Spin Tissue Mini Kit (Invitex) by following manufacturers' instructions. DNA was stored at -20 °C until further analysis.

#### **5.4.3.2. Determination of DNA and RNA concentrations**

DNA and RNA quantifications were either performed with a photometer from Eppendorf or with the NanoPhotometer from DeNovix. Due to the absorbance maxima, nucleic acids were measured by 260 nm and proteins by 280 nm. For working purposes the following OD<sub>260</sub>-concentration relations were used: 1 OD at 260 nm for double stranded DNA = 50 ng/µl of ds DNA, 1 OD at 260 nm for RNA molecules = 40 ng/µl of RNA. DNA and RNA samples were diluted 1:50 in either EB buffer or RNase free water and transferred into a UV cuvette (UVette, Eppendorf). For the NanoPhotometer 1 µl of the undiluted sample was applied. Validation of the purity of the DNA and RNA samples was determined by calculating the ratio of absorbances at 260 nm and 280 nm.  $A_{260}/A_{280}$  ratios above 1.8 for DNA and 2.0 for RNA indicate pure samples, while lower ratio values indicate protein contaminations.

#### **5.4.3.3. RNA precipitation**

For RNA precipitation 500 to 1000 ng RNA were diluted in 50 µl dH<sub>2</sub>O, mixed with 1 µl Pellet paint and vortexed thoroughly. Next, 25 µl of 7.5 M NH<sub>4</sub>Ac were added to the reaction tube and mixed by vortexing. Ethanol (180 µl of 100 %) was added to each sample and vortexed. The reaction tubes were centrifuged for 15 min at 14.000 min<sup>-1</sup> (RT). After centrifugation the supernatant was removed by a vacuum pump (Integra Biosciences), the pellet was washed with ethanol (70 %) and centrifuged again for 5 min at 14.000 min<sup>-1</sup>. After the washing step, pellets were dried at RT for 10-15 min, resolved in 12 µl RNase free water and stored on ice for another 10 min.

#### **5.4.3.4. First strand cDNA synthesis**

For the cDNA synthesis of 1000 ng RNA a mixture of oligo dT nucleotides and random hexamer nucleotides was used. The reaction was performed in a peqSTAR Thermocycler (peqlab). RNA from the precipitation step was dissolved in RNase-free water, transferred into 96-well PCR reaction tubes and incubated at 65 °C. Subsequently, the master mix was added to the RNA template, containing Omniscript

reverse transcriptase, dNTPs, buffer RT and RNase inhibitor (Promega). Next, the RNA template was incubated at 37 °C with the master mix. The setup of a single PCR reaction is stated in table 8. The amplified cDNA was directly diluted 1:10 with RNase free water and stored at -20 °C. For quantitative real time PCR the cDNA solution was further diluted 1:3.3.

**Table 8. Setup for reverse transcriptase PCR**

Components	Volume [μl]
RNA in RNase-free water	12.2
Incubation 5 min by 65° C	
dt-Mix Primer [0.6 pmol/μl]	0.8
N9 Primer [120 pmol/μl]	1.0
Buffer RT, 10x	2.0
RNase Inhibitor [10 U/μl]	1.0
dNTPs (5 M each)	2.0
Omniscript 200 U/μl	1.0
Incubation 1 h by 37° C	

#### 5.4.3.5. Real-time qRT-PCR for mRNA expression

For quantification of PCR products, fluorescent dyes are used (EvaGreen, Axon) that intercalate in double-stranded DNA. The fluorescence increases proportional to the amount of double stranded DNA. A reliable quantification is only possible during the log/exponential phase of the PCR when the reporter fluorescence is greater than the minimal detection level. The starting point of this exponential phase is defined by the  $C_T$  value (Cycle Threshold). The  $C_T$  value is inversely proportional to the amount of template, meaning the more template the lower the  $C_T$  value. The evaluation was done with the CFX-Manager software 3.0 (BioRad) and Excel 2013.

To determine the level of expression of a gene of interest the  $\Delta\Delta C_T$  method is used. In a first step, the  $C_T$  value of a reference gene (b-actin) is subtracted of the  $C_T$  value of the gene of interest resulting in the  $\Delta C_T$  value. Hereby, eventually different amounts of starting materials are considered and corrected. Subsequently, the anti-logarithm of calculated  $\Delta C_T$  values was taken. The values of inducible cKO animals were normalized to the mean value of control animals. The results ( $\pm$  SD/SEM) were processed with GraphPad Prism 7 and analyzed for statistical significance (unpaired t-test, two-tailed). The reactions took place in 96-well plates (Axon) in the CFX96 Real-Time PCR Detection System (BioRad). All samples were carried out in triplicates or

quadruplets. The setup of a single reaction and the temperature program are given in table 9 and 10.

**Table 9. Components for qRT-PCR for gene expression and DNA recombination**

Component	Volume [ $\mu$ l]
cDNA/DNA	4.0
5x Master Mix Hot Start Taq	2.0
forward primer	0.1
reverse primer	0.1
dH <sub>2</sub> O	3.8

**Table 10. qRT-PCR program for the light cycler**

Stage/repetitions	Temperature [ $^{\circ}$ C]	Time [min]
1/1	50	2
2/1	95	15
3/42	95	0:15
3/42 $\rightarrow$ data collection	60	1

#### 5.4.3.6. Real-time qRT-PCR for DNA recombination

The qRT-PCR technique for DNA recombination is similar to the analysis of mRNA expression with slight variations. The primers were positioned in intron stretches to avoid mRNA contamination and the temperature of the PCR program was adapted to DNA as template. The samples of brainstem, cerebellum, cortex and hippocampus were diluted to 10 ng/ $\mu$ l. Samples of the optic nerve were, based on the lower concentration of isolated DNA, diluted to 5 ng/ $\mu$ l. The evaluation was done with the CFX-Manager software 3.0 (BioRad) and Excel 2013. For normalization, the endogene b-actin was used. The anti-logarithm of calculated  $\Delta C_T$  values was taken and the values of inducible cKO animals were normalized to the mean value of control animals or for the TAM study to the mean value of animals that received five time's TAM. The results ( $\pm$  SD/SEM) were processed with GraphPad Prism 7 and analyzed for statistically significance (unpaired t-test, two-tailed). The reactions took place in 96-well plates (Axon) in the CFX96 Real-Time PCR Detection System (BioRad). All samples were carried out in triplicates/quadruplets. For the setup of a single reaction refer to table 10. The temperature programmes are depicted in table 11.

**Table 11. qRT-PCR program of tdTomato, *p2ry1*, *grla1* and GCaMP3 for the light cycl**

Stage/repetitions	Temperature [°C]	Time [min]
1/1	95	10
2/1	95	0:15
3/45	60-62	0:25
3/45→ data collection	72	0:42

**5.4.3.7. Determination of PCR efficiency**

PCR amplification efficiency is the rate, which defines the amount of amplicons generated per cycle in the exponential phase of the PCR amplification. An efficiency of 100 % corresponds roughly to a doubling in amplicon quantity per cycle. To determine the PCR efficiency a dilution series of DNA (undiluted, 1:10; 1:100; 1:1000) was performed to generate a standard curve of the target and the endogene (Fig. 10 A-C). After running this PCR the threshold cycles were plotted against the logarithm of dilution in relative units. The slope of the standard curve is used to determine the exponential amplification (A) and the PCR efficiency (E) by the following formula:

$$A = 10^{(-1/\text{slope})}$$

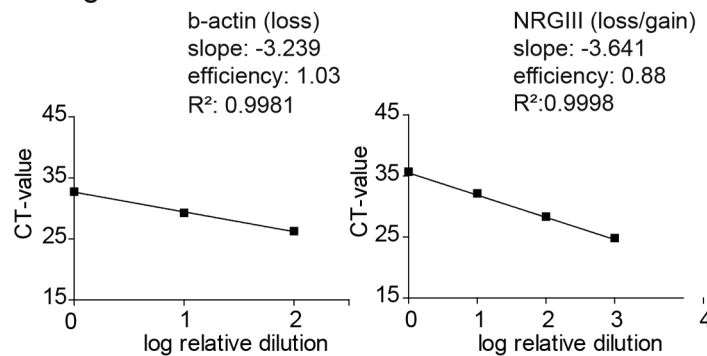
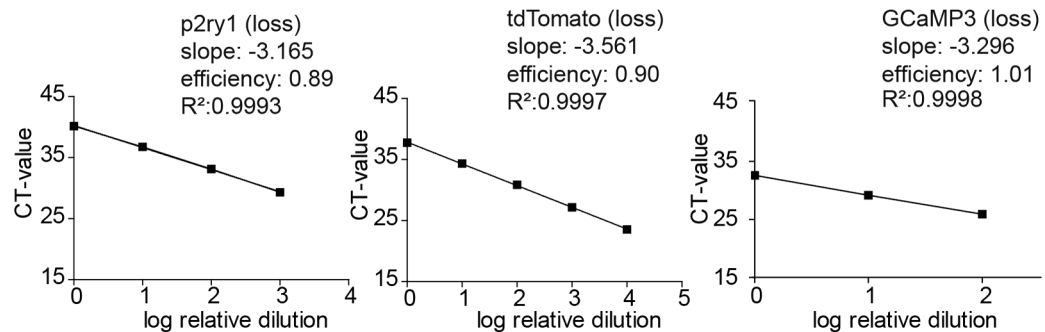
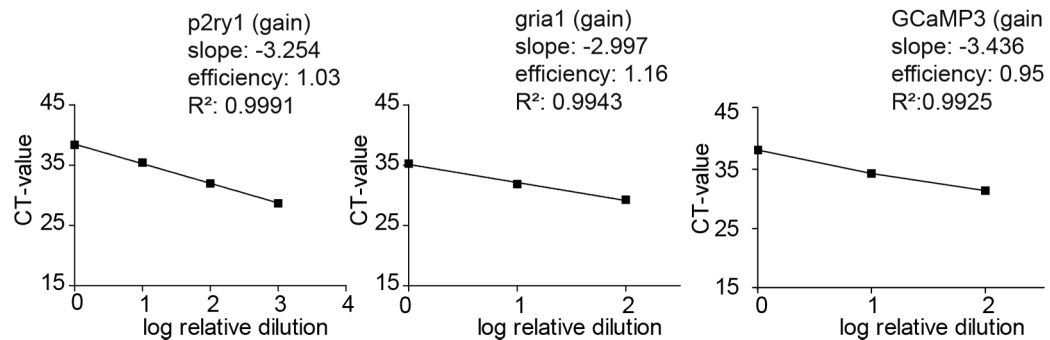
$$E = [10^{(-1/\text{slope})}] - 1$$

Slope = -3.32 → 100% efficiency

Slopes more negative than -3.32 → < 100 % efficiency

To achieve reliable quantitative data it is essential that the efficiency of the target and of the endogene amplification is almost identical. For each PCR reaction one endogene was analyzed to minimize the production of incorrect gene expression data based on different amounts of input material (DNA). But to address questions concerning the absolute amounts of *p2ry1*, *grla1*, GCaMP3 and tdTomato it is absolutely essential to determine PCR efficiencies. In conclusion, PCR efficiencies were determined to confirm the stable endogene performance and to consider possible differences in the PCR performances of the investigated target genes for quantitative analysis.

An efficiency of 1.03 was determined for the endogene b-actin and 0.88 for the endogene NrgIII. The PCR results of the target genes revealed recombination efficiencies of 0.89/1.03, 1.16, 1.01/0.95 and 0.90, respectively. These results were used to evaluate the recombination efficiencies of the investigated mouse lines and allow now the direct comparison of *p2ry1* (loss/gain), *grla1* (gain), GCaMP3 (loss/gain) and tdTomato (loss) (Jahn, Kasakow *et al.*, 2018).

**A****endogenes****B****loss of function****C****gain of function****Figure 10. Primer efficiencies to amplify various gene loci**

(A) Efficiencies were determined for b-actin (loss), NRGIII (loss/gain), tdTomato (loss), *p2ry1* (loss), GCaMP3 (loss) and *p2ry1* (gain), *grla1* (gain) and GCaMP3 (gain). PCRs were run on undiluted, 1:10, 1:100 and 1:1000 diluted samples. Threshold cycles of the dilution were determined and plotted inversely versus the logarithm of the dilution. Data were fitted with a linear regression. The slope was used to determine exponential amplification  $10^{(-1/\text{slope})}$ , efficiency  $[10^{(-1/\text{slope})}] - 1$  of the PCRs and the  $R^2$  value as indicated. Modified after (Jahn, Kasakow *et al.*, 2018).

## **5.5. Cell sorting**

### **5.5.1. Magnetic activated cell sorting (MACS)**

Mice were perfused with cold HBSS for blood removal. Brains were dissected into cortex and cerebellum and chopped into small tissue pieces. The tissue was transferred into Miltenyi C-Tubes and enzyme mix 1 and 2 were added. Dissociation of the tissue was done by the GentleMACS octo dissociator with heaters using the inbuilt programme 37C\_ABDK\_01. The tissue was dissociated to a single cell suspension using a 1000 µl pipette. The cell homogenate was passed through a strainer (70 µm) to remove tissue clots and centrifuged at 300 g for 10 min. The supernatant was discarded and cells were dissolved in 1x D-PBS plus debris removal solution and overlaid with 1x D-PBS. The gradient was centrifuged at 3000 g for 10 min without break. Subsequently, three phases were formed and the upper two were removed completely. Cells were washed with D-PBS and centrifuged (1000 g, 10 min). The supernatant was removed completely and the cell pellet dissolved in 1x D-PBS with 0.5 % BSA. Cells were incubated for 10 min with the FcR blocking reagent. Next, the Anti-ACSA-2 MicroBeads were added for 15 min. After the incubation, cells were washed with 1x D-PBS/BSA buffer and centrifuged (300 g, 10 min). The pellet was dissolved in 500 µl 1x D-PBS/BSA buffer and applied to a MACS MS-column placed in a magnetic field of the MACS separator. The flow through contained all unlabeled cells. The column was washed three times with 1x D-PBS/BSA buffer and removed from the separator for final elution of the labeled cells. The cells were directly eluted into reaction tubes and centrifuged at 500 g for 10 min. The supernatant was discarded and the cell pellet was immediately frozen at -80 °C until further processing. For next generation sequencing (NGS) cell pellets were dissolved in 300 µl RLT buffer plus from the AllPrep DNA/RNA micro kit (Qiagen) and then frozen at -80 °C.

## **5.6. Injury models**

### **5.6.1. Anesthesia and mouse preparation for injury models**

For all surgeries animals were anesthetized with 5 % isoflurane, 47.5 % O<sub>2</sub>, 47.5 % N<sub>2</sub>O (Harvard Apparatus equipment) and fixed with earbars on a heating plate to keep the body temperature at 37 °C. After sedation, the isoflurane was reduced to 2 % and the flow of O<sub>2</sub> and N<sub>2</sub>O to 0.4 l/min (0.8 l/min in total). Eyes were covered with



Bepanthen ointment to protect them from exsiccosis. After the surgery all animals received painkiller for three consecutive days (dexamethasone hydrochlorid 0.2 mg/kg body weight and/or buprenorphine hydrochloride; 0.09 µg/30 g body weight).

For imaging sessions, mice were equally anesthetized as for the surgery. For awake imaging, animals were only slightly anesthetized with 0.5 % isoflurane to fix them in the custom-made treadmill.

### **5.6.2. Cortical stab wound injury**

The scalp was opened along the rostro-caudal axis and the craniotomy was performed with a hand drill (0.7 mm) above the somatosensory cortex (1.5 mm laterally and 2 mm caudally, referring to bregma as 0/0). The center of the craniotomy was stabbed with a surgical scalpel (#11, B/Braun), parallel to the midline and inserted to a depth of 1 mm from the cortical surface. Occuring bleedings were stopped by sponges (Gelastyp, Sanofi Aventis). Afterwards the wound was sutured and animals could recover. The surgery was performed at the age of eight weeks and mice were analyzed seven days post lesion (7 dpl).

### **5.6.3. Cranial window**

The head was cleaned with ethanol and the scalp was opened along the rostro-caudal axis. The wound was disinfected with ethanol (70 %) and Betaisodona solution. The skull was cleaned from remaining hairs and tissue with cortex buffer. At the right hemisphere a 3-4 mm circle was performed with a hand drill (0.7 mm) at the level of the somatosensory cortex (lateral =1.5 mm and longitudinal =2 mm from the bregma). In between drilling bone particles were removed with cortex buffer and bleedings were stopped with sponges (Gelastyp, Sanofi Aventis) and cotton swabs. The skull was thinned until the bone could be removed easily with a forceps (5 SF, 5S, Fine Science Tools). The dura was left intact and kept moist with cortex buffer. A cover slip (5 mm) was fixed over the hole by super glue (Loctite, Henkel). In the next step, a custom-made head holder (5 mm diameter) was fixed to the skull by dental cement (RelyX, 3M ESPE). The surgery was performed at the age of 15-20 weeks and mice were imaged by 2P-LSM at different days post cranial window surgery (dpw).

#### 5.6.4. Microscopy

##### 5.6.4.1. Confocal laser-scanning microscopy

Confocal images were performed at the LSM 710 from Zeiss (Carl Zeiss AG, Jena) with a Plan-Apochromat 40x/1.4 Oil DIC (UV) VIS-IR M27 objective. Fluorescent proteins were excited with the Lasos argon-ion lasers (454 nm, 514 nm) or helium-neon lasers (543 nm, 633 nm). The images were acquired using the software Zen (Zeiss) and processed with ImageJ (Maximum intensity projections (MIP)).

##### 5.6.4.2. Digital slide scanner: AxioScan.Z1

The digital slice scanner AxioScan.Z1 (Zeiss) is an automated microscopy system optimized for many and large tissue sections. Fixed tissue sections are recorded by bright-field and fluorescence illumination. The Axio Scan.Z1 acts as an epifluorescence microscope, using an HBO lamp (HXP 120 V, LEJ). For this purpose, only the reflected fluorescence light is used. A Plan-Apochromat 10x/0.45 objective is applied for coarse focus map on the slides. A Plan-Apochromat 20x/0.8 objective for the fine focus map, with appropriate emission and excitation filters, was applied and images were recorded in 8 µm thick stacks and a variance intensity projection was prepared for analysis.

##### 5.6.4.3. *In vivo* two-photon laser-scanning microscopy (2P-LSM)

*In vivo* 2P-LSM was performed by Laura Stopper (Department of Molecular Physiology) using a custom-built microscope equipped with a 20x water-immersion objective (1.0 NA; Zeiss). Scanning and image acquisition were controlled using custom-written software (ScanImage, (Pologruto *et al.*, 2003)). To minimize photo damage, the excitation laser intensity was kept at a minimum (66-81 mW) for a sufficient signal-to-noise ratio. Laser wavelength was set at 910 nm (Chameleon Ultra II, Ti: Sapphire Laser, Coherent). The emitted light was detected by a photomultiplier tube (R6357, Hamamatsu). The chosen ROI covered 15-25 astrocytes and was located in the somatosensory cortex. Equal imaging settings were selected for all experiments (512x512 px, framerate 0.9-1.5 Hz, pixel time 5.7 µs).

##### Ca<sup>2+</sup> imaging in anesthetized mice

One week after the cranial window surgery animals were fixed with the metal holder on a custom-made head restrainer. Before the imaging session was started, animals were injected with Texas Red-dextran (70 kDa, Invitrogen) via tail vein injection to visualize

blood vessels in the brain. The marked blood vessels served as a map to image the same region of interest (ROI) over several sessions. The astrocytes were labeled with the genetically encoded  $\text{Ca}^{2+}$  indicator GCaMP3. The same image was recorded over 5-10 min to investigate  $\text{Ca}^{2+}$  changes during this period. The total duration of one imaging session lasted 30-60 min. After each session animals were kept on a heating pad until they recovered. All mice were injected with TAM at an age of four weeks and cranial window surgery was performed at an age between 16-20 weeks (Fig 11 A). Mice were imaged at day 3, 4, 8, 10 and 11 post cranial window (Fig 11 B).

#### $\text{Ca}^{2+}$ imaging in awake mice

For  $\text{Ca}^{2+}$  imaging of awake animals mice were habituated before the imaging session. The habituation procedure was adapted from (Guo *et al.*, 2014) and (Kislin *et al.*, 2014). In the first step of habituation animals were accustomed to the scientist (Laura Stopper, Department of Molecular Physiology) therefore, they run freely on the hand for 10 min every day until they behave normal (max 7-10 d). In a second step animals were head restricted but had the opportunity to run freely on a custom-made treadmill for 10-15 min or were kept in a tube for 10-15 min (max 7 d). Only normal behaving animals were used for imaging sessions. Animals were fixed with the head holder to the treadmill, a region of interest was selected in the field of view and anesthesia was removed. The same image was recorded over 5-10 min to investigate the  $\text{Ca}^{2+}$  changes during this period. After 10-20 min animals were released in their cage. All mice were injected with TAM at an age of four weeks and cranial window surgery was performed at an age between 16-20 weeks (Fig 11 A). Mice were imaged at day 4, 8, 10 and 11 post cranial window (Fig 11 C).

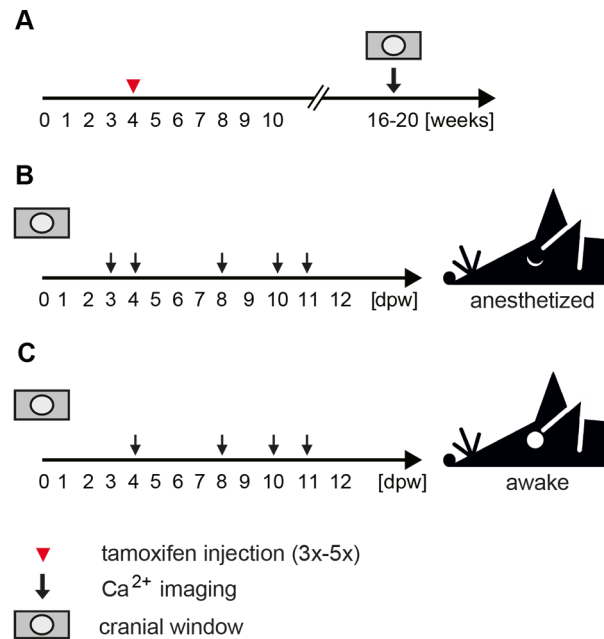


**Figure 11. TAM injection protocol, surgery and imaging preparation**

(A) Mice were injected at an age of four weeks with TAM for five consecutive days. Cranial window surgery was performed at an age between 16 - 20 weeks (grey rectangle) and subsequent imaging sessions are indicated by black arrows (days post cranial window (dpw)). (B) *In vivo* imaging anesthetized: Imaging was performed under 2 % isoflurane. Mice were imaged at day 3, 4, 8, 10 and 11 post cranial window. (C) *In vivo* imaging awake: No anesthesia was used at the time of recording and mice were allowed to move freely on a treadmill. Mice were imaged at day 4, 8, 10 and 11 post cranial window.

## 5.7. Next generation sequencing (NGS)

To analyze the mRNA expression profile of P2Y1R cKO and control mice (n=5), next generation sequencing (NGS) was performed. Mice were perfused with HBSS and astrocytes were isolated via MACS as described before. Astrocytes of the cortex and the cerebellum were dissolved in RLT buffer plus (Qiagen) and directly frozen at  $-80^{\circ}\text{C}$ . NGS was performed at the Department of Psychiatry in collaboration with Prof. Dr. Moritz Rossner (Molecular Neurobiology) at the Ludwig Maximilians University, Munich, Germany.

RNA of cortical and cerebellar samples was extracted, cDNA synthesized and library prepared. Equal quantities of single samples were pooled and sequenced on an Illumina Sequencer. For transcriptome data analysis, reads were validated for sequence- quality and -repeats. Low quality bases and short reads were removed from further analysis. The reads were mapped to *Mus musculus* genome (mm10) and

differentially expressed genes (DEGs) were determined. Genes with at least one log<sub>2</sub>-fold change and adjusted p-value of  $\leq 0.005$  were considered as differentially expressed.

#### **5.7.1. Laboratory and animal handling**

Experimental mice were kept in the animal facility of the Institute of Clinical and Experimental Surgery or in the animal facility of the CIPMM in Homburg. This study was carried out in strict accordance with the recommendations of European and German guidelines for the welfare of experimental animals. Animal experiments were approved by the Saarland state's "Landesamt für Gesundheit und Verbraucherschutz" in Saarbrücken/Germany (animal license number: 72/2010, 34/2016, 36/2016).

## 6. RESULTS

### 6.1. Refined protocols of tamoxifen application for DNA recombination in mouse astrocytes

Induction of DNA recombination in genetically modified mouse lines by application of tamoxifen (TAM) is a favored tool in many labs. The exact time course of TAM metabolism in the liver and the induction of recombination in the brain is not well defined. The concentration of TAM and its metabolites was therefore investigated in a time dependent manner in serum and brain, as well as the influence of varying TAM doses on the DNA recombination efficiency (Jahn, Kasakow *et al.*, 2018).

#### 6.1.1. Fast uptake and clearance of tamoxifen and its bioactive metabolite 4-OH-TAM

To analyze the contribution and time course of TAM and its metabolites N-desmethyl-tamoxifen (NDM-TAM), 4-hydroxytamoxifen (4-OH-TAM) and endoxifen (END) for cell type-specific recombination their pharmacokinetic profile was determined by liquid chromatography-high resolution-mass spectrometry (LC-HR-MS/MS). After a single intraperitoneal injection of TAM, metabolite concentrations were determined in serum and brain at 1, 4, 8, 24 h and 2, 5, 7, 14 and 21 d post injection (pi). In addition, the concentrations were determined after injection of TAM for three consecutive days. Days post injection (dpi) always means time after the first injection, not time after the end of the injection period.

TAM and 4-OH-TAM showed a fast partitioning in the brain reaching maximal levels already at 8 hpi. The metabolite 4-OH-TAM entered the brain equally fast, although it required prior enzymatic hydroxylation of TAM in the liver by cytochrome P450 cyclooxygenases (Fig. 12 A, B). Corresponding TAM samples from the serum displayed profound variability, which was less pronounced for 4-OH-TAM (Fig. 13 B). We attributed this variability to variations of tissue and blood absorption after individual intraperitoneal injections. Both, TAM and 4-OH-TAM were efficiently cleared from brain and blood within 7 dpi (Fig. 12 A, B, Fig. 13 A, B, Table 12). In the brain, TAM was approximately six times enriched in comparison to 4-OH-TAM at 8 hpi as well as at 48 hpi (Fig. 12 A, B). The other two metabolites, NDM-TAM and END, required three to five times longer for reaching their concentration peaks at 24 hpi (Fig. 12C, D,

Fig. 13 C, D, Table 12). Nevertheless, both were cleared completely at 7 dpi (Fig. 12 C, D, Fig. 13 C, D). As expected from its biophysical properties (i.e. also being highly lipophilic), TAM displayed the highest concentration in the brain followed by NDM-TAM and 4-OH-TAM. END showed the lowest concentration (Fig. 12, Fig. 13, Table 12).

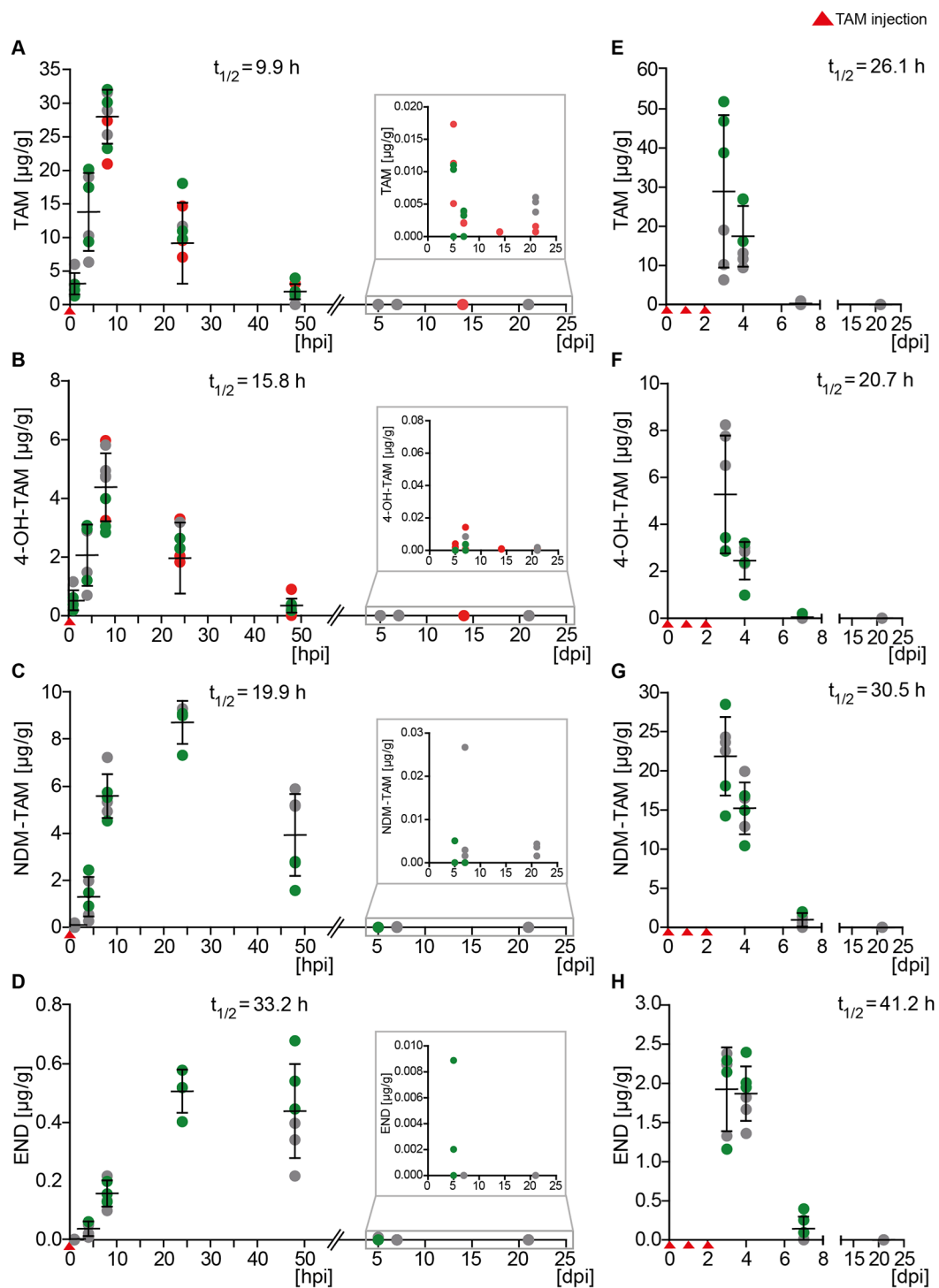
Several consecutive injections of TAM are used frequently to achieve a higher recombination efficiency of floxed alleles as well as for lineage studies. Therefore, we injected TAM for three consecutive days and determined the concentrations of TAM and its metabolites at four different time points focusing at the time required for clearance (Fig. 12 E-H). All four TAM derivatives showed the highest concentration 24 h after the last injection (3 dpi). While TAM and 4-OH-TAM were only slightly enriched, the two metabolites NDM-TAM and END were about 5-fold enriched in comparison to a single injection (Fig. 12 E-H, Table 12). Consecutive injections increased the level of biological active derivatives in the brain and enhance the recombination efficiency.

We determined clearance rates ( $t_{1/2}$ ) from the brain at 9.9 h, 15.8 h, 19.9 h and 33.2 h for TAM, 4-OH-TAM, NMD-TAM and END after one injection, respectively. The clearance rates increased after three daily injections to 26.1 h, 20.7 h, 30.5 h and 41.2 h for TAM, 4-OH-TAM, NMD-TAM and END. Although, levels of TAM and its metabolites were highly variable in the serum, all four compounds were cleared with similar rate constants as in the brain (Fig. 13 A-D and Table 12). This also holds true for consecutive injections over three days (Fig. 13 E-H and Table 12).

In summary, LC-HR-MS/MS data revealed a well-defined time window for optimal bioactivity of TAM and its metabolites, between 4 and 24 h post injection for single applications and 4 h to 5 d for applications over three consecutive days (Fig. 12 and Table 12). All metabolites were cleared effectively to negligible levels at 7 dpi.

**Figure 12. Brain concentrations of TAM and its derivatives peaked between 8 and 24 hpi and showed clearance within 7 dpi**

(A) TAM and (B) 4-OH-TAM peaked at 8 hpi after one TAM injection with 6x more TAM than 4-OH-TAM and subsequent clearance to ineffective levels at 7 dpi. (C) NDM-TAM and (D) END concentrations peaked after one TAM injection later at 24 hpi with 17x more NDM-TAM than END, but were also cleared 7 dpi. Insets show the last three to four examined time points in a higher resolution and half-lives ( $t_{1/2}$ ) are indicated for each derivative. Three consecutive TAM injections led to a prolonged TAM (E), 4-OH-TAM (F), NDM-TAM (G) and END (H) enrichment in the brain with a delayed clearance compared to single TAM injections. The brain concentrations of all TAM derivatives are plotted against the time. Data are shown  $\pm$  SD with  $n = 3-9$ , depicted as single points and with colors (red, green and grey) indicating independent experiments.





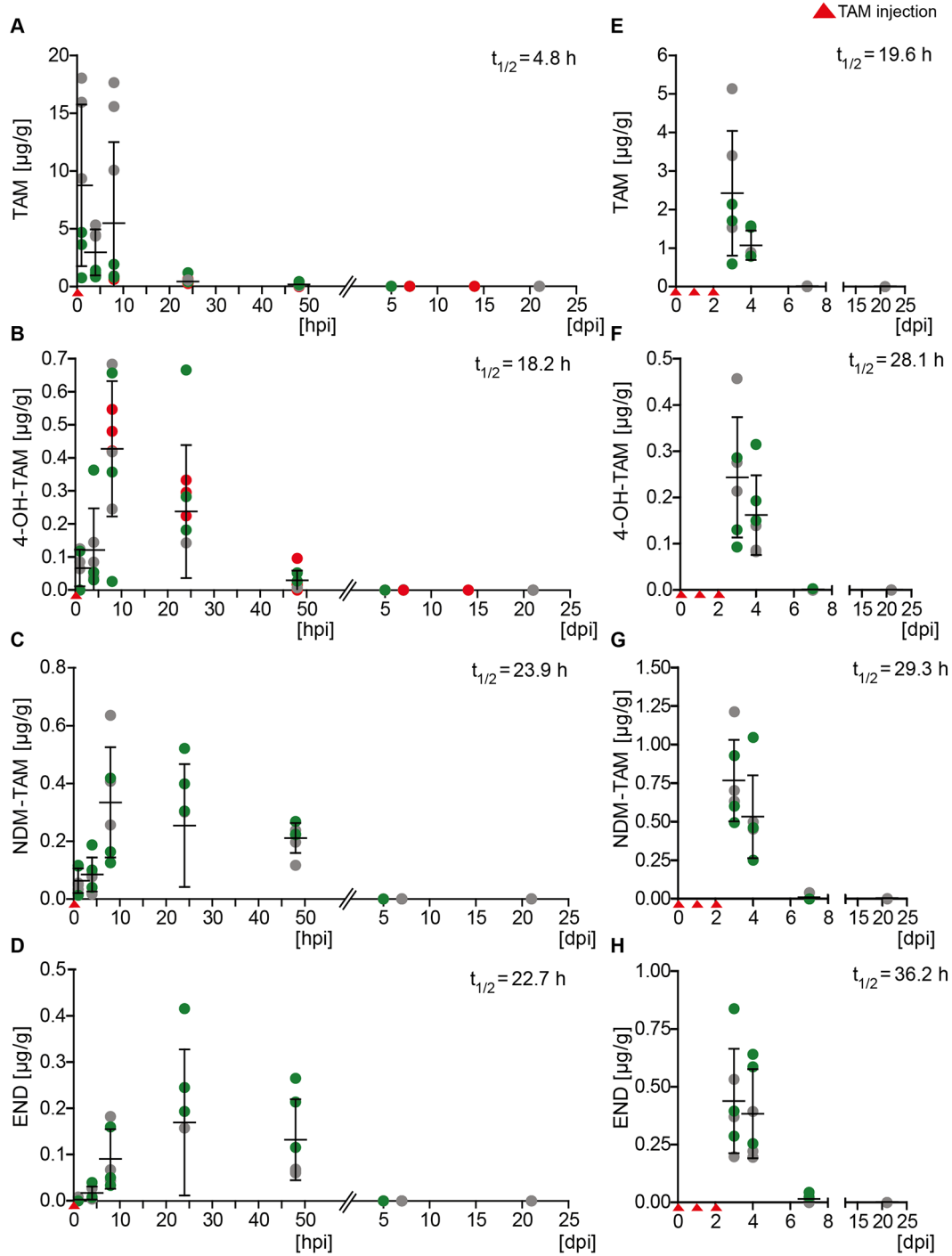


**Figure 13. Serum concentrations of TAM and its metabolites**

(A) Levels of TAM were highly variable after the first 8 hpi in serum after a single TAM injection, while after 24 hpi more uniform levels could be detected. (B) 4-OH-TAM peaked 8 hpi and showed subsequently lower levels at 5 dpi. (C) NDM-TAM and (D) END concentrations peaked after one TAM injection at 24 hpi with only slightly more NDM-TAM than END. Both are equally cleared after 7 dpi. Three consecutive TAM injections led to a higher concentration of TAM (E), 4-OH-TAM (F), NDM-TAM (G) and END (H) up to 48 hpi in the serum with longer half-lives compared to single TAM injections. Serum concentrations of all TAM derivatives are plotted against time. Data are shown  $\pm$  SD with  $n = 3-9$ , depicted as single points and with colors (red, green and grey) indicating independent experiments.

**Table 12. Brain and serum concentrations of TAM and its metabolites**

analysis	brain				serum			
	TAM [ng/g]	4-OHT-TAM [ng/g]	NDM-TAM [ng/g]	END [ng/g]	TAM [ng/ml]	4-OHT-TAM [ng/ml]	NDM-TAM [ng/ml]	END [ng/ml]
<b>single injection</b>								
1 hpi	3067.76	520.01	67.48	0.90	8744.90	65.66	63.38	1.82
4 hpi	13771.25	2055.34	1269.06	36.12	2949.65	120.06	85.08	16.15
8 hpi	27950.56	4373.59	5555.54	156.19	5479.48	426.71	334.40	89.82
24 hpi	9106.04	2513.90	8690.12	504.79	557.63	304.17	381.41	253.13
2 dpi	1875.14	340.05	3901.47	436.85	183.04	28.53	211.26	131.56
5 dpi	9.17	1.28	1.69	3.63	3.75	0.08	–	–
7 dpi	77.57	12.37	5.21	0	2.44	0.29	0.41	0
14 dpi	0.71	0.87	–	–	0.44	0	–	–
21 dpi	3.04	0.86	3.18	0	1.01	0	0.75	0
<b>3 injections</b>								
3 dpi	28853.49	5278.55	21889.77	1925.07	2419.20	242.97	763.76	437.54
5 dpi	17375.64	2457.76	15249.50	1867.61	1068.96	161.36	530.05	382.72
7 dpi	317.43	58.35	999.57	142.47	6.05	0.63	7.45	14.13
21 dpi	5.60	1.72	6.63	0	1.65	0.27	1.94	0

### 6.1.2. Maximal recombination levels are reached by three or five days of TAM injections in cortex or cerebellum, respectively

According to the LC-HR-MS/MS data, substantial levels of TAM and its metabolites were detected in the time window of 1 to 5 dpi depending on the application protocol. To determine the *in vivo* efficiency of TAM to activate Cre<sup>ERT2</sup>, the recombination of two floxed gene loci, *p2ry1* (P2Y1 receptor) and *gria1* (AMPA receptor subunit GluA1) in two different areas of the brain, the cerebellum (cb) and the cortex (ctx), was studied. Respective mouse lines were crossbred to mice expressing Cre<sup>ERT2</sup> from the high-

affinity glutamate aspartate transporter (GLAST; *slc1a3*) locus (GLAST-Cre<sup>ERT2</sup> x-*Gria1*<sup>fl/fl</sup> x *P2Y1*<sup>fl/fl</sup>, Fig. 14 C), generating triple transgenic mice.

Mice received 1, 2, 3 and 5 injections of TAM (100 mg/kg body weight) on consecutive days. Samples were analyzed at 8 hpi, 21 dpi and 200 dpi (Fig. 14 A). After TAM injection recombination of floxed loci was analyzed by qRT-PCR (gain of function, (Fig. 14 B), where successful recombination is indicated by an amplified PCR product. After three TAM injections, both alleles (*p2ry1* and *gria1*) were almost completely recombined in ctx (n = 4, Fig. 14 D, Table 13), and in cb (n = 4, Fig. 14 E, Table 13). Recombination could slightly be enhanced in the cortex for *gria1* when five consecutive injections were applied. This protocol also revealed a difference for *p2ry1* in the cerebellum (n = 4, Table 2).

As expected from LC-HR-MS/MS data, increasing the time period between induction and analysis of recombination from 21 to 200 d did not positively influence the recombination efficiency for both gene loci (n = 2, Table 13). Analyzing the successful recombination already at 8 hpi after a single TAM injection revealed large differences in recombination efficiencies within the different brain regions, but also between the different gene loci. In the ctx only a small percentage of floxed alleles was recombined (n = 3, 14 % *p2ry1*, 3 % *gria1*), while in the cb (n = 3, 36 % *p2ry1*, 33 % *gria1*) the recombination rate was higher (2.5 x and 11 x higher, respectively). As expected from the longer bioavailability of its metabolites, higher degree of recombination was observed at 21 dpi (n = 4) in comparison to 8 hpi (n = 3) after a single TAM injection; (*p2ry1* and *gria1*) in ctx (Table 13). Similarly, three (n = 4) TAM injections were more efficient than only two (n = 3) at 21 dpi (Table 13).

At early time points after TAM injections, (8 hpi) large differences in recombination efficiencies between different alleles and brain regions were detected. Cortical recombination of the *p2ry1* alleles was more than four times larger than *gria1* alleles. In contrast, in the cerebellum almost no difference between the two alleles was detected (Fig. 14 D, E, Table 13). Simultaneously, cerebellar recombination rate was much higher than cortical. At 21 dpi after a single TAM injection, we found more than twice as many recombined *p2ry1* than *gria1* alleles in the ctx. This difference disappeared, when three consecutive injections were applied (Fig. 14 D, E). In addition, both target genes showed different recombination kinetics in ctx and cb. In general, the cb showed faster recombination kinetics as the ctx after one or two injections with comparable recombination after three and five injections (Fig. 14 D, E).

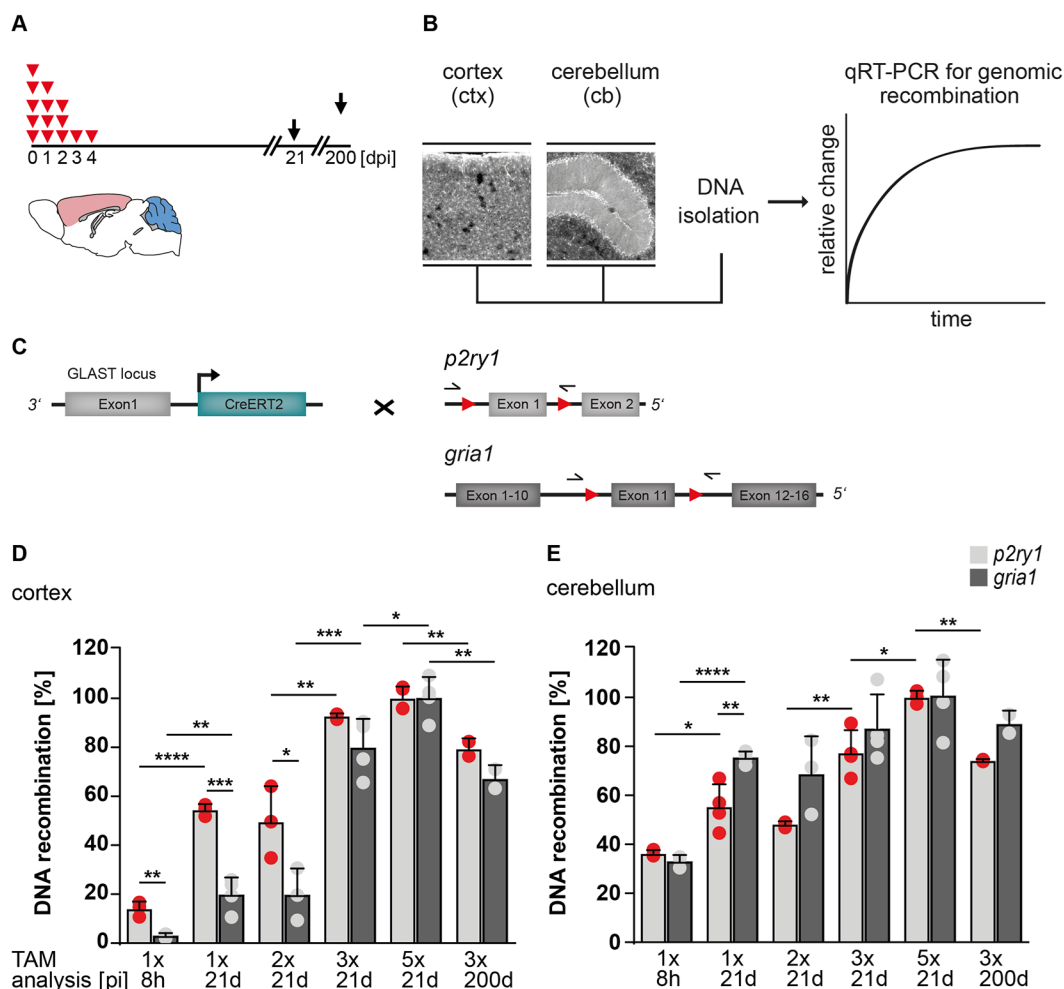


**Figure 14. Three to five daily TAM injections give maximal DNA recombination depending on the brain region**

A) For determination of efficient recombination different TAM injection protocols were used varying between single and five consecutive injections (indicated by red triangles) and were analyzed at different time points (black arrows). (B) DNA isolation from cortical and cerebellar tissue was used for subsequent quantitative RT-PCR (qRT-PCR) from (C) GLAST-Cre<sup>ERT2</sup> x P2Y<sup>1fl/fl</sup> x Gria1<sup>fl/fl</sup> mice. Primers (for the *p2ry1* and *gria1* gene) span both loxP sites with amplification of the flanked sequence after recombination. (D, E) Differences in recombination efficiency between both analyzed alleles, but also both brain regions could be observed with the lowest cortical and cerebellar recombination observed at 8 hpi. Cortical recombination (D) was higher after five consecutive injections for *gria1*, while for *p2ry1* three injections were sufficient. Highest cerebellar recombination (E) could be reached already after three consecutive injections for *gria1* and could be further increased by five injections for *p2ry1*. Per injection protocol three to four animals (exception 200 d, n = 2) were analyzed (colored points) and  $\Delta C_T$ -values were normalized to the mean value of animals which received 5x TAM. The error bars correlate to the SD of the biological replicates (n = 2-4, \* p < 0.05, \*\* p < 0.01, \*\*\* p < 0.001, unpaired t-test).

Additionally, a two-day interval protocol of three consecutive TAM injections, inspired by the rapid drop of 4-OH-TAM at 48 hpi (Fig. 15) and an 8 h interval protocol of three consecutive injections, due to the peak of 4-OH-TAM (Fig. 15), were tested. Based on the LC-HR-MS/MS data that identified a fast clearance in less than 48 h, an interval protocol with one-day pause between injections (i.e. injections at every 2<sup>nd</sup> day) is expected to be less efficient than the daily-injection protocol (Fig. 13, Fig. 15 B, C). Indeed, the interval protocol revealed less recombined alleles in the cortex, with a reduction of 38 % (*p2ry1*) and 61 % (*gria1*) compared to the 5 x injection protocol ( $100 \pm 5\%$  and  $100 \pm 9\%$ , respectively) ( $n = 4$ , Fig. 15 B). In the cerebellum, the recombination was only decreased for the *gria1* locus by 18 % with the interval protocol, while no change was detectable for the *p2ry1* locus. Recombination efficiencies of the interval protocol also reflects again the general higher cerebellar recombination efficiency for both floxed alleles ( $n = 4$ , Fig. 15 C).

The other interval protocol, three times every 8 h, was expected to be more efficient based on the LC-HR-MS/MS data. Peak concentrations were reached after 8 h therefore we assumed, that an injection at that time point will increase TAM and 4-OH-TAM concentrations, leading to a higher recombination efficiency. Samples were collected either 48 h after the last injection or 21 d after the first injection (Fig. 15 B, C). In the cortex about  $77 \pm 21\%$  of the *p2ry1* alleles were recombined and 43 % of *gria1* alleles after 48 h. Compared to the five times injection protocol recombination efficiency was reduced by 57 % for *gria1* alleles (Fig. 15 B). In the cerebellum recombination efficiency was increased for the *p2ry1* locus ( $126 \pm 17\%$ ), while *gria1* showed less recombined alleles ( $40 \pm 6\%$ ) (Fig. 15 C). After 21 dpi recombination efficiency of the *p2ry1* locus was not changed in cortex and cerebellum compared to the 5 x injection protocol. For the *gria1* locus recombination efficiencies were less efficient in both brain regions. In the cortex only  $53 \pm 24\%$  of the alleles were recombined and  $35 \pm 0.7\%$  in the cerebellum, respectively (Fig. 15 B, C). These data suggest an impact of the circadian rhythms on the accessibility of the respective floxed loci, with *p2ry1* favoured in this protocol, while *gria1* declined.

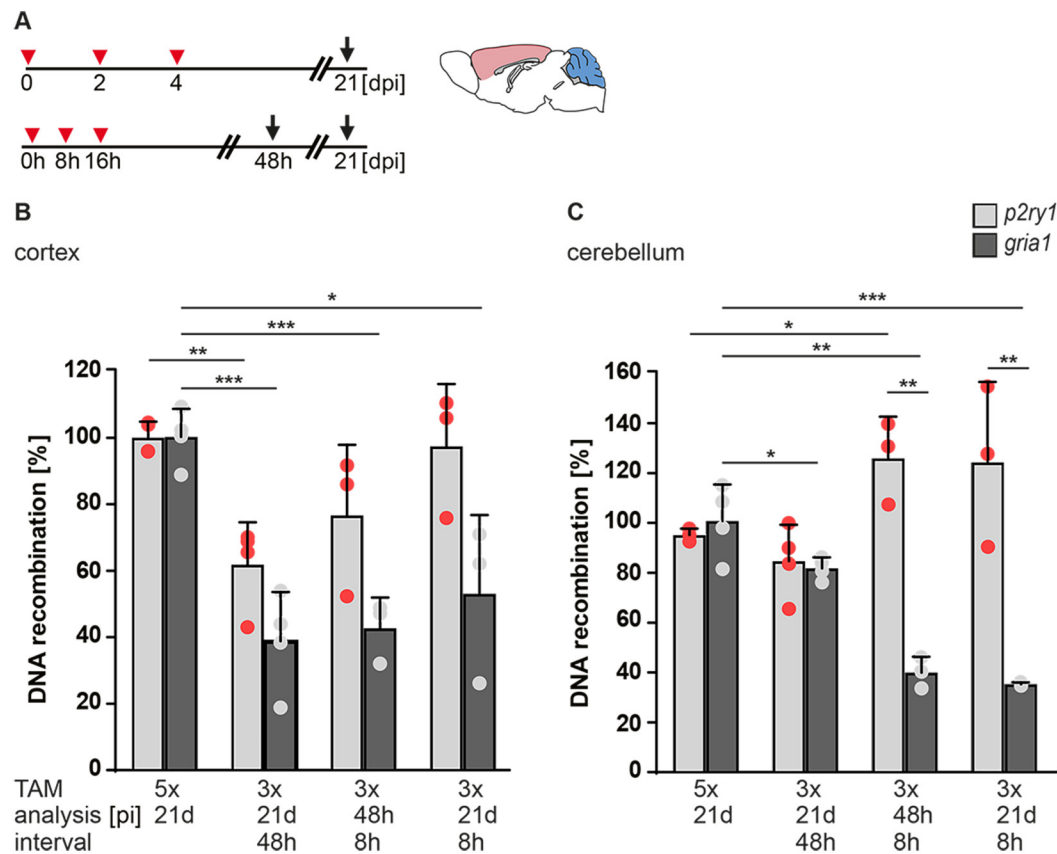


**Figure 15. Interval injections every second day or every 8 h revealed differences in recombination efficiencies of floxed loci**

(A) Interval injection protocols of TAM application (red triangles) and sample preparation after different time points (black arrows). (B) Significant lower cortical recombination of *grla1* alleles in all protocols. Recombination efficiency was reduced for the *p2ry1* locus for the injection protocol every second day, but reached similar levels with the 8 h interval protocols. (C) In the cerebellum all tested interval protocols for the *grla1* locus were less effective than the 5 x injection protocol. *P2ry1* with no difference for the injection protocol every second day, but the 8 h injection protocol revealed an increase in recombination efficiency after 48 h. Three to four animals were analyzed (colored dots) and  $\Delta$ CT-values were normalized to the mean value of animals which received 5 x TAM. The error bars correlate to the SD of the biological replicates ( $n = 3-4$ , \*  $p < 0.05$ , \*\*  $p < 0.01$ , \*\*\*  $p < 0.001$ , unpaired t-test).

In summary, single TAM injections are not sufficient to achieve maximum recombination in cortex and cerebellum. The best recombination efficiency requires three to five days TAM injections. These results indicate that three injections for *p2ry1* in the cortex are sufficient to achieve maximal recombination, whereas in the cerebellum five injections are needed. Exactly the opposite is true for *grla1*, with five injections for cortex and three injections for cerebellum for maximal recombination efficiencies. The interval protocol, with injections every 8 h and a waiting period of 48 h

revealed even higher recombination efficiencies for the *p2ry1* locus, but is more elaborated in scheduling and more stressful for the mice.

**Table 13. Different tamoxifen injection protocols for recombination of the *p2ry1* and *gria1* locus**

	TAM injection	injection intervall	analysis	<i>p2ry1</i> [%]	<i>gria1</i> [%]
<b>ctx</b>	1x	-	8 hpi	14±3	3±1
	1x	-	21 dpi	54±2	20±7
	2x	24 h	21 dpi	50±15	20±11
	3x	24 h	21 dpi	93±1	80±12
	3x	24 h	204 dpi	79±4	67±6
	5x	24 h	21 dpi	100±5	100±9
	3x	48h	21 dpi	62±13	39±15
	3x	8 h	48 hpi	77±21	43±9
	3x	8 h	21 dpi	97±19	53±24
<b>cb</b>	1x	-	8 hpi	36±1	33±2
	1x	-	21 dpi	55±9	76±2
	2x	24 h	21 dpi	48±1	69±15
	3x	24 h	21 dpi	77±9	87±14
	3x	24 h	204 dpi	74±1	89±5
	5x	24 h	21 dpi	100±3	101±15
	3x	48h	21 dpi	74±13	82±4
	3x	8 h	48 hpi	126±17	40±6
	3x	8 h	21 dpi	124±32	35±0.7

### 6.1.3. GLAST-Cre<sup>ERT2</sup> mediated DNA recombination to quantify astroglial cell numbers

Genomic recombination can be determined by qRT-PCR either by generating (1) an amplimer across the newly formed (recombined) genomic DNA with increasing levels of amplimers indicating progress of recombination (Fig. 14, gain), or (2) an amplimer across a single loxP site of the non-recombined locus where reduced amplimer levels indicate successful gene deletion (Fig. 16, loss). The latter approach can be used to

determine the percentage of Cre<sup>ERT2</sup>-expressing cells. If Cre<sup>ERT2</sup> is expressed in a cell type-specific manner, the proportion of this cell type in a given tissue region can be determined. Using the GLAST-Cre<sup>ERT2</sup> mouse line, recombination efficiencies of two different floxed alleles (*stop<sup>fl/fl</sup> tdTomato* and *p2ry1<sup>fl/fl</sup>*) in different brain regions (bs, cb, ctx, hc, opt) were compared and the decrease of non-recombined loxP sites by qRT-PCR was quantified.

Samples from both genders were combined for analysis since no differences were detected (Jahn, Kasakow *et al.*, 2018). Analyzing the floxed *p2ry1* alleles revealed recombination rates between 6 % and 33 % in the brainstem (bs), cb, ctx, hippocampus (hc) and optic nerve (opt) (Figure 16 C). Similar results were obtained for the *tdTomato* allele (bs (89 %), cb (94 %), ctx (79 %), hc (79 %) and opt (73 %)). No differences were found for most brain regions (cb (6 %), ctx (20 %), hc (27 %) and opt (29 %)) (Fig. 16 D, E). In the brainstem, however, the *tdTomato* locus was less recombined than the floxed *p2ry1*. Based on these data, the percentage of GLAST-Cre<sup>ERT2</sup>-positive cells (a rough estimate of astrocytes) varied from 6 to 29 %, dependent on the brain region.

To confirm the qRT-PCR analysis, the number of recombined cortical tdTomato-positive cells was counted. Of all cells (TO-PRO-3 labelled nuclei)  $21 \pm 5$  % were tdTomato-positive (Fig. 16 F), a value well correlating to DNA recombination in the cortex (20 %). In addition, no differences of tdTomato-positive cells could be detected in the cortices of males and females ( $21 \pm 6$  %,  $20 \pm 4$  %, respectively (Jahn, Kasakow *et al.*, 2018)). Our results show that qRT-PCR data of recombined loxP sites obtained from tissue homogenates correlates well to counting of individual recombined cells. Therefore, the recombination rate reflects the percentage of GLAST-positive cells (=astrocytes) in the respective brain regions.



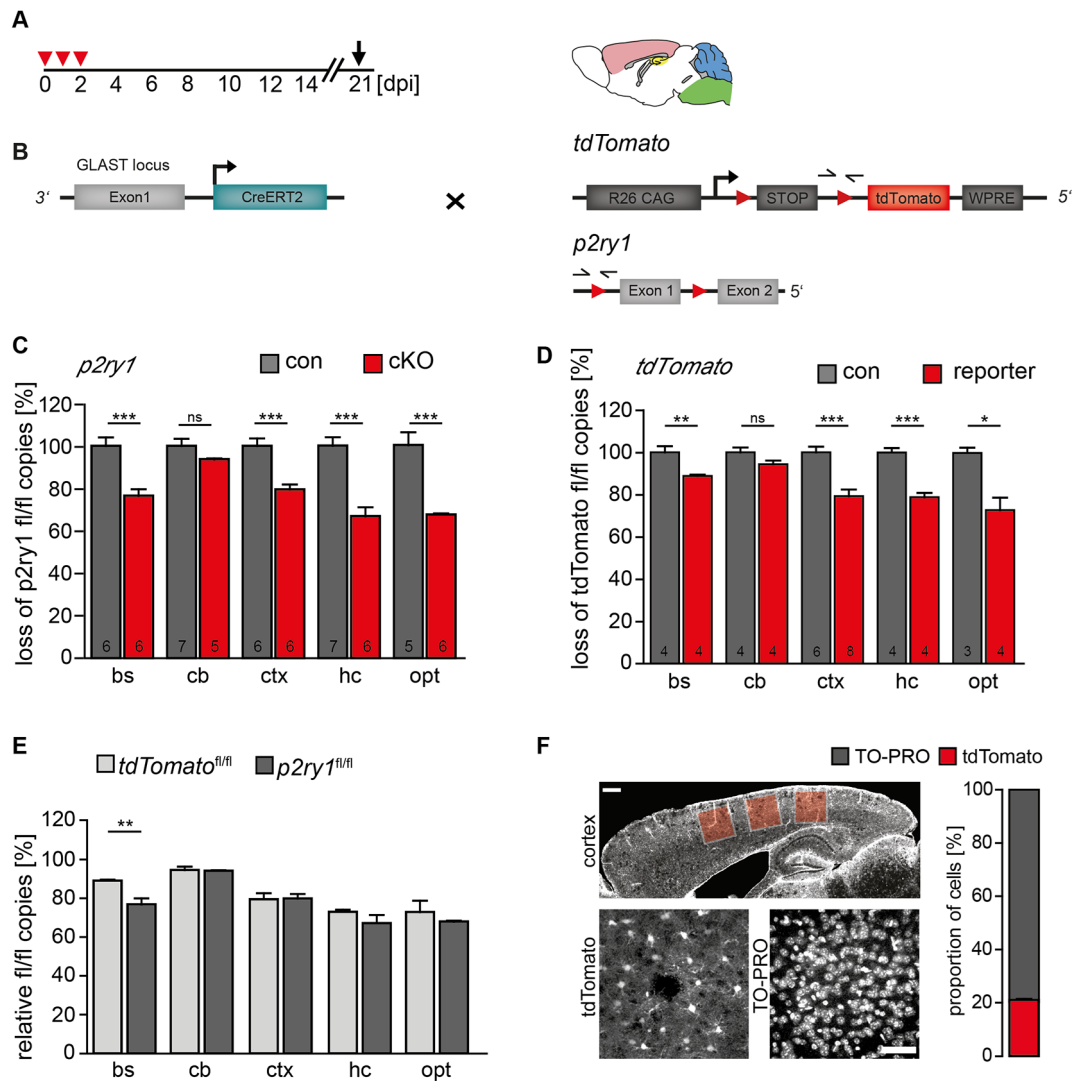


**Figure 16. Recombination efficiencies were constant for target and reporter genes**

(A, B) GLAST-Cre<sup>ERT2</sup> mice crossed to tdTomato<sup>fl/fl</sup> and P2Y1<sup>fl/fl</sup> mice were used for quantification of floxed, non-recombined alleles by qRT-PCR. Arrows indicate the position of primers after TAM injection for three consecutive days and analysis at 21 dpi. Reduction of floxed *p2ry1* alleles (C) and floxed reporter (floxed stop cassette) (D) in bs, cb, ctx, hc and opt of transgenic animals compared to non-recombined alleles (100 %) showed (E) no differences in all brain regions with the exception of the bs, where the reporter allele was recombined at a lower level than the floxed receptor gene. The error bars correlate to the SEM of the biological replicates ( $n$  = as indicated in bars (C, D),  $*p < 0.05$ ,  $**p < 0.01$ ,  $***p < 0.001$ , unpaired t-test). (F) Micrograph of a representative cortical vibratome section prepared from a GLAST-Cre<sup>ERT2</sup> x tdTomato mouse showing the extent of fluorescent recombined astrocytes. Colored squares represent the position of confocal images for stereological analysis. The scale bar corresponds to 500  $\mu$ m. Counting of TO-PRO-3+ and tdTomato+ cells in cortices of GLAST-Cre<sup>ERT2</sup> x tdTomato vibratome sections resulted in  $21 (\pm 3) \%$  tdTomato positive cells. The scale bar corresponds to 50  $\mu$ m.

In summary, already at 8 hpi 28 % of the injected, non-metabolized TAM (100 %) partitioned into brain tissue. In addition, 10% of injected TAM reached the brain as the liver metabolites NDM-TAM (5.6 %), 4-OH-TAM (4.4 %) and END (0.2 %) (36.1 ng/g). While more than one third of TAM accumulated in the brain quickly, only 4-OH-TAM and END are bioactive and can induce DNA recombination. At 24 hpi significant portions of TAM and the major bioactive metabolite 4-OH-TAM were already cleared from the brain (decrease of TAM to 9.1 % and of 4-OH-TAM to 3 %). Simultaneously, NDM-TAM (9 %) and END (0.5 %) piled up (Fig. 17 A).

For maximal cortical or cerebellar recombination (driven by Cre<sup>ERT2</sup> expression under control of the GLAST locus), the ideal injection protocol depends on the investigated floxed loci: *p2ry1* (cb) and *gria1* (ctx) five TAM injections; *p2ry1* (ctx) and *gria1* (cb) three TAM injections (Fig. 17 B).

We determined the percentage of astrocytes in a given brain region (by defining GLAST-Cre<sup>ERT2</sup> positive cells largely as astrocytes): 17 % (n=10) in the brainstem; 6 % (n=9) in the cerebellum; 20 % (n=14) in the cortex; 27 % (n=10) in the hippocampus and 29 % (n=10) in the optic nerve (Fig. 17 C).

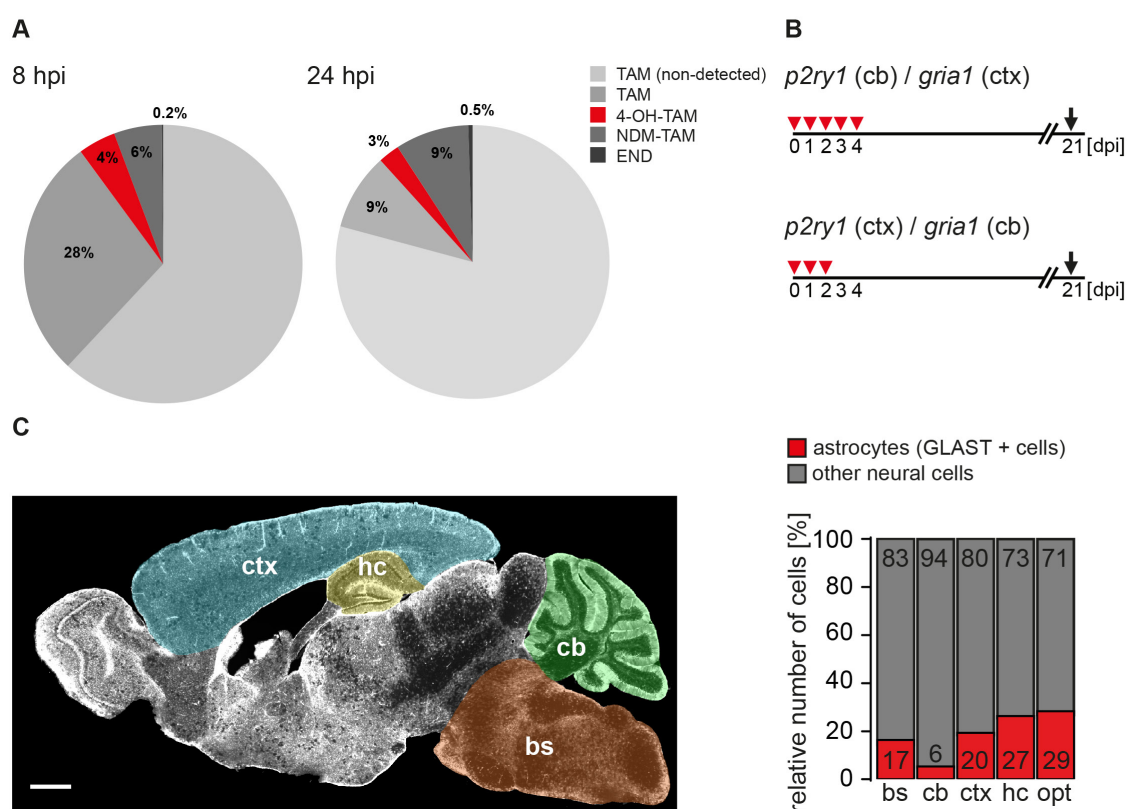


### Figure 17. Inducible DNA recombination in mouse astroglia

(A) Concentrations of TAM and its derivatives after single TAM injections revealed that about 28 % of the originally injected TAM could be detected in the brain while only 4 % 4-OH-TAM, 6 % NDM-TAM and negligible amount of END could be found at 8 hpi. While TAM (9 %) and 4-OH-TAM (3 %) decreased 24 hpi, NDM-TAM (9 %) and END (3x higher) increased their concentrations in the brain. (B) The optimized injection protocol for GLAST-CreERT2 mice: 5xTAM for p2ry1 (cb) and *gria1* (ctx); 3xTAM for p2ry1 (ctx) and *gria1* (cb). (C) In a brain of a young adult mouse, astrocytes account for 17 % (n=10) in the bs, 6 % (n=9) in the cb, 20 % (n=14) in the ctx, 27 % (n=10) in the hc and 29 % (n=10) in the optic nerve (setting GLAST-positive cells as astrocytes).

## 6.2. Tamoxifen-independent recombination

Tamoxifen-independent recombination of floxed alleles, mediated by the inducible Cre DNA recombinase, was observed during control experiments for the recombination study (6.1). Therefore, several Cre<sup>ERT2</sup> driver lines were tested for tamoxifen-independent recombination by expression of two different reporter lines to evaluate the impact of non-induced recombination for our experiments. Here, homologous as well as non-homologous recombined mouse lines were compared. Percentage of tamoxifen-independent reporter expression was measured and compared to injected animals and to Cre<sup>ERT2</sup> wildtype controls.

### 6.2.1. IHC analysis and quantification of different astrocyte-specific

#### Cre<sup>ERT2</sup> driver lines crossbred to the reporter mouse lines GCaMP3 and tdTomato

To study tamoxifen-independent recombination, two different Cre<sup>ERT2</sup> driver lines were compared and analyzed by immunohistochemical analysis after reporter recombination. As astrocyte-specific mouse lines with Cre<sup>ERT2</sup> expression: GLAST-Cre<sup>ERT2</sup> as a knockin and GFAP-Cre<sup>ERT2</sup> (Cre<sup>ERT2</sup> expression controlled by a part of the human GFAP-promoter) were compared. Lines were crossbred with both reporters to investigate any impact of the reporter on tamoxifen-independent recombination. The GCaMP3 signal was stained with  $\alpha$ -GFP due to the loss of signal during the fixation of the brain. For better comparison, the tdTomato signal was additionally stained with  $\alpha$ -DsRed. The percentage of recombined cells in both mouse lines was investigated using the Orbit image analysis software. Therefore, raw images (czi files) of whole sagittal brain slices, generated by the AxioScan, were used. Inclusion and exclusion models were created, as described before, to detect only the fluorescence of the

recombined cells. Fluorescence intensities were converted into percentage reporter expression with the injected, Cre<sup>ERT2</sup> expressing mice set to 100 % (positive control) and all other conditions were standardized (Fig. 20 and 23).

All mice were analyzed at an age of seven weeks (Fig. 18-23 A). Animals heterozygously expressing Cre<sup>ERT2</sup> (ct2/wt) and injected for three consecutive days with TAM (+TAM) represent maximum reporter expression (positive control, ct2/wt/+TAM (1)). Wildtype animals without Cre<sup>ERT2</sup> served as negative controls (wt/wt/ $\pm$ TAM (2)) with no apparent recombination. Some of these animals were also injected with TAM to exclude any recombination in the absence of Cre<sup>ERT2</sup> induced by TAM ( $\pm$  TAM). The other two tested conditions expressed Cre<sup>ERT2</sup> either heterozygously (ct2/wt/-TAM (3)) or homozygously (ct2/ct2/-TAM (4); only tested for knockin line) and did not receive TAM. Reporter lines were only used homozygously floxed. For the GFAP-Cre<sup>ERT2</sup> line, generated by non-homologous recombination, the fourth group (ct2/ct2/-TAM) was excluded.

Sagittal brain overviews of all seven genotypes and magnifications of cortex (corpus callosum, hippocampus) and cerebellum (Fig. 18-23) were analyzed.

#### **6.2.1.1. Non-induced recombination of GLAST-Cre<sup>ERT2</sup> mice**

TAM injected GLAST-Cre<sup>ERT2</sup> animals crossbred to GCaMP3 reporter showed an expected overall expression of the reporter in astrocytes with a very high expression in the cerebellum (Fig. 18 B) (Jahn *et al.*, 2015, Saab *et al.*, 2012). Positive (Fig. 20 C, 102.4 %) and negative controls (Fig. 20 C, 1.9 %) revealed expected results, with high recombination compared to no reporter expression. In heterozygous mice without induction (ct2/wt/-TAM) only a few cells were recombined in the forebrain, while main tamoxifen-independent recombination could be found in the cerebellum (Fig. 18 D, 9.3 % for whole brain (Fig. 20 C)). The number of recombined cells in non-induced homozygous mice (ct2/ct2/-TAM) was slightly increased in forebrain and cerebellum (Fig. 18 E) reaching 10 % reporter expression (Fig. 20 C).

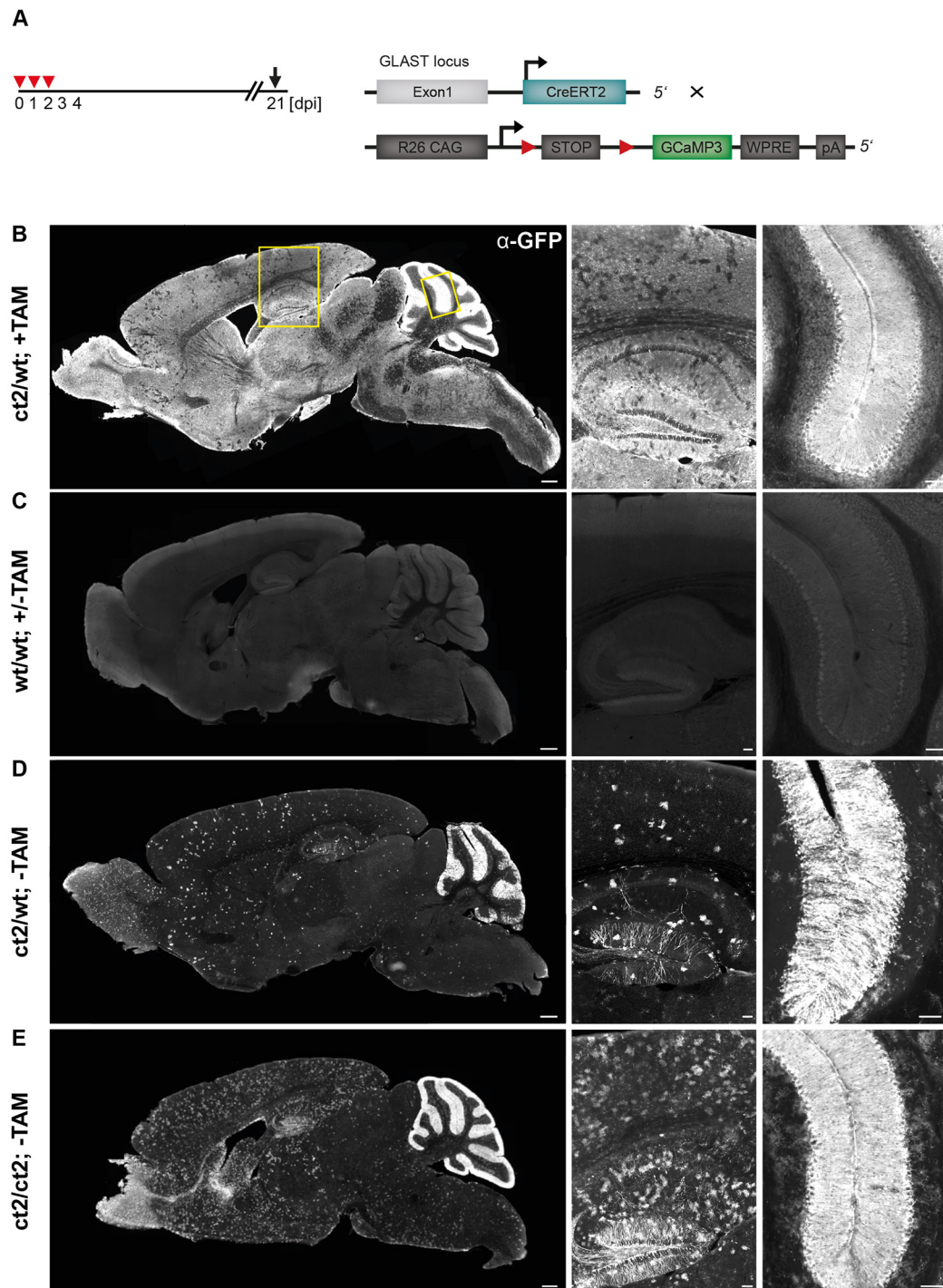


**Figure 18. Tamoxifen-independent recombination of the GLAST-Cre<sup>ERT2</sup> line indicated by high Gfap reporter expression**

(A) GLAST-Cre<sup>ERT2</sup> mice crossbred to the reporter line Rosa26-GCaMP3, were injected with TAM (positive control) at an age of four weeks and analyzed 21 dpi. (B-E) Whole sagittal brain slices with four different Cre<sup>ERT2</sup> genotypes and magnifications of cortex and cerebellum. (B) The positive con (ct2/wt/+TAM) revealed an overall high expression of GCaMP3 in astrocytes and (C) lacking GCaMP3 in the negative con

(wt/wt/ $\pm$ TAM). (D) Heterozygous non-induced animals (ct2/wt/-TAM) with single recombined astrocytes in the fore- and midbrain and high cerebellar reporter expression. (E) Homozygous non-induced animals (ct2/ct2/-TAM) showed more astrocytes, with even comparable cerebellar reporter expression to the positive con. ctx: cortex; cc: corpus callosum; hc: hippocampus; cb: cerebellum. Scale bars correspond to 500  $\mu$ m in sagittal overviews and 100  $\mu$ m in magnifications, respectively.

The GLAST-Cre<sup>ERT2</sup> driver line crossbred to the tdTomato reporter showed similar results compared to GCaMP3, with high astrocytic tdTomato expression after TAM treatment all over the brain (101.1 % reporter expression, Fig. 19 B and 20 C). No reporter was expressed in the negative control (wt/wt/ $\pm$ TAM, 0.7 %, Fig. 19 C and 20 C). Non-injected animals, expressing Cre<sup>ERT2</sup> either heterozygously or homozygously, showed few recombined astrocytes in the forebrain, but an overall high reporter expression in the cerebellum (5.3 % and 9.7 % reporter expression, respectively, Fig. 19 D, E and 20 C). Direct visual comparison of expressed GCaMP3 and tdTomato in GLAST-Cre<sup>ERT2</sup> mice revealed a higher expression level of the GCaMP3 reporter.

The reporter GCaMP3 was additionally stained with  $\alpha$ -GFP. To exclude higher fluorescence intensities due to antibody labeling, also tdTomato was stained with  $\alpha$ -DsRed (IHC data not shown), revealing a higher fluorescence signal compared to the original signal: (1) 100.6 %; (2) 8.6 %; (3) 16.8 %; (4) 30.1 %. But also the background signal for the negative control was increased due to staining from 0.7 % to 8.6 % (Fig. 20 C).



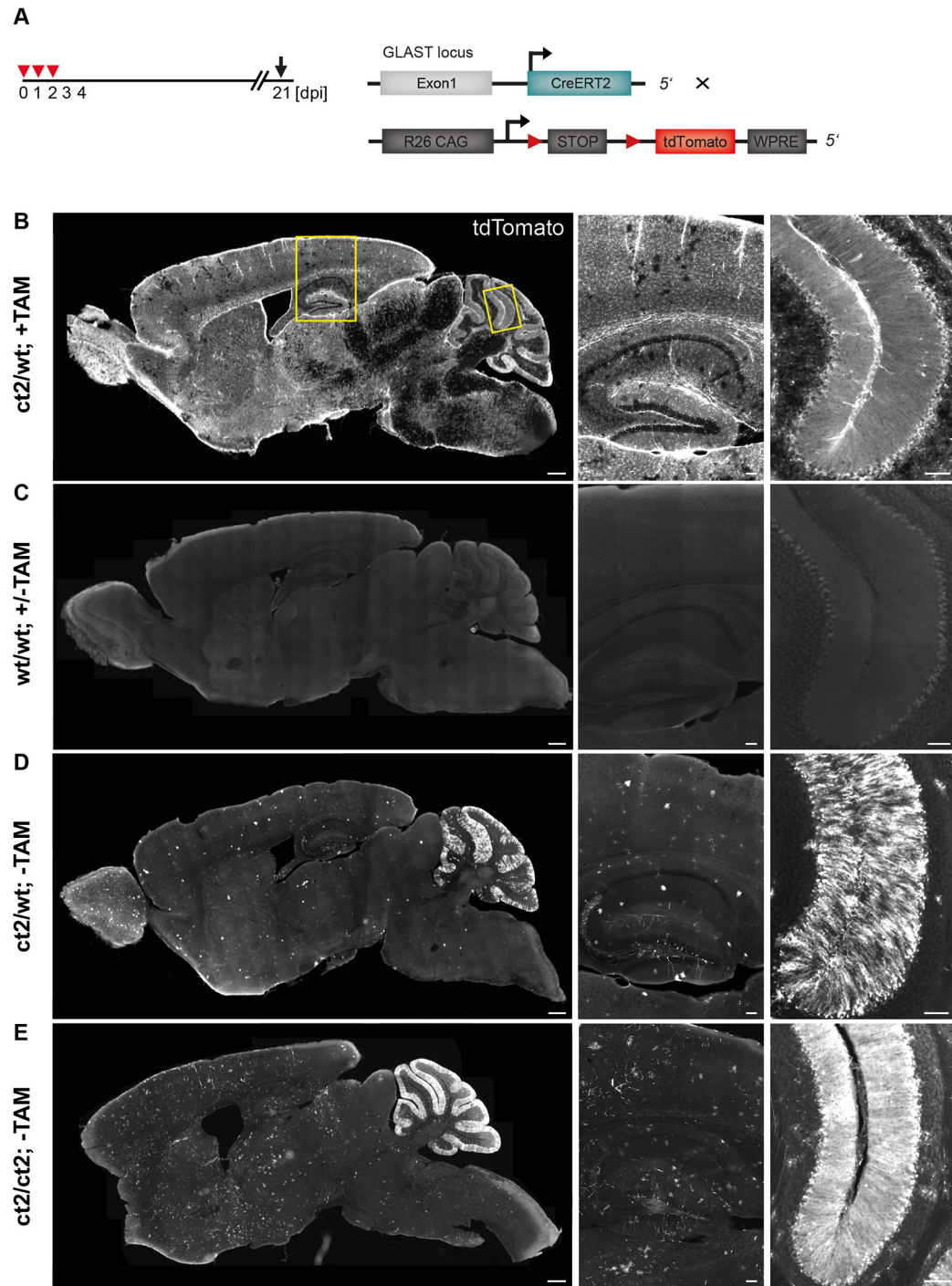


**Figure 19. Tamoxifen-independent recombination of GLAST-Cre<sup>ERT2</sup> x Rosa26-tdTomato mice**

(A) GLAST-Cre<sup>ERT2</sup> mice were crossbred to the reporter line Rosa26-tdTomato, injected with TAM (positive control) at an age of four weeks and analyzed 21 dpi. (B-E) Whole sagittal brain slices of four different Cre<sup>ERT2</sup> genotypes and magnifications of cortex and cerebellum, of original tdTomato signal without additional staining. (B) Positive con (*ct2/wt; +TAM*) with overall high expression of tdTomato in astrocytes,

while (C) the negative con (wt/wt±TAM) expressed no reporter. (D) Heterozygous non-induced animals (ct2/wt/-TAM) with only few recombined astrocytes in the fore- and midbrain and a high cerebellar reporter expression. (E) Homozygous non-induced animals (ct2/ct2/-TAM) revealed more recombined astrocytes in cortex and cerebellum compared to heterozygous animals. ctx: cortex; cc: corpus callosum; hc: hippocampus; cb: cerebellum. Scale bars correspond to 500  $\mu$ m in sagittal overviews and 100  $\mu$ m in magnifications, respectively.

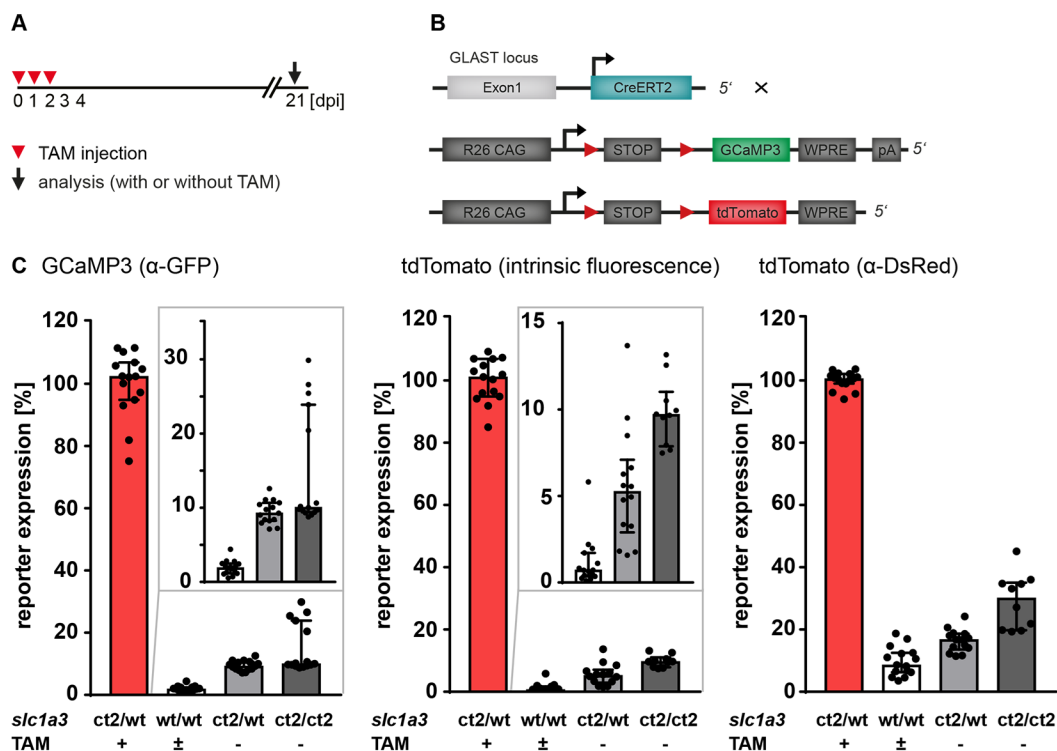


**Figure 20. Quantification of tamoxifen-independent recombination of the GLAST-Cre<sup>ERT2</sup> driver line revealed high reporter expression**

(A) Animals were injected with TAM at the age of four weeks for three consecutive days and analyzed 21 dpi (positive con; ct2/wt+TAM) (B) GLAST-Cre<sup>ERT2</sup> driver line crossbred to reporter lines GCaMP3 and tdTomato. (C) Analysis of recombination (Orbit) in GLAST-Cre<sup>ERT2</sup> mice revealed a difference between ct2/wt+TAM animals compared to the negative con (wt/wt±TAM), the heterozygous (ct2/wt/-TAM) and the homozygous (ct2/ct2/-TAM) condition for both reporter and the additional reporter staining. Differences in reporter expression between wt compared to the heterozygous and homozygous condition could be found. Homozygous non-induced animals revealed for tdTomato expression and α-DsRed staining a higher recombination than heterozygous animals, while GCaMP3 expression was comparable ( $p = 0.0555$ ). The error bars correlate to the median ± interquartile range of the biological replicates ( $n = 2-3$ ), table 14 and 15.



#### 6.2.1.2. Tamoxifen-independent recombination is mainly absent in GFAP-Cre<sup>ERT2</sup> mice

To evaluate if tamoxifen-independent recombination occurs in astrocyte-specific Cre<sup>ERT2</sup> driver lines, non-homologous TgN (hGFAP-Cre<sup>ERT2</sup>) mice (Hirrlinger *et al.*, 2006) were analyzed. Injected animals of the GFAP-Cre<sup>ERT2</sup> line showed reporter positive (GCaMP3) astrocytes all over the brain with a higher expression rate in the hindbrain (Fig. 21 B) and less recombination efficiency in cortex and cerebellum compared to GLAST-Cre<sup>ERT2</sup> mice (Jahn *et al.*, 2015, Jahn, Kasakow *et al.*, 2018). IHC data and Orbit image analysis revealed no reporter expression in negative controls (Fig. 21 C and 23 C). Heterozygous Cre<sup>ERT2</sup>-expressing animals showed only isolated recombined cells in cortex and cerebellum (Fig. 21 D), also reflected by only 1.1 % reporter expression (Fig. 23 C). Therefore, this mouse line showed less tamoxifen-independent recombination in heterozygous mice than the GLAST-Cre<sup>ERT2</sup> mouse line, using the GCaMP3 reporter (1.1 % to 9.3 %, respectively).

Analysing tdTomato reporter expression in GFAP-Cre<sup>ERT2</sup> mice revealed similar results compared to GCaMP3 but with higher background signal in negative controls (5.5 %) (Fig. 22 C and 23 C). Positive controls showed reporter expression all over the brain with highest recombination in midbrain and brainstem and only sparse cortical and hippocampal recombination (Fig. 22 B). The negative control did not recombine (Fig. 22 C). Heterozygous, non-injected animals showed almost no TAM-independent recombination. Less than 50 cells per sagittal section could be detected (Fig. 22 D). These findings were also reflected by Orbit image analysis, revealing 2.1 % reporter expression (Fig. 23 C). Staining with  $\alpha$ -DsRed antibody revealed higher fluorescence signals compared to the original signal, revealing (1) 102.2 %; (2) 19.2 % and (3) 22.1 %. However, background signal for the negative control was again increased due to the staining from 5.5 % to 19.2 % (Fig. 23 C).

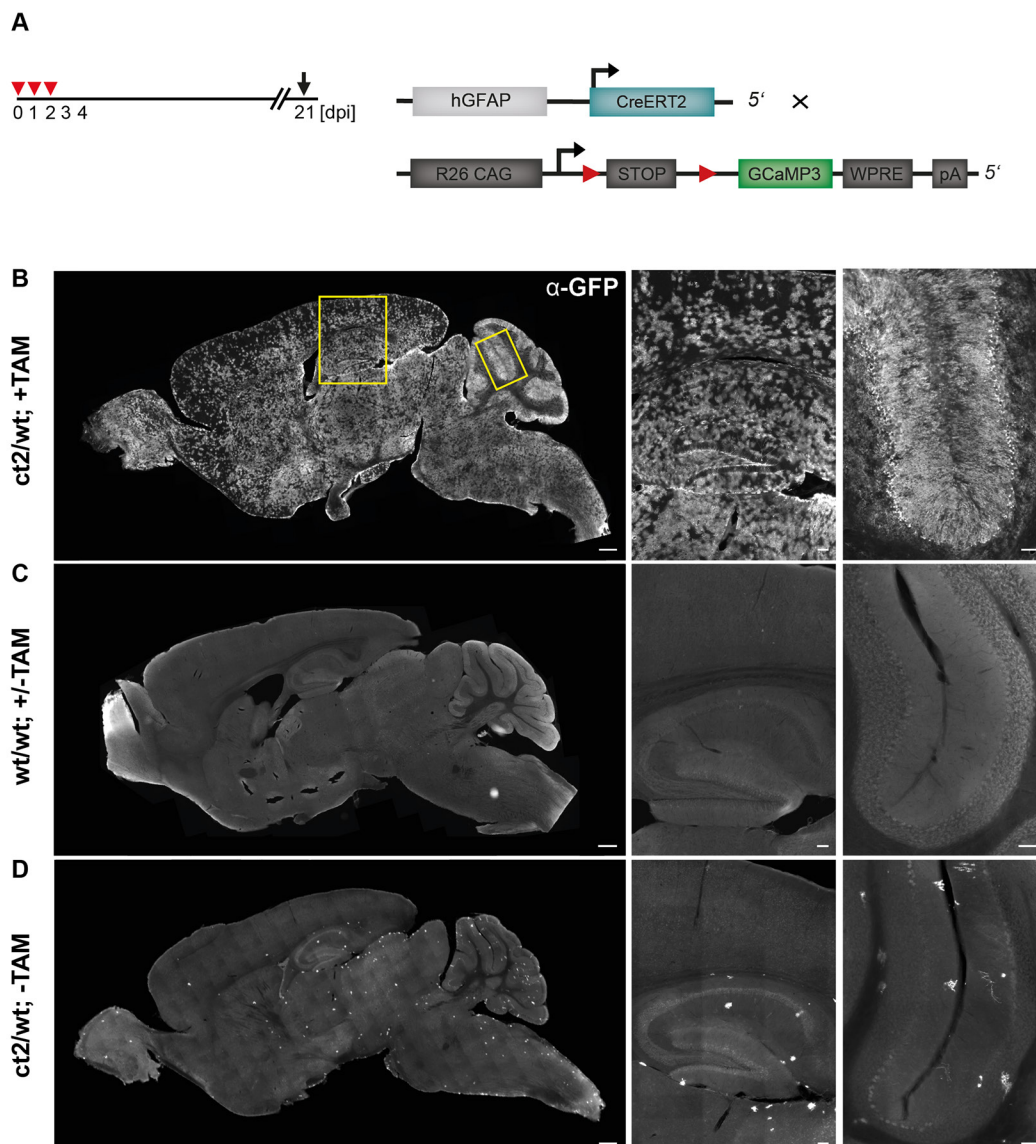


**Figure 21. Negligible non-tamoxifen-induced recombination of GCaMP3 in GFAP-Cre<sup>ERT2</sup> mice**

(A) Mice were injected with TAM (positive control) at an age of four weeks and analyzed 21 dpi. GFAP-Cre<sup>ERT2</sup> mice were crossbred to the reporter line Rosa26-GCaMP3, and (B-D) sagittal brain slices with three different Cre<sup>ERT2</sup> genotypes and magnification of cortex and cerebellum. (A) The positive con (ct2/wt/+TAM) revealed an overall high expression of the GCaMP3 in astrocytes with a different expression pattern compared to the GLAST-Cre<sup>ERT2</sup> line. More astrocytes are recombined in the mid- and hindbrain, while cortical recombination was sparse. (C) Negative con (wt/wt/±TAM) with no expression of the reporter. (D) Heterozygous non-induced animals (ct2/wt/-TAM) with single recombined astrocytes in midbrain and only sparsely recombined Bergmann glia cells. ctx: cortex; cc: corpus callosum; hc: hippocampus; cb: cerebellum. Scale bars correspond to 500 µm in sagittal overviews and 100 µm in magnifications, respectively.

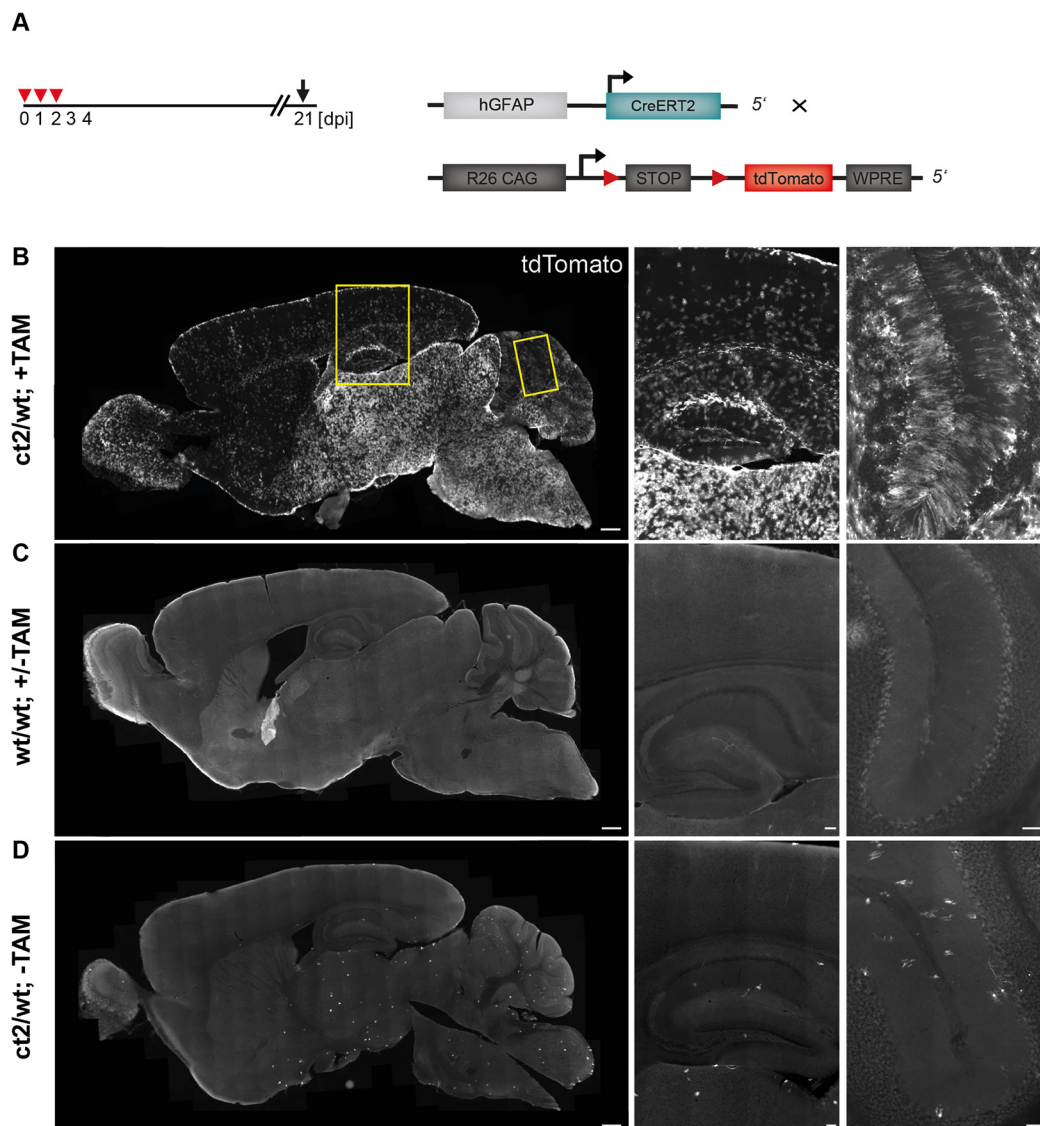


**Figure 22. Fewer cells expressed tdTomato in GFAP-Cre<sup>ERT2</sup> mice**

(A) GFAP-Cre<sup>ERT2</sup> mice were crossbred to the reporter line Rosa26-tdTomato, injected with TAM (positive control) at an age of four weeks and analyzed 21 dpi. (B-D) Sagittal brain slices with three different Cre<sup>ERT2</sup> genotypes and magnification of cortex and cerebellum. (B) The positive con (ct2/wt/+TAM) revealed a similar expression pattern to GCaMP3 in astrocytes but less bright. (C) No reporter expression was detected in negative con (wt/wt/ $\pm$ TAM). (D) Heterozygous non-induced animals (ct2/wt/-TAM) showed almost no tdTomato reporter positive cells in forebrain, midbrain and cerebellum. Here, the original tdTomato signal without additional staining is depicted. ctx: cortex; cc: corpus callosum; hc: hippocampus; cb: cerebellum. Scale bars correspond to 500  $\mu$ m in sagittal overviews and 100  $\mu$ m in magnifications, respectively.

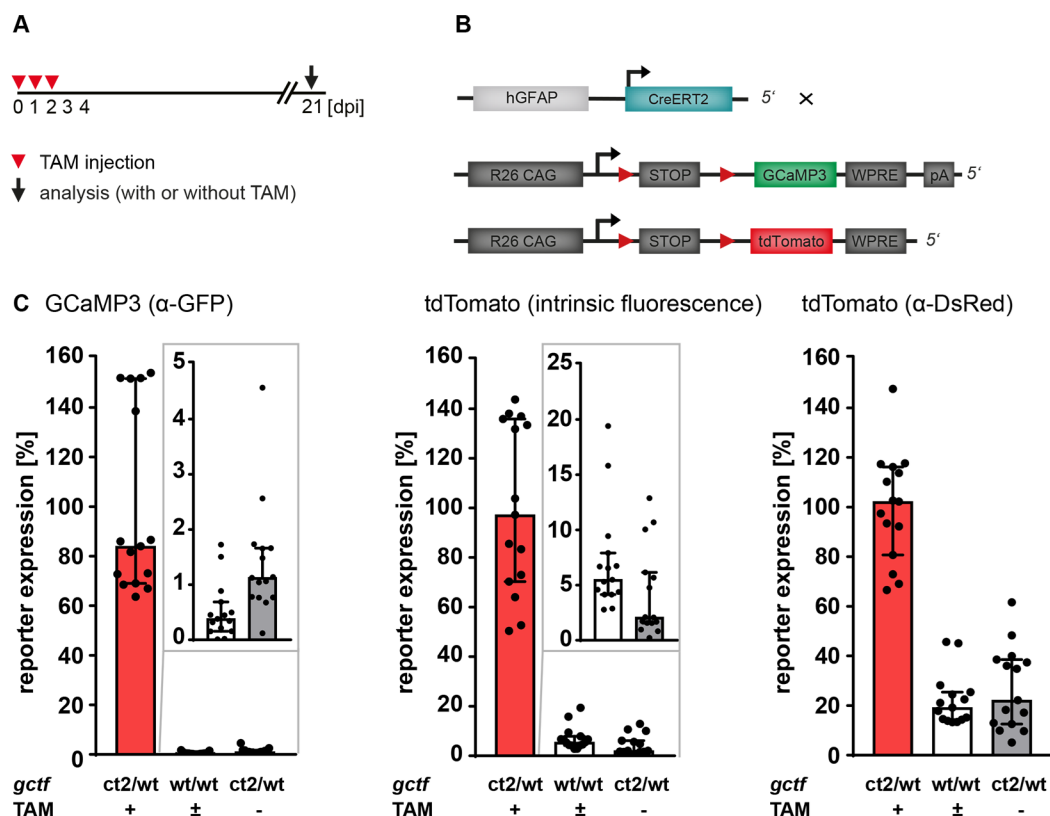


**Figure 23. Quantification of low reporter expression after tamoxifen-independent recombination in GFAP-Cre<sup>ERT2</sup> mice**

(A) Animals were injected with TAM at an age of four weeks for three consecutive days and analyzed 21 dpi (positive con; ct2/wt/+TAM) (B) GFAP-Cre<sup>ERT2</sup> driver lines were crossbred to reporter lines GCaMP3 and tdTomato. (C) Comparison of reporter expression in GFAP-Cre<sup>ERT2</sup> mice (GCaMP3 (α-GFP), tdTomato, tdTomato (α-DsRed)) of positive con (ct2/wt/+TAM), negative con (wt/wt/±TAM) and the heterozygous condition (ct2/wt/-TAM). GCaMP3 expression of heterozygous non-injected animals was higher compared to negative con, while tdTomato expression was lower and α-DsRed staining revealed no difference. The error bars correlate to the median ± interquartile range of the biological replicates (n = 3), table 14 and 15.

Fluorescence intensities (median) of all mouse lines are depicted in table 14, respective statistical analysis is stated in table 15.

**Table 14. Percentage of fluorescence intensities of the GLAST-Cre<sup>ERT2</sup> and GFAP-Cre<sup>ERT2</sup> mouse lines (median; standardized to ct2/wt/+TAM)**

<b>GCaMP3</b>		<b>slc1a3 [%]</b>	<b>gctf [%]</b>
ct2/wt	+ TAM	102.4	84.0
wt/wt	± TAM	1.9	0.4
ct2/wt	- TAM	9.3	1.1
ct2/ct2	- TAM	10.0	-
<b>tdTomato</b>		<b>slc1a3 [%]</b>	<b>gctf [%]</b>
ct2/wt	+ TAM	101.1	97.2
wt/wt	± TAM	0.7	5.5
ct2/wt	- TAM	5.3	2.1
ct2/ct2	- TAM	9.7	-
<b>tdTomato</b>		<b>slc1a3 α-DsRed [%]</b>	<b>gctf α-DsRed [%]</b>
ct2/wt	+ TAM	100.6	102.2
wt/wt	± TAM	8.6	19.2
ct2/wt	- TAM	16.8	22.1
ct2/ct2	- TAM	30.1	-

**Table 15. Statistical comparison of the different mouse lines and Cre<sup>ERT2</sup> genotypes**

	<b>Genotype</b>	<b>TAM</b>	<b>wt/wt / ±TAM</b>	<b>ct2/wt / -TAM</b>	<b>ct2/ct2 / -TAM</b>
<b>GLAST-Cre<sup>ERT2</sup>/GCaMP3</b>	ct2/wt	(+)	****	****	****
	wt/wt	(±)		****	****
	ct2/wt	(-)			ns (p=0.0555)
<b>GLAST-Cre<sup>ERT2</sup>/tdTomato</b>	ct2/wt	(+)	****	****	****
	wt/wt	(±)		****	****
	ct2/wt	(-)			***
<b>GLAST-Cre<sup>ERT2</sup>/α-DsRed</b>	ct2/wt	(+)	****	****	****
	wt/wt	(±)		***	****
	ct2/wt	(-)			****
<b>GFAP-Cre<sup>ERT2</sup>/GCaMP3</b>	ct2/wt	(+)	****	****	
	wt/wt	(±)		**	
<b>GFAP-Cre<sup>ERT2</sup>/tdTomato</b>	ct2/wt	(+)	****	****	
	wt/wt	(±)		*	
<b>GFAP-Cre<sup>ERT2</sup>/α-DsRed</b>	ct2/wt	(+)	****	****	
	wt/wt	(±)		ns (p=0.3629)	

### 6.2.2. Quantitative real time PCR analysis of the same mouse lines confirm results of Orbit image quantification

Tamoxifen-independent recombination was additionally investigated by qRT-PCR analysis. Separately analysis of cortex and cerebellum was performed to address regional expression differences. Cortex and cerebellum of the GLAST-Cre<sup>ERT2</sup> x and GFAP-Cre<sup>ERT2</sup> x Rosa26-GCaMP3 mouse line were dissected and genomic DNA isolated (Fig. 24 A, B). The same three/four groups of animals were investigated: (1) ct2/wt/+TAM, (2) wt/wt/±TAM, (3) ct2/wt/-TAM and (4) ct2/ct2/-TAM by gain of function qRT-PCR. All animals were homozygously floxed for the *gcamp3* alleles. Data were normalized to tamoxifen-injected animals (positive control/ ct2/wt/+TAM (1)) as for the immunohistochemistry quantification (Orbit). Wildtype animals for Cre<sup>ERT2</sup> (wt/wt/±TAM (2)), were used as negative controls. All negative controls of the gene loci in cortex and cerebellum showed less than 0.5 % recombination and were therefore estimated as not recombined.

GLAST-Cre<sup>ERT2</sup> induced reporter expression revealed in non-induced heterozygous animals (ct2/wt/-TAM) only 1.7 % recombined cortical *gcamp3* alleles, while in homozygous (ct2/ct2/-TAM) animals around 14 % were recombined. A higher tamoxifen-independent cerebellar recombination was detected as already seen in the IHC data (Fig. 18, 19). Cerebellar homozygous non-induced (ct2/ct2/-TAM) animals reached similar recombination of floxed alleles (63 %) as the injected positive controls (ct2/wt/+TAM). Heterozygous animals showed recombination of 22 % floxed alleles with a high SD (± 15) (Fig. 24 C, Table 16).

In contrast, GFAP-Cre<sup>ERT2</sup> induced GCaMP3 expression was absent in cortex and cerebellum of non-injected animals. In cortex, heterozygous non-induced animals revealed 0.16 %, in the cerebellum 0.4 % recombined *gcamp3* alleles (Fig. 24 D, Table 16).

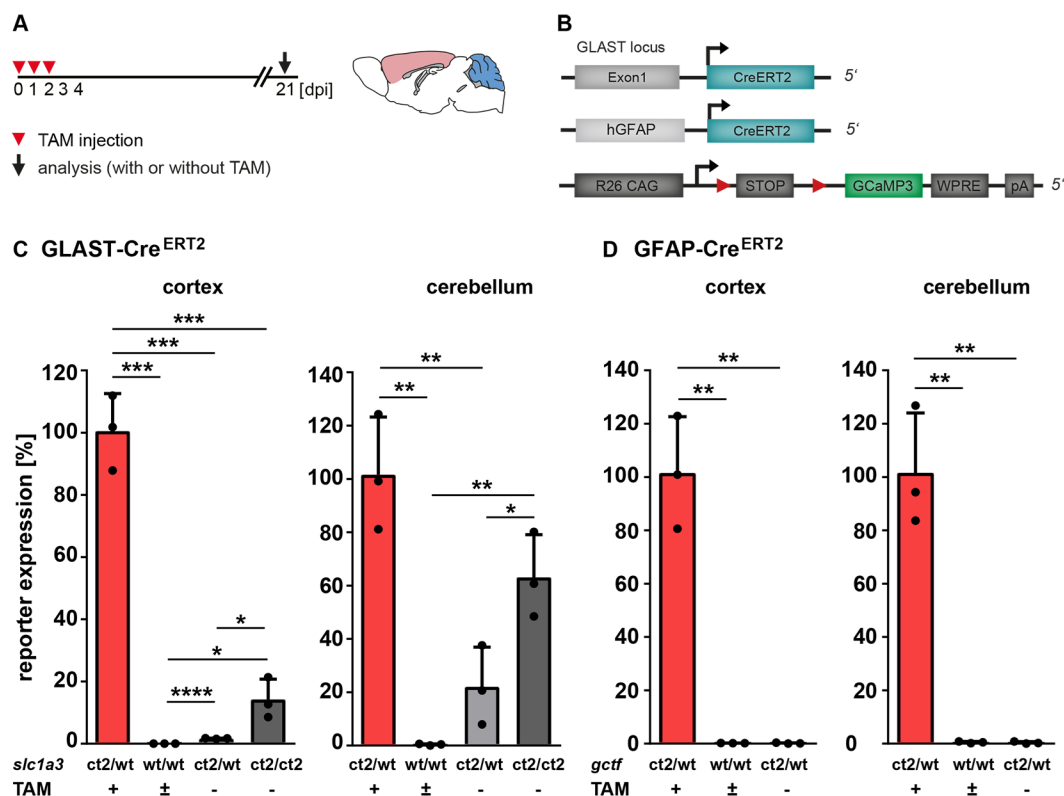


**Figure 24. Primarily GLAST-Cre<sup>ERT2</sup> driven tamoxifen-independent recombination of the reporter GCaMP3 in the cerebellum**

(A) Mice were injected with TAM at an age of four weeks and were analyzed 21 dpi. (B) GLAST-Cre<sup>ERT2</sup> and GFAP-Cre<sup>ERT2</sup> crossbred to the Rosa26-GCaMP3 line. (C, D) Quantitative real-time PCR results of *gcamp3* recombination in cortex and cerebellum. Three/four groups of animals, depending on the mouse line, were investigated: (1) ct2/wt/+TAM, (2) wt/wt/±TAM, (3) ct2/wt/-TAM and (4) ct2/ct2/-TAM. (C) Cortical tamoxifen-independent recombination revealed less than 2 % recombined *gcamp3* alleles in heterozygous animals, while homozygous animals revealed 14 %. In the cerebellum 22 % (ct2/wt/-TAM) and 63 % (ct2/ct2/-TAM) floxed alleles were recombined, respectively. Homozygous non-induced animals revealed similar cerebellar recombination efficiencies as TAM-induced mice (ct2/wt/+TAM), while cortical non-induced recombination was negligible. (D) Minor GFAP-Cre<sup>ERT2</sup> driven, non-induced recombination of *gcamp3* alleles in heterozygous animals in cortex and cerebellum. Three animals were analyzed per group and  $\Delta$ CT-values were normalized to the mean value of animals which received 3x TAM (table 16). The error bars correlate to the SD of the biological replicates (n = 3, \* p < 0.05, \*\* p < 0.01, \*\*\* p < 0.001, unpaired t-test).



**Table 16. GLAST-Cre<sup>ERT2</sup> and GFAP-Cre<sup>ERT2</sup> driven recombination of *gcamp3* alleles**

		<b>GLAST-Cre<sup>ERT2</sup> ctx</b>	<b>GFAP-Cre<sup>ERT2</sup> ctx</b>
ct2/wt	+ TAM	101 ± 12	102 ± 21
wt/wt	± TAM	0.03 ± 0.02	0.2 ± 0.02
ct2/wt	- TAM	1.7 ± 0.1	0.2 ± 0.09
ct2/ct2	- TAM	14.2 ± 6.6	-
		<b>GLAST-Cre<sup>ERT2</sup> cb</b>	<b>GFAP-Cre<sup>ERT2</sup> cb</b>
ct2/wt	+ TAM	102 ± 22	102 ± 22
wt/wt	± TAM	0.4 ± 0.3	0.5 ± 0.3
ct2/wt	- TAM	22 ± 15	0.2 ± 0.09
ct2/ct2	- TAM	63 ± 16	-

In addition, GLAST-Cre<sup>ERT2</sup> x P2Y1<sup>fl/fl</sup> x Gria1<sup>fl/fl</sup> x Rosa26-GCaMP3 mice were investigated (Fig. 25 A; B) to evaluate the extent of non-induced recombination on floxed target alleles. As shown before, recombination efficiencies of floxed alleles differ after tamoxifen-induced recombination. All animals were homozygously floxed for *p2ry1*, *gria1* and *gcamp3* and the same Cre<sup>ERT2</sup> genotypes were analyzed as described before. Tamoxifen-independent recombination of the *p2ry1* locus was almost absent in the cortex (0.5 % recombined alleles in heterozygous non-induced mice (ct2/wt/-TAM) and 4 % in homozygous non-induced mice (ct2/ct2/-TAM)) (Fig. 25 C). Higher recombination was detected in the cerebellum of non-injected animals for *p2ry1*, with around 6 % recombined alleles in heterozygous (ct2/wt/-TAM), and almost three times more (16.5 %) recombined alleles in homozygous (ct2/ct2/-TAM) animals without TAM (Fig. 25 D). Cerebellar recombination was twelve times higher in heterozygous (ct2/wt/-TAM) mice and four times higher in homozygous mice (ct2/ct2/-TAM) compared to cortical recombination, respectively. TAM-induced recombination of the *gria1* locus was, compared to *p2ry1*, less efficient (Fig. 14). Lower recombination was also observed for non-induced recombination. At the *gria1* locus non-injected animals (ct2/wt or ct2/ct2) showed no cortical recombination (Fig. 25 C). Cerebellar recombination of the *gria1* locus was also negligible in heterozygous and homozygous non-induced mice ( $\leq 1$  %) (Fig. 25 D). Only 1.7 % of cortical GCaMP3 alleles were recombined in non-injected heterozygous animals (ct2/wt/-TAM), whereas almost 10 % of the alleles were recombined in the cortex of homozygous animals without TAM (ct2/ct2/-TAM) (Fig. 25 C). These data are well in line with reporter recombination data of the GLAST-Cre<sup>ERT2</sup> line (Fig. 24 C). Explicit higher recombination efficiencies were



found for the reporter in GLAST-Cre<sup>ERT2</sup> x P2Y1<sup>fl/fl</sup> x Gria1<sup>fl/fl</sup> mice compared to GLAST-Cre<sup>ERT2</sup> mice. In the cerebellum, one quarter (26.5 %) of the alleles was recombined in heterozygous animals without TAM (ct2/wt/-TAM). GLAST homozygous animals without injection (ct2/ct2/-TAM) showed a very high recombination rate of GCaMP3 alleles, revealing no difference to the positive control (Fig. 25 D). Similar results were found for the GLAST-Cre<sup>ERT2</sup> mouse line, revealing 22 % and 63 % recombined reporter alleles in heterozygous and homozygous mice, respectively. Recombination efficiency of homozygous mice reached comparable levels as the positive control. All these data show a higher recombination rate of the reporter in the cerebellum compared to cortex for the three floxed alleles, while target gene alleles remained unaffected. Mean values  $\pm$  SD and statistical analysis are stated in table 17 and 18, respectively.

In summary, non-induced recombination rate of the cerebellum was higher than cortical recombination and more *p2ry1* alleles were recombined compared to *gria1* alleles without TAM. These data represent the same tendencies already observed in data of the tamoxifen-induced recombination. Negligible target allele recombination (*p2ry1*, *gria1*) was found for the cortex without TAM. For following experiments, mainly performed in the cortex, non-induced recombination could be neglected.

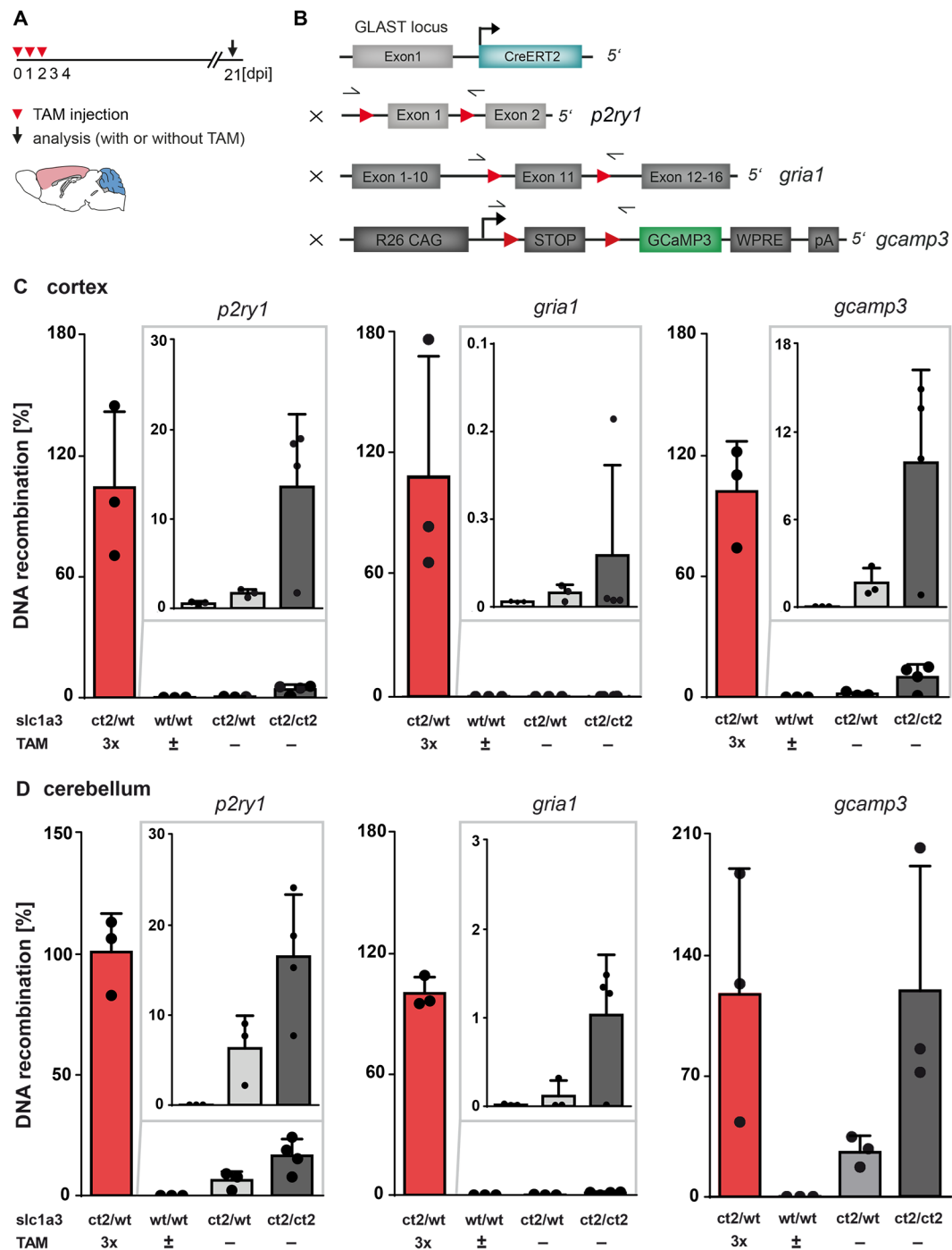


**Figure 25. Tamoxifen-independent recombination of the floxed reporter**

(A) Mice were injected with TAM at an age of four weeks and analyzed 21 dpi. (B) Constructs of GLAST-Cre<sup>ERT2</sup> x P2Y1<sup>fl/fl</sup> x Gria1<sup>fl/fl</sup> x Rosa26-GCaMP3 line with location of respective gain of function primers for qRT-PCR. (C) Four groups of animals were investigated: (1) ct2/wt+TAM, (2) wt/wt±TAM, (3) ct2/wt-TAM and (4) ct2/ct2-TAM. Cortical tamoxifen-independent recombination was almost absent in GLAST heterozygous animals of all investigated floxed loci. In GLAST homozygous non-injected animals around 4 % *p2ry1* alleles and 10 % *gcamp3* alleles were recombined.

The *gria1* locus was not recombined in ct2/wt/-TAM (3) and ct2/ct2/-TAM (4) mice. (D) Cerebellar qRT-PCR results of the same animals. Tamoxifen-independent recombination in GLAST heterozygous animals revealed recombination of about 6 % for *p2ry1*, 0.1 % for *gria1* and 27 % for *gcamp3* alleles. In GLAST homozygous animals without TAM 17 % of *p2ry1*, 1.0 % of *gria1* and 120 % of *gcamp3* alleles were recombined. Three animals were analyzed per group and  $\Delta$ CT-values were normalized to the mean value of animals which received 3x TAM. The error bars correlate to the SD of the biological replicates (n = 3, \* p < 0.05, \*\* p < 0.01, \*\*\* p < 0.001, unpaired t-test, table 17).

**Table 17. Recombination of floxed *p2ry1*, *gria1* and *gcamp3* alleles in ctx and cb**

		<i>p2ry1</i> ctx	<i>gria1</i> ctx	<i>gcamp3</i> ctx
ct2/wt	+ TAM	104 ± 38	110 ± 59	102 ± 25
wt/wt	± TAM	0.2 ± 0.1	0.01 ± 0.0	0.03 ± 0.0
ct2/wt	- TAM	0.5 ± 0.1	0.02 ± 0.01	1.7 ± 1.0
ct2/ct2	- TAM	4.1 ± 2.4	0.01 ± 0.0	9.9 ± 6.4
		<i>p2ry1</i> cb	<i>gria1</i> cb	<i>gcamp3</i> cb
ct2/wt	+ TAM	101 ± 9	100 ± 8	118 ± 72
wt/wt	± TAM	0.01 ± 0.0	0.02 ± 0.01	0.03 ± 0.0
ct2/wt	- TAM	6.3 ± 3.6	0.12 ± 0.18	26.5 ± 8.8
ct2/ct2	- TAM	16.5 ± 6.9	1.03 ± 0.7	120 ± 71

**Table 18. Statistical comparison of the floxed alleles with different GLAST genotype**

	Genotype	TAM	wt/wt / ±TAM	ct2/wt / -TAM	ct2/ct2 / -TAM
<i>p2ry1</i> ctx	ct2/wt	(+)	**	**	**
	wt/wt	(±)		*	*
	ct2/wt	(-)			ns (p=0.0563)
<i>p2ry1</i> cb	ct2/wt	(+)	***	***	***
	wt/wt	(±)		*	**
	ct2/wt	(-)			ns (p=0.0703)
<i>gria1</i> ctx	ct2/wt	(+)	*	*	*
	wt/wt	(±)		ns (p=0.1349)	ns (p=0.1390)
	ct2/wt	(-)			ns (p=0.1805)
<i>gria1</i> cb	ct2/wt	(+)	****	****	****
	wt/wt	(±)		ns (p=0.3861)	ns (p=0.0535)
	ct2/wt	(-)			ns (p=0.0770)
<i>gcamp3</i> ctx	ct2/wt	(+)	**	**	***
	wt/wt	(±)		*	*
	ct2/wt	(-)			ns (p=0.0822)
<i>gcamp3</i> cb	ct2/wt	(+)	*	ns (p=0.0947)	ns (p=0.9748)
	wt/wt	(±)		**	*
	ct2/wt	(-)			ns (p=0.0878)

### 6.2.3. Pathological conditions can trigger tamoxifen-independent recombination in GFAP-Cre<sup>ERT2</sup> mice

GFAP upregulation was induced by two independent pathological models: (1) stab wound injury (SWI) model and (2) cuprizone treatment. To prove that pathological conditions can induce tamoxifen-independent recombination, GFAP-Cre<sup>ERT2</sup> x Rosa26-tdTomato mice were analyzed after SWI (Laura Caudal, Department of Molecular Physiology). Under physiological conditions GFAP-Cre<sup>ERT2</sup> mice without TAM did not recombine. However, after SWI recombined astrocytes could be observed at the lesion site (Fig. 26 E). Another pathological model revealed similar results. Feeding cuprizone, mimics multiple sclerosis (MS) and induced recombination without TAM application in the demyelinated and astroglial activated corpus callosum of GFAP-Cre<sup>ERT2</sup> x Rosa26-tdTomato mice (Alyssa Price, Department of Molecular Physiology) (Fig. 26 D).

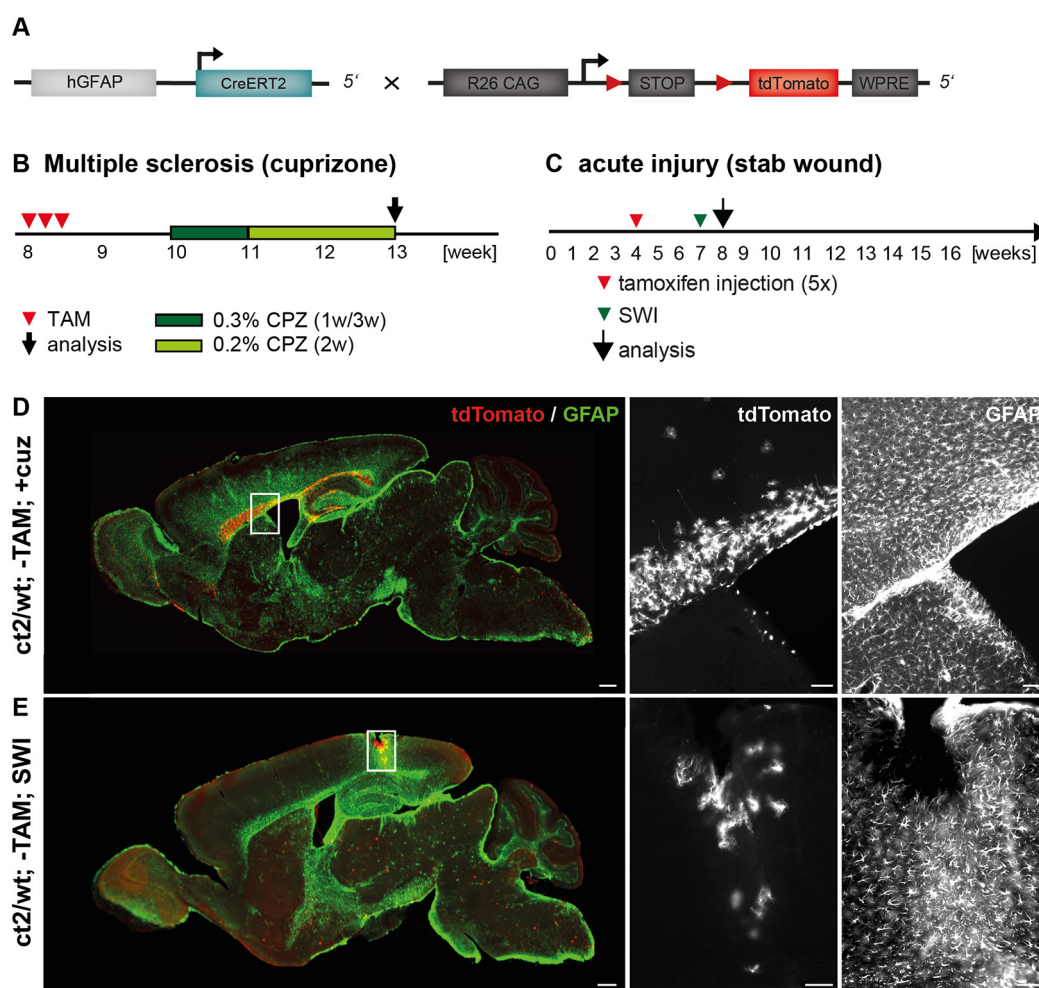


**Figure 26. Tamoxifen-independent recombination after GFAP upregulation under pathological conditions**

(A) GFAP-CreERT2 x Rosa26-tdTomato mice were investigated with two pathological models. (B) Mice were injected with TAM at an age of eight weeks for three consecutive days, treated with cuprizone to induce demyelination for three consecutive weeks and analyzed with 13 weeks. (C) The same mouse line was injected with TAM at an age of four weeks for three consecutive days. SWI was performed at an age of seven weeks and animals were analyzed seven days later. (D) Animals without TAM but with cuprizone treatment (ct2/wt/-TAM/+cuz), revealed high non-induced reporter expression in the hippocampus and particularly in the corpus callosum, where cuprizone leads to demyelination (Gudi *et al.*, 2014). (E) Mice without TAM injection but SWI showed GFAP upregulation around the lesion core, indicating tamoxifen-independent recombination under pathological conditions. Scale bars correspond to 500  $\mu$ m in sagittal overviews and 100  $\mu$ m in magnifications, respectively.

### 6.3. P2Y1 receptor cKO mice

As previously described, optimal TAM injection protocols are crucial to induce maximal DNA recombination of floxed loci. Three to five injections are sufficient to reach maximal recombination. In addition, tamoxifen-independent recombination was mainly absent in the cortex for the floxed *p2ry1* locus.

#### 6.3.1. High reduction of P2Y1R mRNA on astrocytes

Homogenates of P2Y1R cKO and control mice were analyzed for expression of *p2ry1* mRNA. After TAM application, exon 1 of the *p2ry1* gene is excised, leading to no PCR product (loss of function) (Fig. 27 B). Mice were injected for three consecutive days with TAM at an age of four weeks and were analyzed 21 dpi. mRNA was isolated from total tissue homogenates of brainstem (bs), cerebellum (cb), cortex (ctx) and hippocampus (hc) (Fig. 27 A). P2Y1 control mice without Cre<sup>ERT2</sup> expression represented 100 % mRNA expression and cKO animals were calculated accordingly. In all brain regions a reduction in mRNA expression could be achieved (22 % in bs, 63 % in cb, 50 % in ctx and 43 % in hc) (Fig. 27 C). As shown before (Fig. 16) tamoxifen-induced P2Y1R cKO also led to a reduction in all brain regions at the DNA level (23 % in bs, 6 % in cb, 20 % in ctx, 33 % in hc and 32 % in the opt).

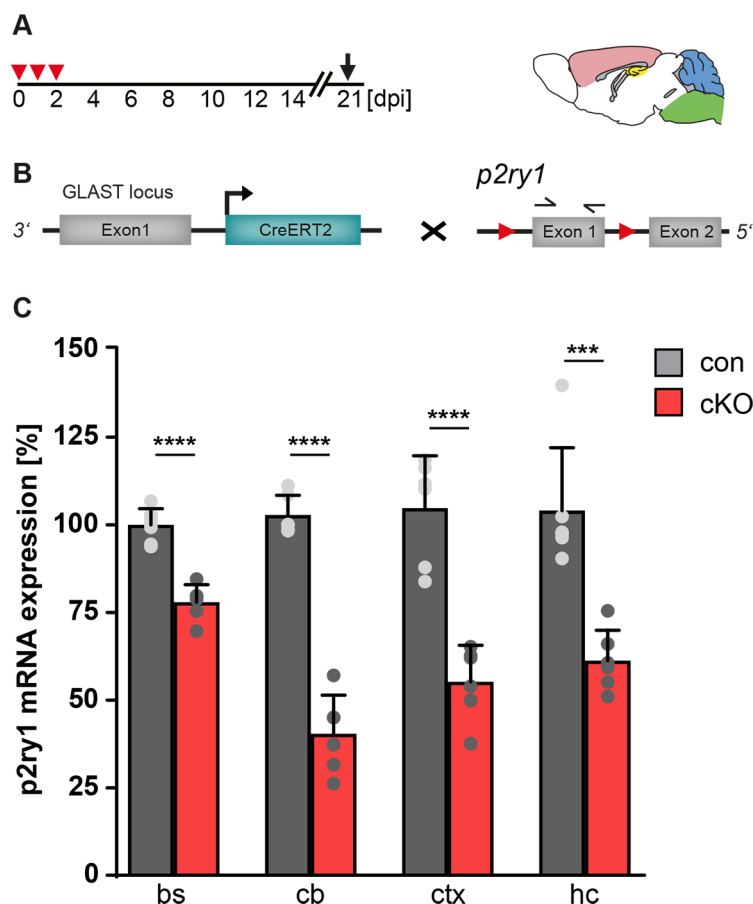


**Figure 27. Reduction of P2Y1R mRNA in homogenates of various brain regions**

(A) GLAST-Cre<sup>ERT2</sup> x P2Y1<sup>fl/fl</sup> mice were injected with TAM at an age of four weeks and analyzed 21 dpi later. (B) Primers were positioned in exon 1 of the *p2ry1* gene. Upon Cre<sup>ERT2</sup> activity exon 1 is excised and no PCR product generated. (C) Total homogenates of bs, cb, ctx and hc of con and cKO mice were analyzed. Reductions in mRNA expression to 78 % in bs, 40 % in cb, 55 % in ctx and 61 % in hc compared to con animals were detected. Six to seven animals were analyzed and  $\Delta$ CT-values were normalized to the mean value of con animals. The error bars correlate to the SD of the biological replicates (n = 6-7, \* p < 0.05, \*\* p < 0.01, \*\*\* p < 0.001, unpaired t-test).

### 6.3.2. DNA data of MACS isolated astrocytes and mRNA expression data from NGS confirm observations of total homogenates

P2Y1R ablation was additionally investigated on purified astrocytes. Astrocytes were isolated from tissue homogenates by magnetic activated cell sorting (MACS). Genomic DNA of isolated astrocytes from cKO and control mice was further analyzed by qRT-PCR to evaluate recombination efficiency of cortical and cerebellar floxed *p2ry1* loci. In addition, reduction in mRNA expression after induction of the cKO was investigated by next generation sequencing (NGS).

Controls and cKOs of GLAST-Cre<sup>ERT2</sup> x P2Y1<sup>fl/fl</sup> mice (Fig 28 B) were injected at an age of four weeks for five consecutive days and analyzed 21 dpi (Fig 28 A). Cortical and cerebellar astrocytes were separated from other cell types by MACS. Genomic DNA was isolated and further analyzed by qRT-PCR as previously described. Control animals without Cre<sup>ERT2</sup> expression represent 100 % floxed alleles (no recombination) and cKO samples were calculated accordingly (loss of function qRT-PCR strategy). Identically isolated astrocytes were diluted in RLT buffer plus and further analyzed by NGS.

In the cortex, a reduction of 60 % of floxed *p2ry1* alleles was detected in the cKO, while in the cerebellum a reduction of 30 % was determined (Fig 28 C). Compared to control animals a reduction in cKO mice could be achieved for both brain regions, but no absolute receptor ablation. Expression data of isolated astrocytes revealed a reduction of *p2ry1* mRNA of about 50 % for both investigated brain regions (Fig 28 D). In line with the DNA data, a total ablation of the P2Y1R on astrocytes could not be achieved.

In total homogenates 20 % (ctx) and 6 % (cb) reduction of *p2ry1* alleles could be detected (Fig 16 C), leading to an increase in reduction of 30 % and 24 % in MACS purified astrocytes at the DNA level, respectively.

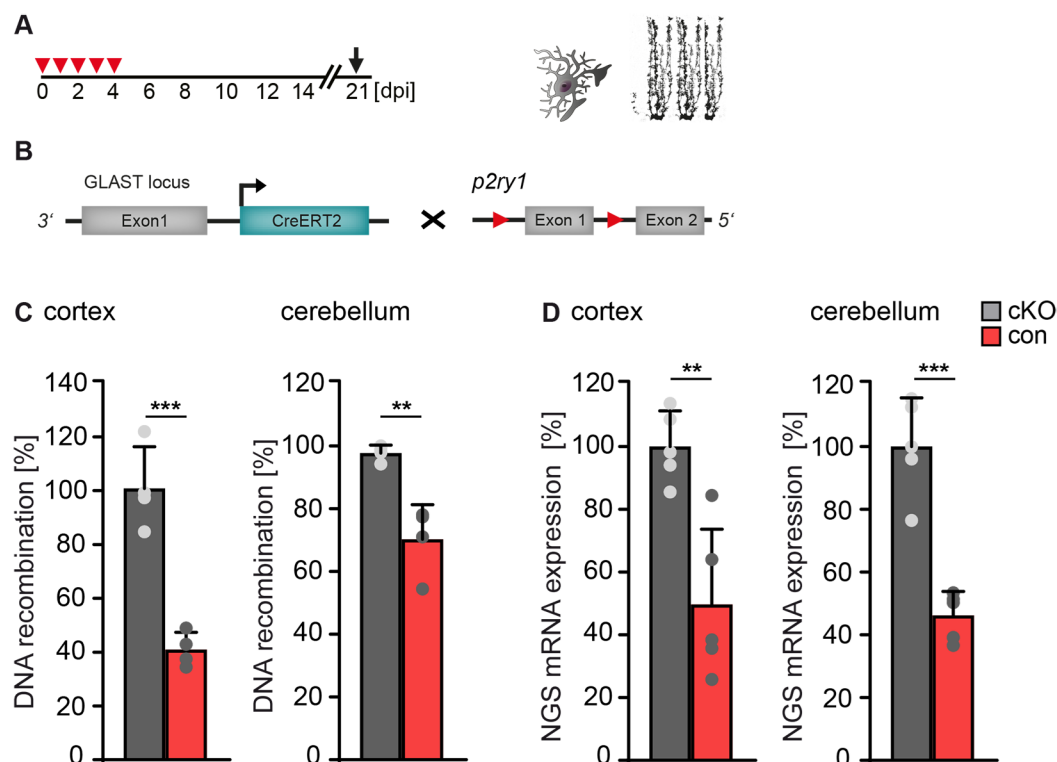


**Figure 28. Reduction of floxed *p2ry1* alleles at the DNA and mRNA level of MACS isolated astrocytes**

(A-B) GLAST-Cre<sup>ERT2</sup> x P2Y1<sup>fl/fl</sup> mice were injected at an age of four weeks with TAM for five consecutive days and were analyzed 21 dpi. (C) A reduction of floxed *p2ry1* alleles to 40 % in cortex and 70 % in cerebellum was achieved compared to con animals. (D) mRNA expression was reduced about 50 % in cKOs of cortex and cerebellum. Four con and cKO animals were analyzed and  $\Delta$ CT-values were normalized to the mean value of con animals / five animals for con and cKO were processed for NGS. The error bars correlate to the SD of the biological replicates (n = 4-5, \* p < 0.05, \*\* p < 0.01, \*\*\* p < 0.001, unpaired t-test).

The mRNA of sorted astrocytes was analyzed for expression of astroglial (Glutamate transporter-1 (Glt1), Aldehyde dehydrogenase 1 family member I1 (Aldh1l1), Glutamine synthetase (GS) and Aquaporin4 (Aqp4)), microglial (Itgam), neuronal (NeuN), NG2 glial (PDGFR $\alpha$ ) and oligodendroglial (MBP) markers, to evaluate contamination of astrocytic population with other neural cell types after sorting (Fig 29). A contamination with neurons or other glial cells could explain the incomplete P2Y1R ablation. mRNA expression was normalized to the ubiquitous astrocyte marker Glt1 and all other markers were calculated accordingly. Aldh1l1 (41 %), was less expressed compared to Glt1 (100 %), GS (140 %) and Aqp 4 (140 %). Other cell markers like Itgam (5.5 %), MBP (7.3 %), PDGFR $\alpha$  (7.3 %) and NeuN (2 %) could also be detected in the



astrocytic cell population. These data indicate a contamination of the astroglial population with microglia, neurons, NG2 glia and oligodendrocytes.

Almost the same markers (GLAST instead of Aldh111) were investigated using the NGS data. GLAST (116 %), was higher expressed compared to Glt1 (100 %), GS (26 %) and Aqp4 (29 %). The other cell markers like Itgam (0.06 %), MBP (8 %), PDGFR $\alpha$  (0.15 %) and NeuN (1.1 %) could also be detected in the astrocytic cell population. NGS data revealed lower mRNA expression of other neural cell types compared to qRT-PCR results, but also the astrocytic markers GS and Aqp4 were lower expressed. In general, we could demonstrate an enrichment of astrocytic markers, but the purity of the sorting process should be further improved.

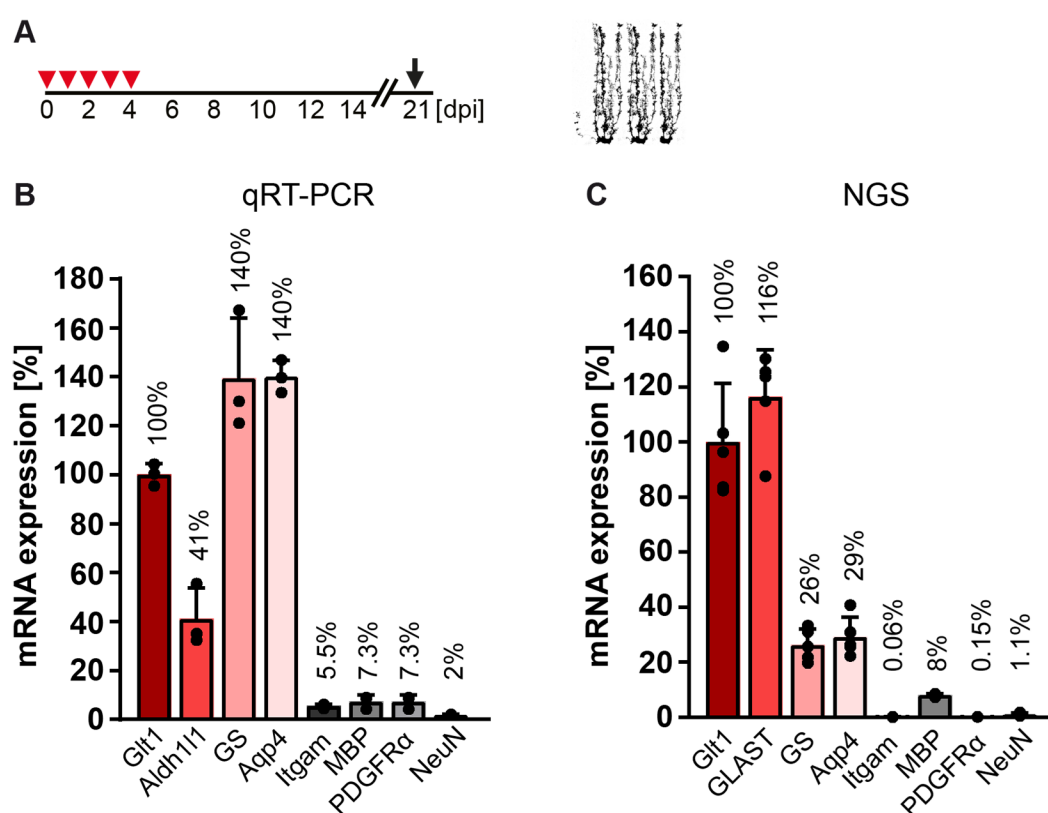


**Figure 29. Contamination of astrocytic population after MACS with microglia, neurons, NG2 glia and oligodendrocytes**

(A) Mice were injected for five consecutive days with TAM and analyzed 21 dpi. Cortical and cerebellar astrocytes were purified via MACS and analyzed by qRT-PCR or NGS. mRNA of purified astrocytes was analyzed for astrocytic, microglial, oligodendroglial, NG2 glial and neuronal cell markers. (B, C) mRNA expression of all markers was normalized to the ubiquitous astrocytic marker Glt1. Data revealed high mRNA expression of astrocytic markers, but also of other neural cells. The error bars correlate to the SD of the biological replicates (n = 3-5).

### 6.3.3. Differentially expressed genes after P2Y1R ablation

The mRNA expression profile of P2Y1R cKO and control mice was investigated by next generation sequencing (NGS) to identify changes in expression pattern of other astrocytic receptors and to determine signaling pathways involved in the adaption to the cKO condition. Cortical astrocytes were isolated by MACS as described before and samples were processed by NGS.

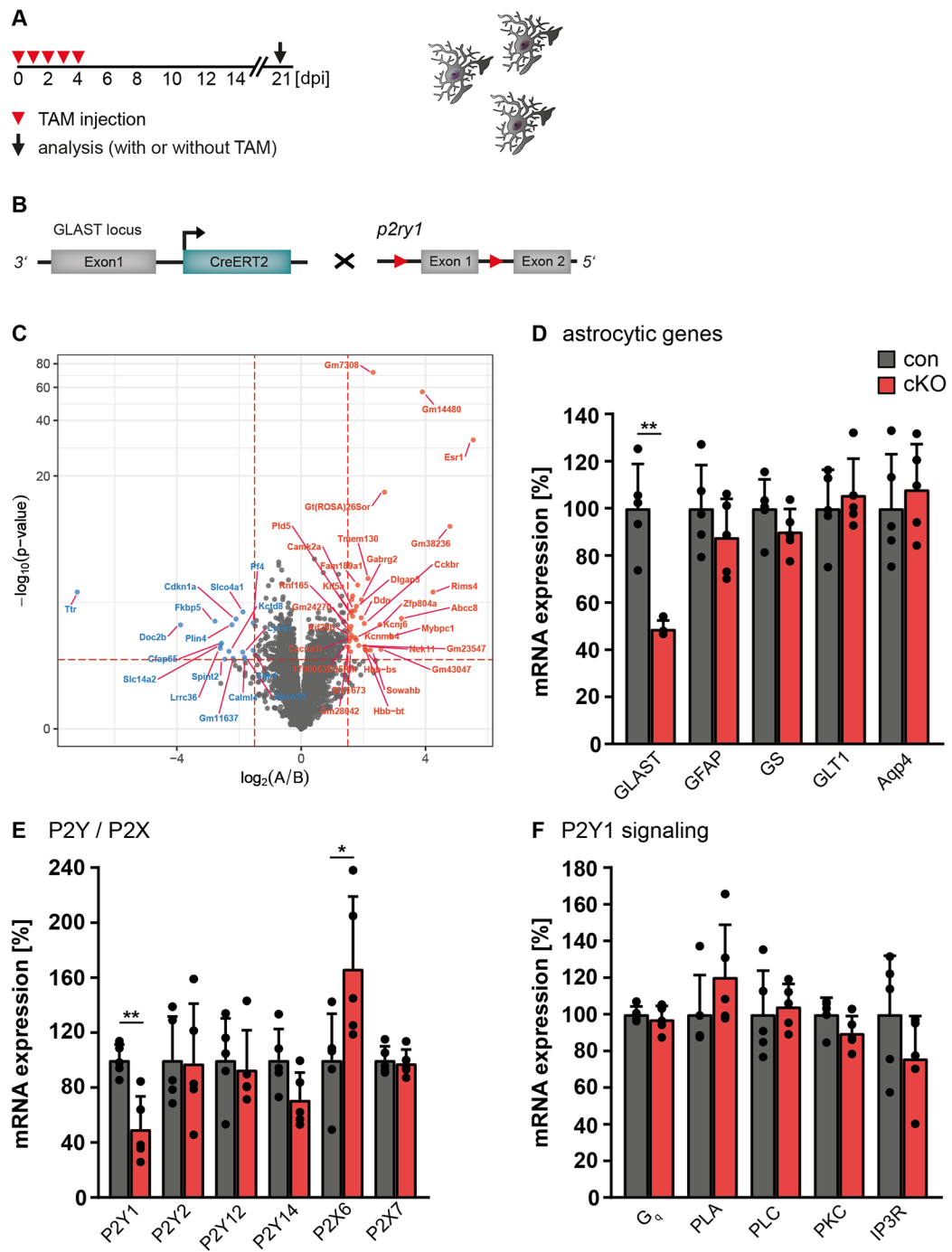
Volcano plot revealed profound differences in gene expression between control and cKO of cortical astrocytes. Several genes are differentially expressed in the cKO condition (Fig. 30 C). Some genes like *Ddn* (Dendrin) and *Rims4* (Regulating synaptic membrane exocytosis 4) were upregulated (red dots), while *Ttr* (Transthyretin), *Doc2b* (Double C2 domain beta) and *Plin4* (Perilipin 4) were downregulated (blue dots) in the cKO.

Representative astrocytic markers were not changed in cKOs, with the expected exception of the *GLAST* locus. Here, 50 % reduction was detected for the cKO due to the knockin of *Cre<sup>ERT2</sup>* (Fig. 30 D, Saab *et al.*, 2012).

Expression of several P2Y and P2X receptors were compared, revealing 50 % reduction at the *p2ry1* locus and an increase of *p2rx6* mRNA after P2Y1R ablation (Fig. 30 E). Molecules involved in the downstream signaling cascade of the P2Y1R were not altered (Fig. 30 F).

**Figure 30. Next generation sequencing revealed 50 % reduction of *p2ry1* alleles in the cKO and an upregulation of *p2rx6***

(A) Mice were injected with TAM at an age of four weeks for five consecutive days and cortical astrocytes were isolated by MACS. (B) P2Y1R cKO and control mice were analyzed by NGS. (C) Volcano plot revealed differential expressed genes (up- or downregulated) in cKO mice compared to controls. (D) High expression of astrocytic markers indicate an enriched astrocytic population. Expression of these markers were comparable between control and cKO, with exception of the *GLAST* locus. cKOs revealed a reduction of 50 %, due to the heterozygous expression of *Cre<sup>ERT2</sup>* at the *GLAST* locus. (E) Expression of P2Y1R revealed about 50 % reduction in the cKO, while other P2Y receptors remained unchanged. Expression of the P2X6 receptor was increased in the cKO, while P2X7 remained unaltered. (F) Several genes involved in P2Y1R signaling were not changed in cKO mice. Five cKO and control animals were analyzed. The error bars correlate to the SD of the biological replicates (n = 5, \* p < 0.05, \*\* p < 0.01, \*\*\* p < 0.001, unpaired t-test).



#### 6.4. Astroglial P2Y1 receptor knockout had no impact on acute injuries

The influence of the astroglial P2Y1R under pathological conditions was analyzed by stab wound injury (SWI) experiments. SWI was performed 21 d after TAM treatment and animals were analyzed 7 d post lesion (dpl) (Fig. 31 A and 33 A, respectively). Coronal vibratome sections (40  $\mu$ m) were prepared and stained with DAPI, GFP, GFAP and Iba1. P2Y1 cKO mice were crossbred with either the reporter mouse line tdTomato or GCaMP3, respectively. For controls, either littermates without Cre<sup>ERT2</sup> (tdTomato) or animals without floxed *p2ry1* alleles (GLAST-Cre<sup>ERT2</sup> x Rosa26-GCaMP3) were used (Fig 31 B and 33 B).

cKO animals showed expression of the reporter tdTomato (Fig. 31 C), whereas control animals were not recombined. GCaMP3 expressing mice were additionally stained with  $\alpha$ -GFP (Fig. 33 C (A-E)). All sections (n = 4-7; 6 sections per animal) were analyzed using the ImageJ Plugin LROI (Fig. 7). Fluorescence intensities across the lesion site of the respective reporter and the markers Iba1 for microglia and GFAP for activated astrocytes were simultaneously analyzed ipsi- and contralaterally. On the ipsilateral side the lesion core defines the mid position of the 25 ROIs (Fig. 32 and 34).

##### 6.4.1. Loss of astroglial P2Y1 receptors without impact on acute brain injury

cKO mice and controls of P2Y1<sup>fl/fl</sup> x Rosa26-tdTomato mice revealed no differences for the astroglial marker GFAP on the ipsilateral side. Both, cKO mice and controls, showed higher fluorescence intensities due to an increase in astrocyte cell number at the lesion core with a GFAP upregulation. On the contralateral side fluorescence intensities were similar without any peak in fluorescence (Fig. 32 A). The microglial marker Iba1 showed higher fluorescent intensities compared to GFAP, because more microglia cells surround the lesion site and were also equally distributed contralaterally without difference between cKO and control. Ipsilaterally, a peak in Iba1 fluorescence of cKO and control sections could be detected with no difference (Fig. 32 B). The tdTomato reporter showed a peak in cKO mice due to cell activation but no increase in fluorescence on the contralateral side. No fluorescence could be detected ipsi- and contralaterally of control (wt for Cre<sup>ERT2</sup>) mice due to no reporter expression (Fig. 32 C).

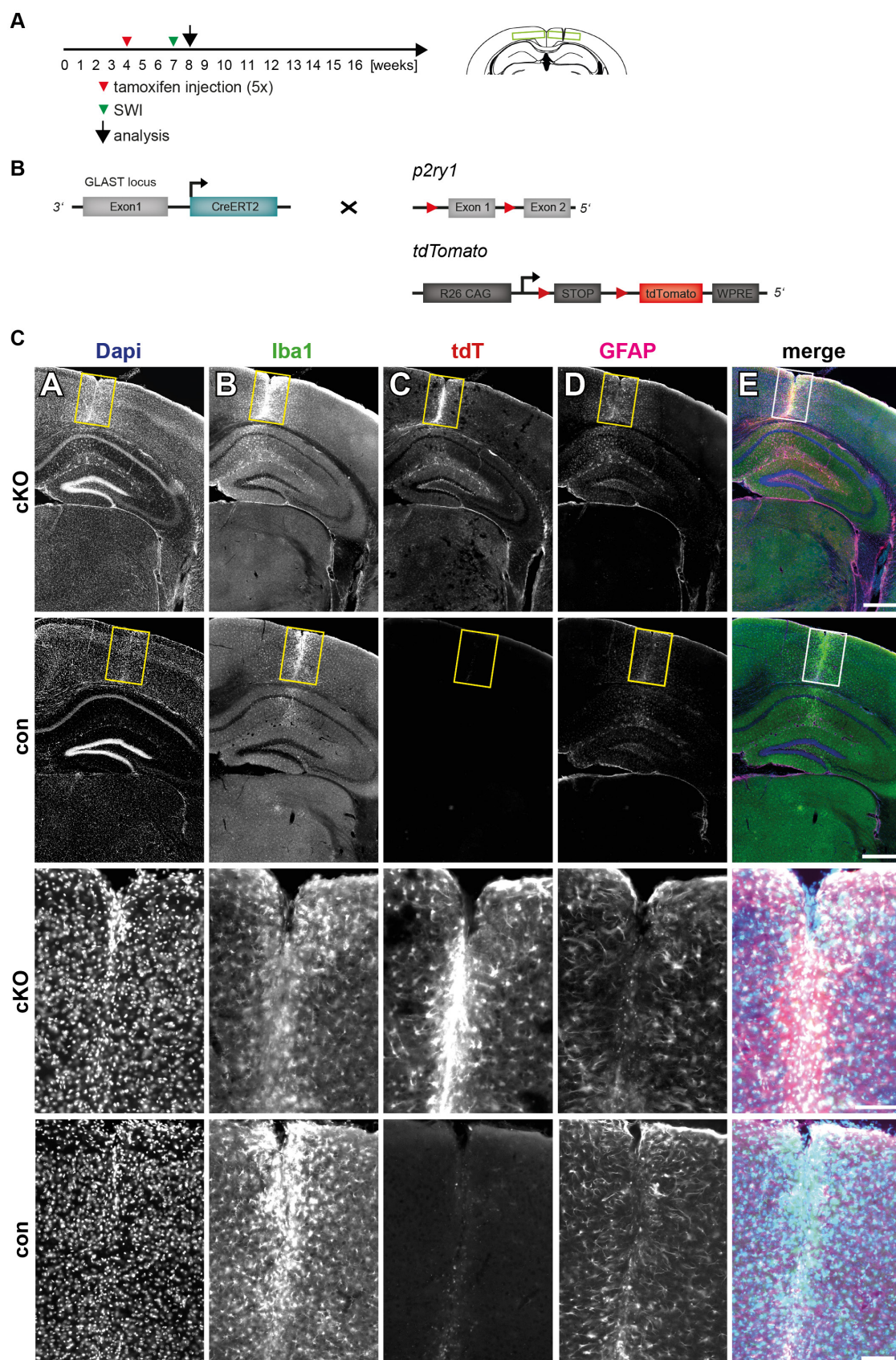


**Figure 31. No difference between cKO and control mice after SWI on glial activation**

(A) Mice were injected at the age of four weeks for three consecutive days. Stab wound injury was performed 21 dpi and mice were analyzed 7 d post lesion (dpi). Con animals did not express the reporter tdTomato (Cre<sup>ERT2</sup> negative). (B) Mouse constructs of the investigated mouse lines: GLAST-Cre<sup>ERT2</sup>, floxed P2Y1 and floxed tdTomato. (C) Frontal brain slices depicting the lesion site. Sections were stained for DAPI, Iba1 and GFAP. cKOs showed tdTomato expression, while con were reporter negative. The two upper panels depict cKO and con of overviews, lower panels the magnification of the highlighted region (yellow rectangle). An increase of cells (DAPI<sup>+</sup>) could be detected surrounding the lesion site (A) with an alike upregulation of Iba1 (B) and GFAP (D) in con and cKOs. The scale bars correspond to 500  $\mu$ m in overviews and 100  $\mu$ m in magnifications, respectively.

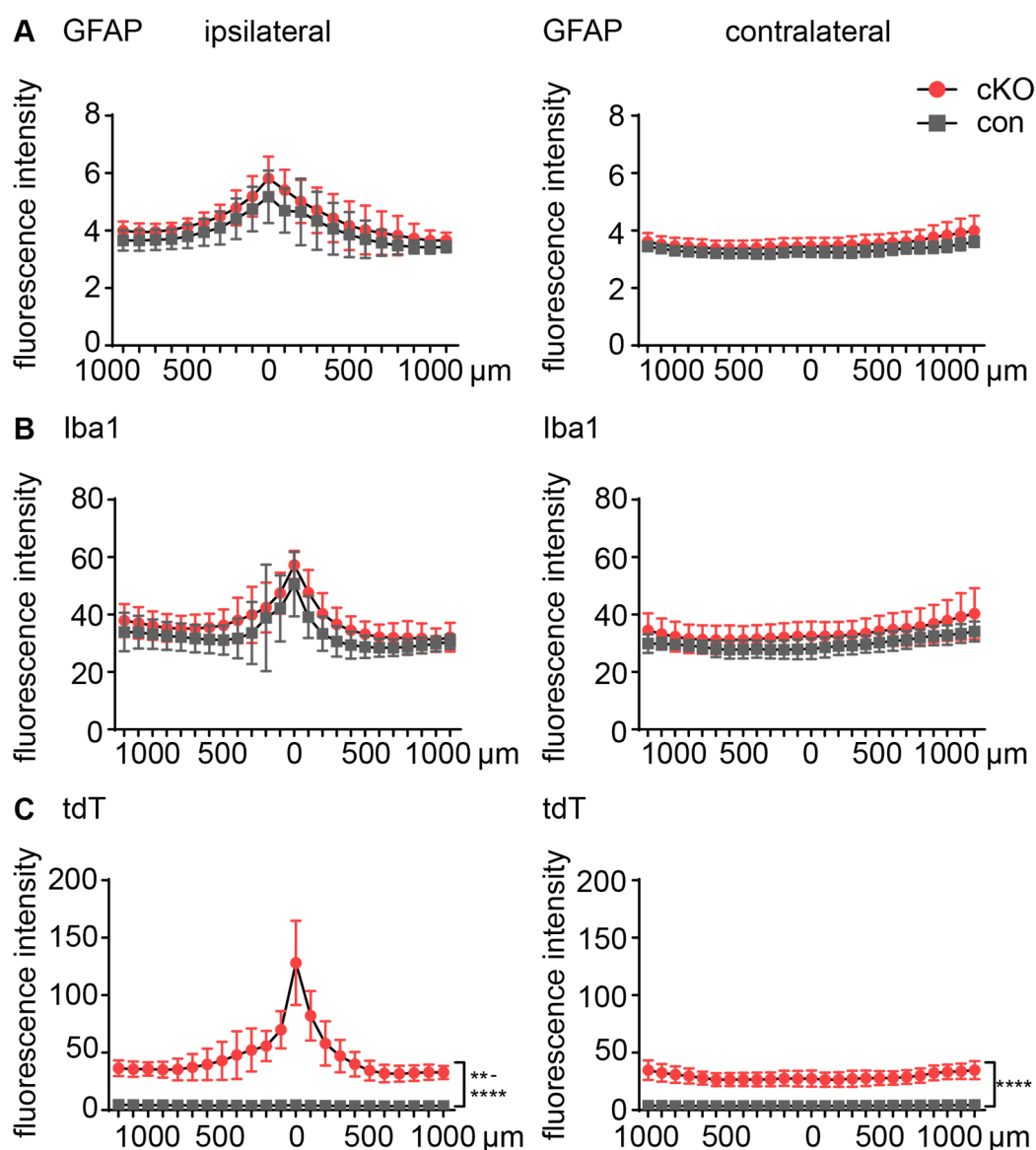




**Figure 32. Quantification of astroglial and microglial activation after acute injury revealed no differences between cKO and control mice**

Frontal slices of cKO and con were analyzed with the ImageJ plugin LRoi to calculate fluorescence intensities of 25 ROIs along the lesion site (ipsilateral) as well as on the contralateral side. Three different proteins were analyzed in parallel: GFAP, Iba1 and tdTomato. (A) Fluorescence intensities of GFAP increased ipsilaterally in cKO and con mice due to astrocytic activation. Contralaterally, fluorescence intensities of cKO and con were similar. (B) Iba1 was upregulated in the lesion site without differences between cKOs and con. (C) The reporter signal was decreased ipsilaterally and contralaterally in con due to lack of reporter expression. The cKO revealed an upregulation in fluorescence intensity at the lesion site. The error bars correlate to the SD of the biological replicates (n = 4-7, \*p<0.05, \*\*p< 0.01, \*\*\*p<0.001, 2way Anova).

**6.4.2. GCaMP3 reporter expression led to an increase in GFAP expression upon astroglial P2Y1R ablation**

The analysis of cKO and control mice by LRoi revealed ipsilaterally differences between  $\alpha$ -Iba1 and  $\alpha$ -GFAP stained sections. GFAP expression was upregulated in the lesion core of cKO sections while Iba1 expression was downregulated (Fig. 34 A, B). The reporter GCaMP3 revealed no change in fluorescence intensity in cKOs and con at the lesion site (Fig. 34 C). On the contralateral side GFAP expression was two times higher in cKO mice, while Iba1 expression was alike in cKO and control mice (Fig. 34 A, B). Contralaterally, fluorescence intensities of the reporter in cKO sections were doubled in signal intensity (Fig. 34 C) in contrast to the use of tdTomato as reporter.

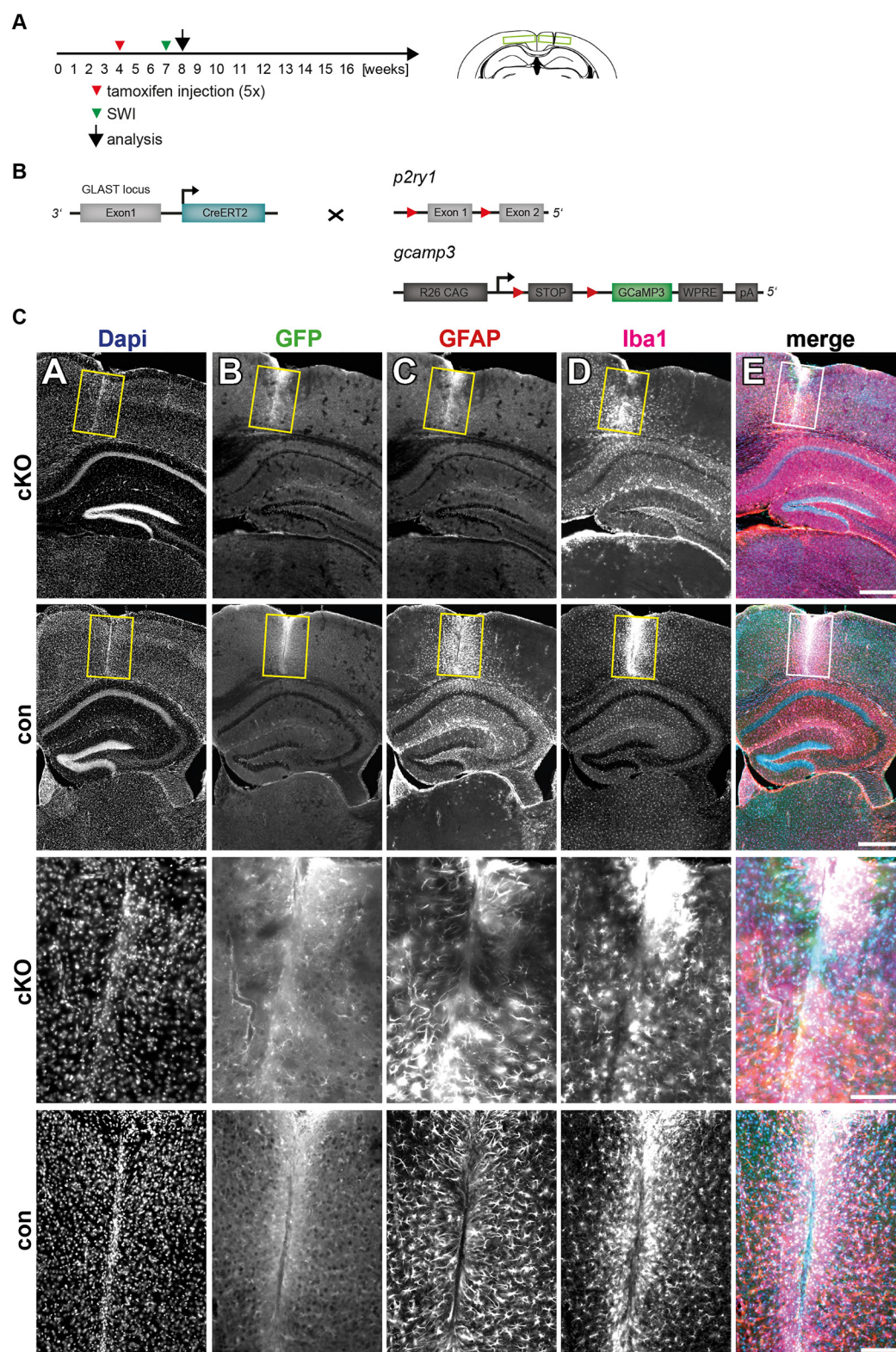




**Figure 33. Differences between cKO and control mice after SWI on glial activation when GCaMP3 is expressed**

(A) Mice were injected at an age of four weeks for three consecutive days. Stab wound injury was performed 21 dpi and mice were analyzed 7 d post lesion (dpi). (B) Mouse constructs of the investigated mouse lines: GLAST-Cre<sup>ERT2</sup>, floxed P2Y1 and floxed Rosa26-GCaMP3. Here, cKO and con mice expressed the reporter due to Cre<sup>ERT2</sup> activity and tamoxifen-induction. (C) Frontal brain slices depicting the lesion site. Sections were stained for DAPI, GFP, GFAP and Iba1. GCaMP3 was additionally stained with  $\alpha$ -GFP. The two upper panels depict cKO and con of overviews, lower panels the magnification of the highlighted region (yellow rectangle). An increase of cells (DAPI<sup>+</sup>) could be detected surrounding the lesion site (A) with an upregulation of GFAP (C) and a downregulation of Iba1 in cKOs, while GCaMP3 expression ( $\alpha$ -GFP, B) was alike in cKOs and con. The scale bars correspond to 500  $\mu$ m in overviews and 100  $\mu$ m in magnifications, respectively.

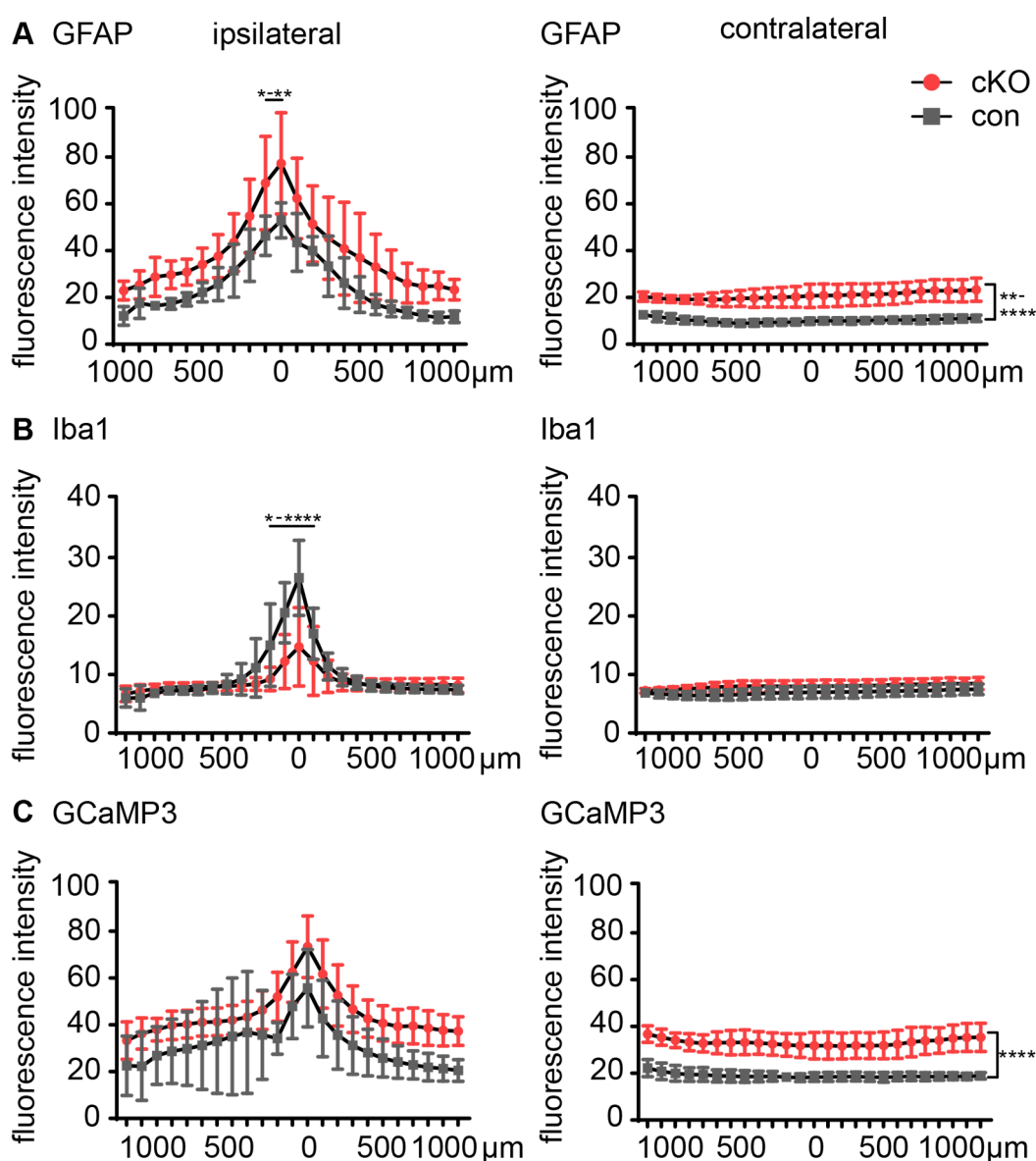


**Figure 34. GFAP upregulation ipsilaterally and contralaterally of P2Y1R cKO mice**

Frontal slices of cKO and con were analyzed with the ImageJ plugin LROI to calculate fluorescence intensities of 25 ROIs along the lesion site (ipsilateral) as well as on the contralateral side. Three different proteins were analyzed in parallel: GFAP, Iba1 and GCaMP3 ( $\alpha$ -GFP). (A) Fluorescence intensities revealed an GFAP upregulation at the lesion site of cKO and con with higher signals in cKO mice. Contralaterally, fluorescence intensities of the GFAP staining were increased in the cKO. (B) Iba1 was upregulated in the lesion site of con, while contralaterally expression was similar in cKO and con. (C) GCaMP3 ( $\alpha$ -GFP) signal revealed ipsilaterally no difference between cKO and con. Contralaterally, a higher reporter expression was detected in cKO mice. The error bars correlate to the SD of the biological replicates ( $n = 5-7$ ,  $*p < 0.05$ ,  $**p < 0.01$ ,  $***p < 0.001$ , 2way Anova).

## 6.5. $\text{Ca}^{2+}$ signaling in astrocytes

$\text{Ca}^{2+}$  signaling in astrocytes represents one of the main communication routes between astrocytes and other cells. To functionally evaluate, if this signaling is disturbed upon P2Y1R ablation, *in vivo*  $\text{Ca}^{2+}$  signals of astrocytes expressing the  $\text{Ca}^{2+}$  indicator GCaMP3 were analyzed by 2-photon laser-scanning microscopy (2P-LSM).

### 6.5.1. Smaller and shorter $\text{Ca}^{2+}$ signals in cKO mice under anesthetized and awake conditions

P2Y1R cKO and control mice were investigated by 2P-LSM to analyze changes in  $\text{Ca}^{2+}$  signaling upon P2Y1R ablation *in vivo*. Mice were injected with TAM at an age of four weeks for five consecutive days. Cranial window surgery was performed at an age of 16-20 weeks. Several imaging sessions per animal were performed and  $\text{Ca}^{2+}$  data were pooled and depicted as box plots. Investigated parameters were amplitude (signal strength) and duration (signal length).  $\text{Ca}^{2+}$  signals of analyzed astrocytes were divided into signals of the processes (gliapil) and signals of the cell bodies (soma).  $\text{Ca}^{2+}$  signals were additionally divided into three signal types that represent the magnitude of the respective signals. Therefore, each graph shows signals of the first (1 SD), second (2 SD) and third standard deviation (3 SD), representing the small, medium sized and large  $\text{Ca}^{2+}$  signals, relating to strength not size.  $\text{Ca}^{2+}$  signals were automatically classified by MSparkles. Signal amplitudes of the three classes were also analyzed for their duration. MSparkles also calculated the percentage of each  $\text{Ca}^{2+}$  signal class, resulting in the signal composition (Fig 35-37) and generated heatmaps for each analysis time point (Appendix Fig. 42).

#### **6.5.1.1. Smaller and shorter Ca<sup>2+</sup> signals in anesthetized P2Y1R cKO mice**

Animals were treated and prepared for 2P-LSM and imaging sessions were performed 3, 4, 8, 10 and 11 days after cranial window surgery (days post window surgery, dpw). During the imaging sessions animals were constantly anesthetized with 2 % isoflurane (0.8 l/min in total) (Fig 35 A).

Ca<sup>2+</sup> signals of the gliapil were smaller in their amplitudes in P2Y1 cKO mice compared to controls for all classes of Ca<sup>2+</sup> signals. Small signals were about 1.5 x smaller, while medium sized and large signals were twice as weak as the respective control signals. Signal durations were also changed in cKO mice with shortened small and medium sized signals, while large signals remained unaltered (Fig. 35 B).

Ca<sup>2+</sup> amplitudes of the soma showed similar results compared to the gliapil. In cKO all observed Ca<sup>2+</sup> signals had smaller amplitudes compared to controls. However, the duration of small and medium sized signals was not changed, while large signals were shorter in cKOs (Fig. 35 C). Signal composition of control and cKO in the gliapil revealed the highest percentage of small (1 SD) signals (52 % and 49 %, respectively) followed by medium sized (2 SD) (26 % and 29 %) and large (3 SD) signals (22 % and 22 %). Signal composition of the soma was comparable in control and cKO with 54 % and 56 % small signals, 23 % and 26 % medium sized signals and 23 % and 18 % large signals, respectively (Fig. 35 D). Overall, no differences between cKOs and controls could be found in their signal composition in soma and processes.

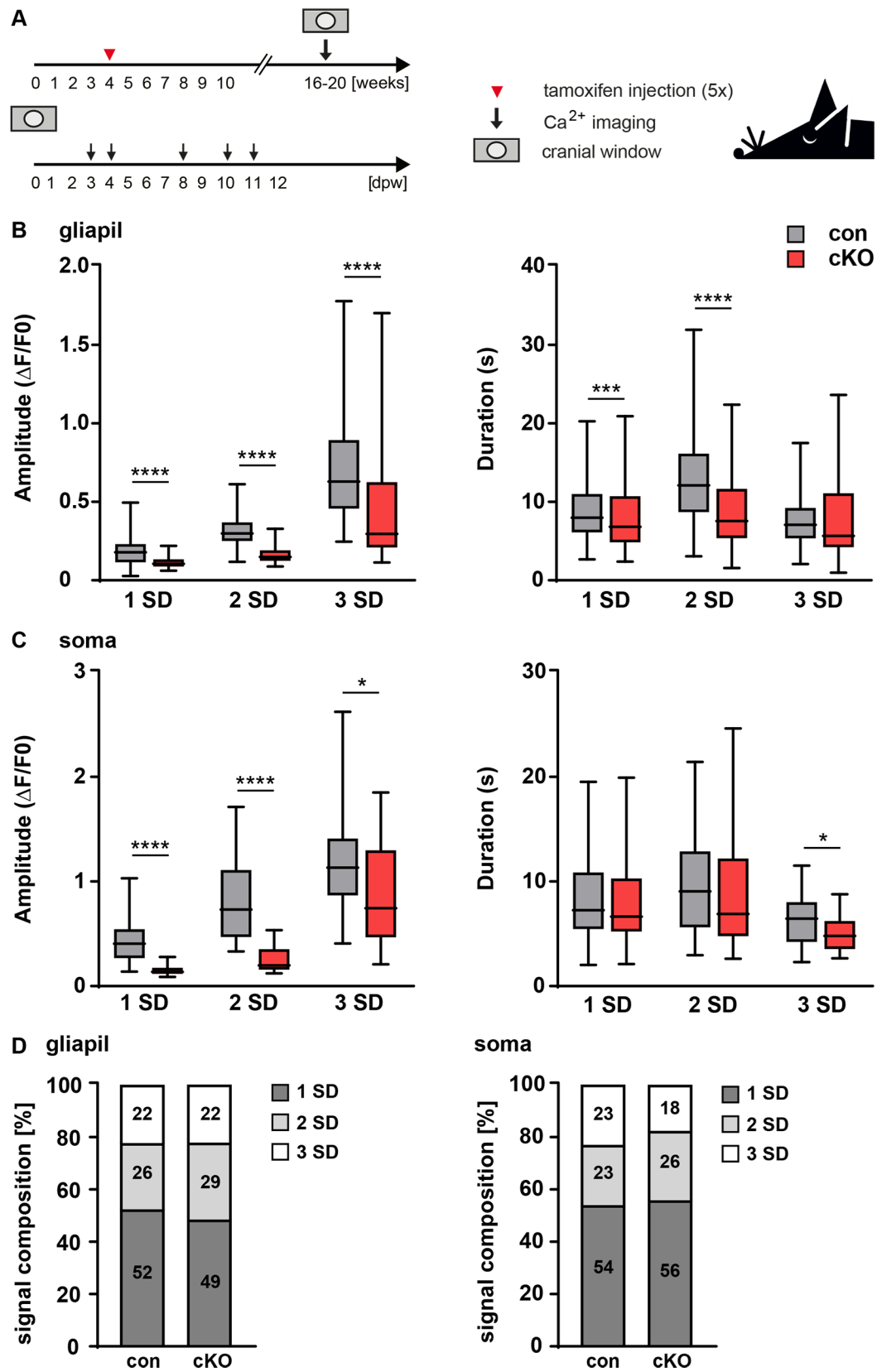


**Figure 35. Anesthetized P2Y1 cKO mice had smaller and shorter Ca<sup>2+</sup> signals in gliapil and soma**

(A) Animals were injected at an age of four weeks for five consecutive days with TAM. Cranial window surgery was performed between 16-20 weeks and imaging sessions were performed 3, 4, 8, 10 and 11 dpw. (B) Ca<sup>2+</sup> signals of the gliapil were smaller in cKO compared to con in all three classes of signals. Respective signal durations of small and medium sized signals were shorter, while large signals were not changed in P2Y1 cKO. (C) Somatic signals were smaller after astroglial P2Y1R deletion in all classes of Ca<sup>2+</sup> signals, while signal durations were shorter in large Ca<sup>2+</sup> signals and not changed in small and medium sized signals. (D) The overall signal composition revealed no difference between cKO and con in gliapil and soma with the highest percentage of small signals (1 SD) followed by medium sized and large signals. The error bars correlate to the median  $\pm$  interquartile range of the biological replicates (n = 1-2, \* p 0.01-0.05; \*\* p 0.001-0.01; \*\*\* p 0.0001-0.001; \*\*\*\* p > 0.00001, Mann-Whitney test).

**6.5.1.2. Ca<sup>2+</sup> signals of awake P2Y1R cKO mice were smaller in gliapil and soma and overall shorter**

Animals were treated and prepared for 2P-LSM as described before. Imaging sessions were performed 4, 8, 10 and 11 dpw. Before the first imaging session animals were habituated to the experimentator and the setup (Fig 8 and Fig. 36 A).

Signal strength of the gliapil was weaker in small (1 SD) and large (3 SD) Ca<sup>2+</sup> signals and not changed in medium sized (2 SD) signals of cKO. The signal duration was not changed in small signals but medium sized and large signals were shortened in P2Y1 cKO animal (Fig. 36 B). Compared to anesthetized mice, signal amplitudes of controls and cKO were generally stronger in awake mice, while signal duration was shorter or unaltered (Appendix Fig. 45). Somatic medium sized (2 SD) and large (3 SD) signals were again smaller in the cKO compared to controls, while amplitudes of small signals did not change. The length of small Ca<sup>2+</sup> signals was not changed between control and cKO mice, while the medium sized and large signals were shorter (Fig. 36 C). Comparison to anesthetized mice revealed stronger somatic signals in awake mice, while their signal duration was not changed (Appendix Fig 45). Signal composition of gliapil and soma revealed for controls the highest percentage of small signals (52 %/ 57 %) followed by medium sized (26 %/ 24 %) and large (22 %/ 19 %) signals. Small, medium sized and large signals (32 %/ 35 %, 29 %/ 30 % and 39 %/ 35 %, respectively) were equally distributed in cKO mice (Fig. 36 D). In awake mice, the signal composition changed in gliapil and soma of cKO, revealing a higher proportion of large signals and therefore less small signals, while under anesthetized conditions the signal composition remained in same proportions as controls.

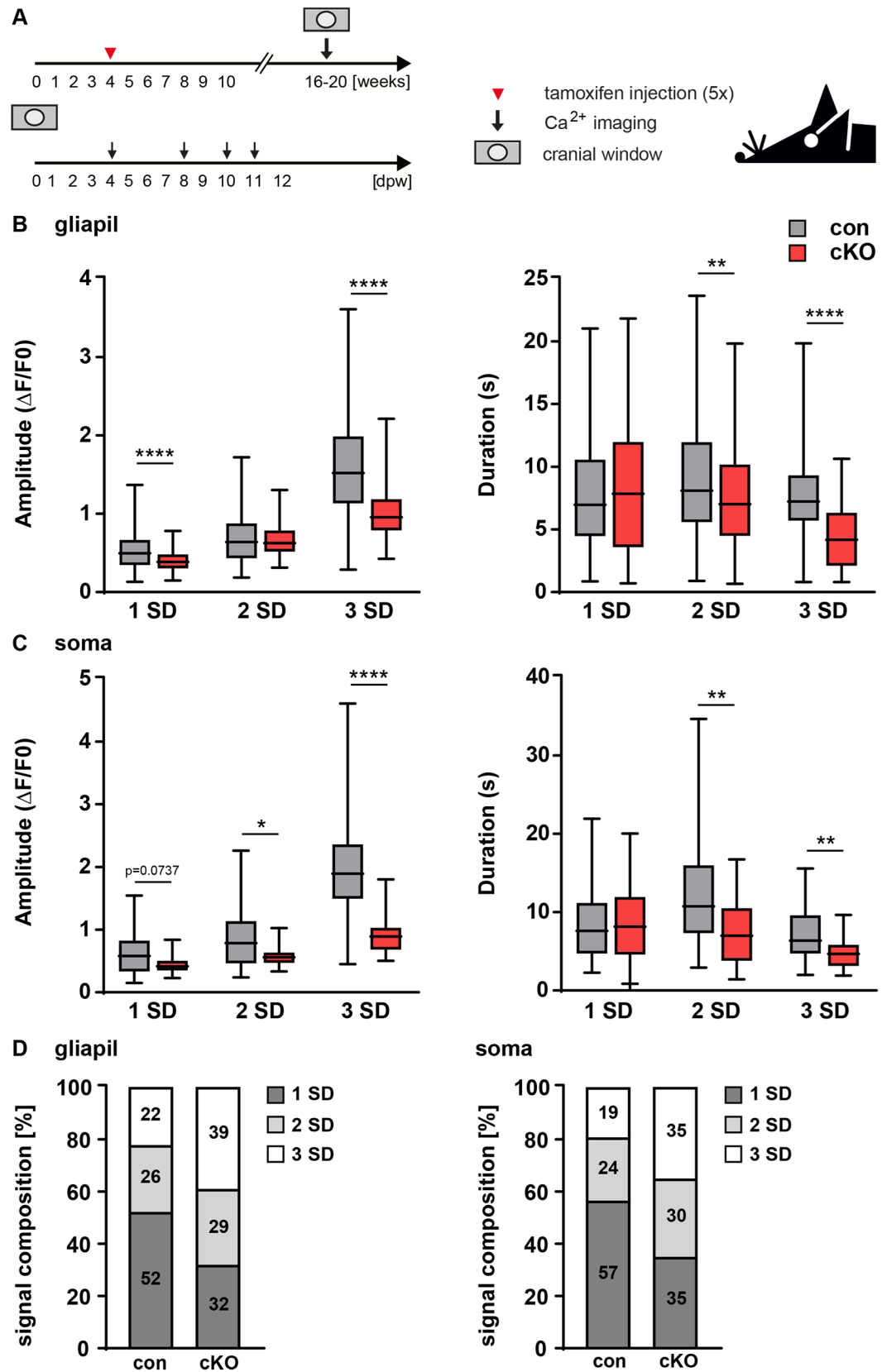


**Figure 36. Smaller and shorter Ca<sup>2+</sup> signals of awake P2Y1R cKO mice in gliapil and soma**

(A) Animals were injected at an age of four weeks for five consecutive days with TAM. Cranial window surgery was performed between 16-20 weeks and imaging sessions were performed 4, 8, 10 and 11 dpw. (B) Small and large signals of the gliapil were smaller in cKOs, whereas medium sized signals were not changed. Medium sized and large signals were shorter in cKO mice, while signal duration of small signals was not changed. (C) Somatic signals of medium sized and large signals were smaller in cKOs, but no changes occurred in small signals. The cKO had shorter medium sized and large signals, but no changes in small signals. (D) Signal composition of the cKO revealed a similar distribution of small, medium sized and large signals for gliapil and soma, while in con mice more small signals were found followed by medium sized and large signals. The error bars correlate to the median  $\pm$  interquartile range of the biological replicates (n = 1-2, \* p 0.01-0.05; \*\* p 0.001-0.01; \*\*\* p 0.0001-0.001; \*\*\*\* p > 0.00001, Mann-Whitney test).

**6.5.1.3. Stimulation of purinergic receptors by ATP application led to higher signal amplitudes under control conditions**

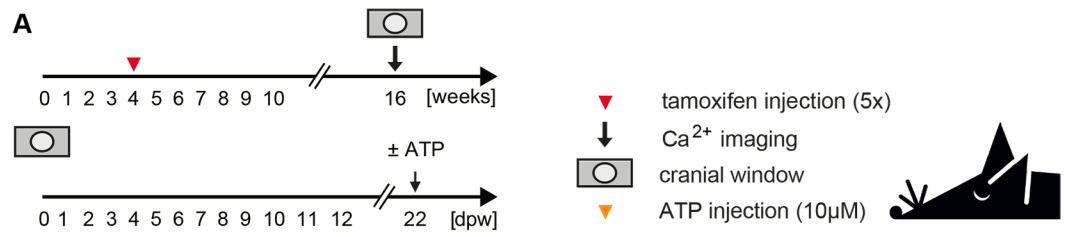
A control mouse (wt for P2Y1R) was injected at an age of four weeks with TAM for five consecutive days. Cranial window surgery was performed at an age of 16 w and the animal was imaged with and without ATP application 22 d after the surgery. The animal was anesthetized with 2 % isoflurane during imaging sessions (Fig. 37 A).

After ATP application to the brain of the control animal, Ca<sup>2+</sup> signals of all classes in the gliapil were larger. All classified signal amplitudes increased after ATP application about four to five times, while signal durations were shorter (1.5 x to 2.4 x times) (Fig. 37 B).

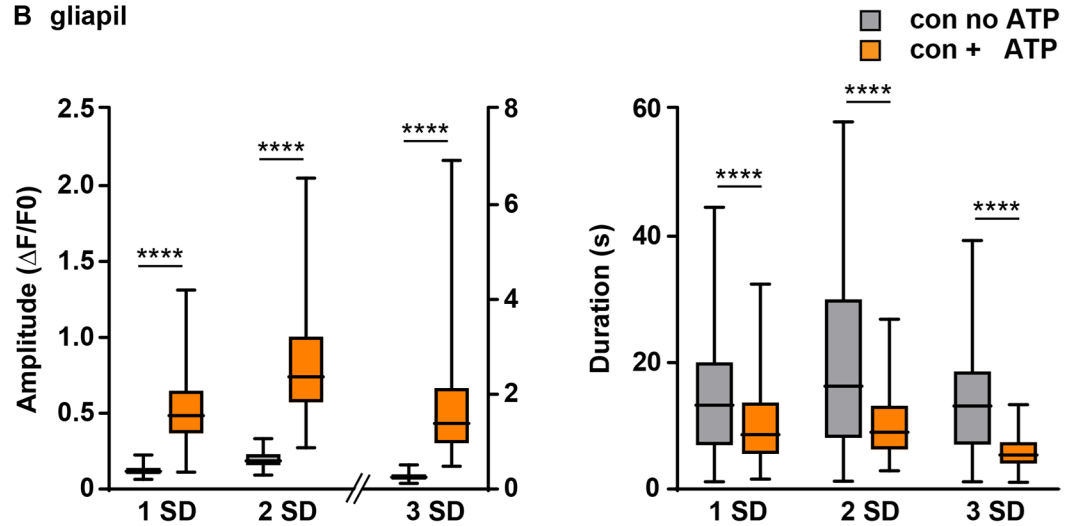
Somatic signals were increased (about 2.4 x to 4.5 x) in all classes of Ca<sup>2+</sup> signals upon ATP treatment. Duration of small and medium sized signals remained unaltered, while large signals were shorter (Fig. 37 C).

The signal composition of the gliapil revealed before ATP application similar distribution of small, medium sized and large signals as anesthetized control animals (Fig. 35 D). After ATP treatment the percentage of large (20 %) signals increased, while the percentage of small signals decreased (49 %). Highest percentage of small signals was found in the soma with or without ATP, but medium sized and large signals increased after ATP application (Fig. 37 D).

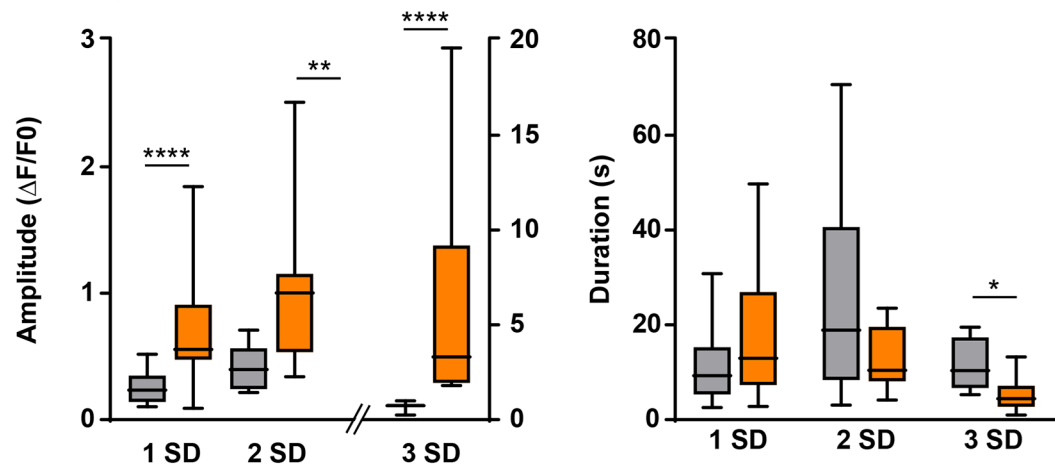
Here, we demonstrated the influence of a non-selective P2Y1R agonist on Ca<sup>2+</sup> signals in a control mouse, revealing stronger but shorter signals. The opposite effect was observed for Ca<sup>2+</sup> signals of a cKO mouse without ATP stimulation, revealing smaller signals while duration was also shortened.



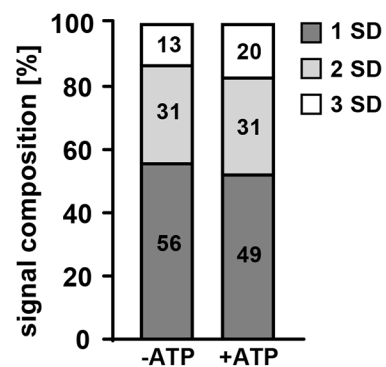
**B gliapil**



**C soma**



**D gliapil**



**soma**

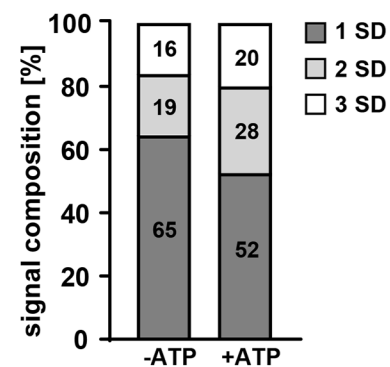




**Figure 37. Stronger and shorter Ca<sup>2+</sup> signals in gliapil and soma**

(A) Animals were injected at an age of four weeks for five consecutive days with TAM and cranial window surgery was done at an age of 16 w. Imaging sessions were performed 22 dpw with or without ATP application. (B) Signal amplitudes of the gliapil were increased after ATP application in all classified Ca<sup>2+</sup> signals, while duration was shortened. (C) Somatic signal amplitudes were stronger after ATP application in all groups of Ca<sup>2+</sup> signals. Large signals were shortened, while small and medium sized signals remained unaltered. (D) Signal composition of the gliapil revealed a higher percentage of large signals after ATP application. In the soma medium sized and large signals increased after ATP application. The error bars correlate to the median  $\pm$  interquartile range of the biological replicates (n = 1, \* p 0.01-0.05; \*\* p 0.001-0.01; \*\*\* p 0.0001-0.001; \*\*\*\* p > 0.00001, Mann-Whitney test).

## 7. DISCUSSION

Main results of this thesis:

1. Identification of an optimal tamoxifen injection protocol to induce maximal gene recombination.
2. Tamoxifen-independent recombination of the GLAST-Cre<sup>ERT2</sup> driver line does not affect cortical target genes.
3. Profound changes of Ca<sup>2+</sup> signaling in P2Y1R cKO *in vivo*.
4. High P2Y1R expression on astrocytes revealed by mRNA expression data.
5. Under pathological conditions no effect of P2Y1R ablation.

### 7.1. Tamoxifen-induced recombination

For efficient genomic DNA recombination protocols in the brain, a precise knowledge of the bioavailability of tamoxifen (TAM) and its metabolites is fundamental. Here, the GLAST-Cre<sup>ERT2</sup> knockin mouse line was used for optimization of induction protocols for DNA recombination. The bioavailability of TAM and its metabolites in brain and serum by liquid chromatography-high resolution-mass spectrometry (LC-HR-MS/MS) was analyzed and compared to the recombination efficiencies of gene loci in different brain regions after various TAM injection protocols. The main goal was to establish a TAM protocol with the best recombination efficiency using the lowest TAM concentration to reduce side effects. In addition, the Cre<sup>ERT2</sup>/loxP system was used to determine the proportion of astroglia in various brain regions (Fig. 38).

#### 7.1.1. Pharmacokinetic profile of tamoxifen and its metabolites revealed fast accumulation and clearance of all metabolites in the brain

TAM and 4-OH-TAM showed peak values already 8 hpi after a single injection, while the other metabolites NMD-TAM and END peaked at 24 hpi (Jahn, Kasakow *et al.*, 2018). All four compounds were cleared within 7 dpi (Fig 38 B), similar to a recent study, where different doses of TAM (up to 400 mg/kg body weight within 24 h) were compared (Valny *et al.*, 2016). Within the first 40 h all four substances were reduced by half after a single dose of TAM. 4-OH-TAM concentrations were quite high after a single injection (4.4 µg/g brain weight at 8 hpi), while others (Valny *et al.*, 2016) observed after two injections only 2.1 µg/g at 6 hpi. After three consecutive injections, all four substances accumulated. It is well known that high doses of TAM are toxic, but

our standard TAM concentration for injections of 100 mg/kg revealed a low mortality rate of 3.7 % in adult mice (older than 21 days,  $n = 4.080$ ). The general mortality rate of our animal facility over the last five years was not significantly lower (3.4 %;  $n = 25.731$ ). Hence, the here used TAM protocol does not increase the mortality rate of injected animals.

The minimal effective concentration of 4-OH-TAM has been determined at  $38 \pm 22$  ng/g (Valny *et al.*, 2016). This value is slightly lower than the concentration we detected in the brain at seven days when TAM was injected for three consecutive days (58.4 ng/g, 7 dpi). Long presence of 4-OH-TAM is important for genetic experiments in which extended gene excision is required. Recent studies revealed END as another TAM metabolite with high affinity to estrogen receptors (Ahmad *et al.*, 2010). END and 4-OH-TAM have a 100 times stronger affinity to estrogen receptors compared to TAM (Katzenellenbogen *et al.*, 1984, Robertson *et al.*, 1982). Regarding Cre<sup>ERT2</sup>-driven recombination END has a similar induction capacity as 4-OH-TAM (Felker *et al.*, 2016, Benedykowska *et al.*, 2016). END is higher in serum and brain compared to 4-OH-TAM 48 hpi (single) or 7 dpi (three injections), showing either a slower excretion for END or a prolonged generation from TAM in line with published data (Valny *et al.*, 2016). Therefore, it is conceivable that late recombination is not only due to 4-OH-TAM, still present in the brain, but also to slow accumulation of END.

In summary, our tamoxifen study revealed that upon application the metabolization to 4-OH-TAM in the liver by diverse cytochrome P450 isoenzymes (CYPs) takes place within 8 h (Fig. 38 A, B). The other effective TAM metabolite endoxifen showed a delayed peak after 24 h. In the brain mainly 4-OH-TAM induces the translocation of Cre<sup>ERT2</sup> into the nucleus to mediate recombination. All metabolites were cleared from the brain within 7 d, although the largest amount was already gone during the first 48 h after TAM application.

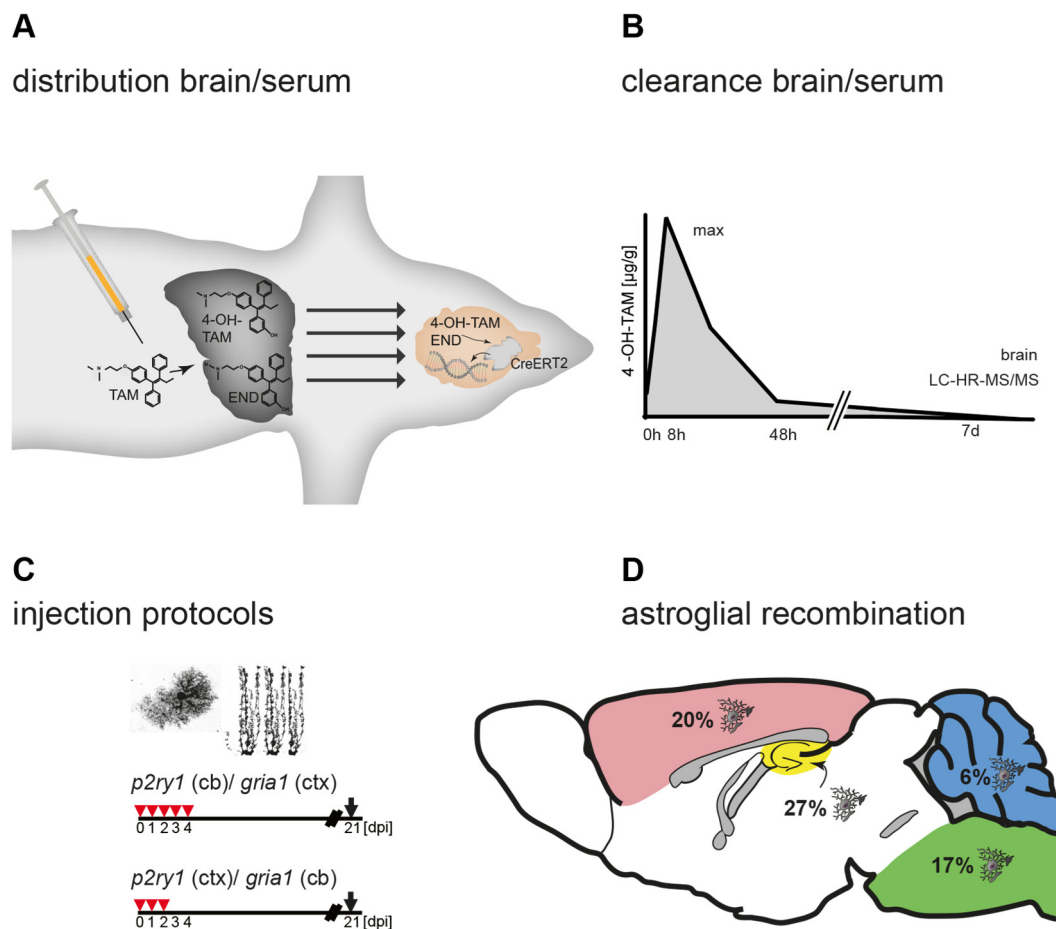


**Figure 38. Overview and conclusion of the tamoxifen study**

(A) TAM is metabolized in the liver to 4-OH-TAM and END. 4-OH-TAM induces DNA recombination in the brain. (B) Upon TAM application it took 8 h for the TAM and its active metabolite 4-OH-TAM to reach maximal level in the brain. Within 48 h the concentration of TAM and 4-OH-TAM decreased and was cleared from the brain after 7 d. (C) TAM protocols for *p2ry1* and *grla1* revealed differences for the two floxed alleles and the investigated brain region. (D) Quantitative analysis of two floxed alleles revealed the total amount of recombined astrocytes in different brain regions with: 20 % in cortex, 6 % in cerebellum, 27 % in hippocampus, 17 % in brainstem and 29 % in the optic nerve.

### 7.1.2. TAM injections for three or five consecutive days revealed highest recombination efficiencies dependent on brain region and floxed allele

DNA recombination efficiency of different floxed alleles (*p2ry1*, *grla1*) was analyzed by qRT-PCR. Three to five days of consecutive injections of TAM (100 mg/kg) induced maximal recombination, while fewer injections (once or twice) were less efficient (Jahn, Kasakow *et al.*, 2018). Similarly inefficient was a protocol with a pause between

injections (three injections with a pause of 48 h in between) since TAM and 4-OH-TAM were eliminated too quickly as observed by the LC-HR-MS/MS data. Application of TAM every eight hours for three consecutive injections revealed profound differences in recombination efficiencies for *p2ry1* and *gria1*. We expected, due to the application of TAM at the concentration peak, higher recombination efficiencies. Recombination of *p2ry1* alleles was comparable to the five times injection protocol or even higher, while *gria1* alleles were poorly recombined. These findings indicate different accessibilities of the gene loci for recombination during the injection period of 24 h. *Gria1* undergoes diurnal rhythms of expression (6 am and 6 pm) (Parekh *et al.*, 2017). For the eight hours interval protocol, mice were injected at 6 am, 2 pm and 10 pm, leading to less efficient TAM doses during ideal gene accessibility. In conclusion, circadian rhythms of respective genes play an important role in gene accessibility.

Kinetic differences in gene recombination based on different brain regions and/or floxed alleles were compensated after 21 days with at least three injections, but not after a single or two injections. Differences in recombination kinetics between (1) *gria1* and *p2ry1* and (2) the different brain regions (ctx vs. cb) could be caused by different chromatin structures, leading to less accessible *gria1* locus for Cre<sup>ERT2</sup> than *p2ry1*. Local chromatin structure and consequently, the potential for gene expression, are regulated by a number of post-translational, covalent modifications of histone-amino terminals, like methylation or acetylation (Takizawa & Meshorer, 2008, Namiyama *et al.*, 2008, Imamura *et al.*, 2014). Within euchromatin structures the degree of condensation or DNA accessibility varies depending on gene activity (Allen, 2008). Different DNA modifications of *p2ry1* and *gria1*, in combination with structural changes dependent on the circadian rhythms, but also between ctx and cb, could lead to the observed different recombination efficiencies. Therefore, for each new allele-of-interest a thorough DNA recombination analysis should be performed to reach maximal recombination.

Taken together, recombination efficiency after different TAM injection protocols is highly dependent on the floxed loci and the time point of analysis after the injection. Also the investigated brain region has to be taken into account. For the *p2ry1* gene five injections and 21 dpi led to maximal recombination in the cerebellum whereas three injections were sufficient for the cortex. For the *gria1* gene the contrary is the case: three injections for the cerebellum and five for the cortex (Fig. 38 C).

### 7.1.3. GLAST-Cre<sup>ERT2</sup>-driven recombination to determine the percentage of astrocytes in different brain regions

Exact numbers and proportions of different glial cell types (astrocytes, oligodendrocytes and microglia etc.) in various brain regions are missing in the literature. Therefore, we quantified the number of astrocytes in the murine brain based on DNA recombination. The loss of floxed alleles was taken as a measurement for astrocytes (GLAST+ cells) in a given brain region. Data revealed that in brainstem 17 %, in cerebellum 6 %, in cortex 20 %, in hippocampus 27 % and in optic nerve 29 % of all cells account for astrocytes (Fig. 38 D). In line with these data, cell counting of tdTomato+ cells resulted in 21 % astrocytes in the cortex (Jahn, Kasakow *et al.*, 2018). Similar to our data, counting of S100B+ cells in rat cortex revealed 18.5 % astrocytes (Ren *et al.*, 1992). We regarded GLAST+ cells as astrocytes and neglected different patterns of GLAST expression in astrocytic subpopulations or expression in neurogenic radial glia (Jahn *et al.*, 2015). The advantage of this cell quantification approach is the possible use of simple homogenates to estimate the total amount of astrocytes obtained from defined brain regions.

### 7.2. Tamoxifen-independent recombination had no effect on floxed receptor alleles in the cortex

Non-induced recombination was mainly present in GLAST-Cre<sup>ERT2</sup> expressing mice, while in GFAP-Cre<sup>ERT2</sup>, PLP-Cre<sup>ERT2</sup> and NG2-Cre<sup>ERT2</sup> mice almost no tamoxifen-independent recombination was observed. In addition, the impact of unintended recombination seemed to be highly dependent on the chosen floxed loci.

Orbit image analysis of whole sagittal slices of the GLAST-Cre<sup>ERT2</sup> mouse line crossbred to the GCaMP3 or tdTomato reporter revealed highest non-induced expression in GCaMP3 reporter mice.

GFAP-Cre<sup>ERT2</sup> induced tamoxifen-independent recombination was lower but detectable for both tested reporter lines. The low non-induced reporter expression of GFAP-Cre<sup>ERT2</sup> mice indicates that tamoxifen-independent recombination is not an astrocyte-driver dependent phenomenon. GFAP-Cre<sup>ERT2</sup> mice were, in contrast to GLAST-Cre<sup>ERT2</sup> mice, generated via non-homologous recombination. To evaluate, if non-induced recombination is influenced by the type of gene insertion (homologous vs. non-homologous recombination), two more mouse lines were investigated: TgN (PLP-

Cre<sup>ERT2</sup>) and TgH (NG2-Cre<sup>ERT2</sup>). Both mouse lines revealed less reporter expression than GLAST-Cre<sup>ERT2</sup> mice (Appendix Fig. 41).

Taken together, non-induced recombination is not caused by astrocyte-specific Cre<sup>ERT2</sup> driver lines, because GFAP-Cre<sup>ERT2</sup> mice remained unaffected. Influence of mouse generation strategy via homologous or non-homologous recombination could also be excluded, because NG2-Cre<sup>ERT2</sup> mice were not recombined without TAM. All these data indicate that tamoxifen-independent recombination is mainly dependent on GLAST-Cre<sup>ERT2</sup> driven recombination in combination with the reporter GCaMP3.

Protein data were confirmed by non-induced recombination of GCaMP3 at the DNA level. Therefore, the GLAST-Cre<sup>ERT2</sup>, GFAP-Cre<sup>ERT2</sup> and NG2-Cre<sup>ERT2</sup> mouse lines were analyzed for non-induced recombination of floxed reporter alleles (Fig. 24 C, D and Appendix Fig 41 E). Data revealed highest tamoxifen-independent recombination of floxed alleles in the cerebellum of GLAST-Cre<sup>ERT2</sup> mice, with almost the same recombination efficiency as the tamoxifen-induced positive control. In contrast, GFAP- and NG2-Cre<sup>ERT2</sup> driven recombination was mainly absent. DNA recombination data substantiate the results at the protein level and demonstrate a brain region dependent recombination with higher cerebellar non-induced recombination due to higher GLAST expression in Bergmann glia cells compared to GFAP (based on NGS, Data not shown).

Non-induced GLAST-Cre<sup>ERT2</sup> activity was additionally evaluated for the target genes *p2ry1* and *gria1* in comparison to reporter recombination. Heterozygous and homozygous GLAST-Cre<sup>ERT2</sup> mice revealed the expected high recombination of *gcamp3* alleles, while *p2ry1* and *gria1* alleles were less recombined. qRT-PCR data also revealed significant differences between cortex and cerebellum, as already seen in IHC data of sagittal slices. Cerebellar non-induced recombination at the *p2ry1* locus of heterozygous mice was similar to cortical recombination, while in homozygous mice a four times higher recombination could be detected. Still, compared to the tamoxifen-induced positive control, recombination rate of homozygous mice at the *p2ry1* locus was very low. Recombination of the *gria1* locus was low in both brain regions and could be neglected, while cerebellar recombination of *gcamp3* alleles was higher in heterozygous and homozygous mice compared to the negative control.

In general, homozygously Cre<sup>ERT2</sup> expressing mice revealed always higher non-induced recombination than heterozygous mice independent of the floxed locus with the highest recombination in the cerebellum.

One explanation for high reporter expression could be the length of the floxed region (Fig. 39). We compared the number of base pairs in between loxP sites of the *p2ry1*, *gria1*, *gcamp3* and *tdtomato* locus and an increasing length of floxed base pairs resulted in lower tamoxifen-independent recombination. Floxed regions of the reporter alleles include less base pairs than floxed *p2ry1* and *gria1* alleles. Although the largest floxed region was found for the *p2ry1* locus, *gria1* was even less recombined without TAM application. These findings are in line with the tamoxifen-induced recombination data, revealing a less accessible gene structure at the *gria1* locus due to circadian rhythms. Our data indicate that not only accessible DNA structure, but also the length of the floxed sequence influence recombination efficiency. Increase of non-induced recombination with shortening of floxed sequence length, was also observed by others (oral discussion with Amit Agarwal, Institute for Anatomy and Cell Biology, Heidelberg University). In general, it is crucial to evaluate the correlation between length of the floxed loci and the extent of unintended recombination with other floxed alleles.

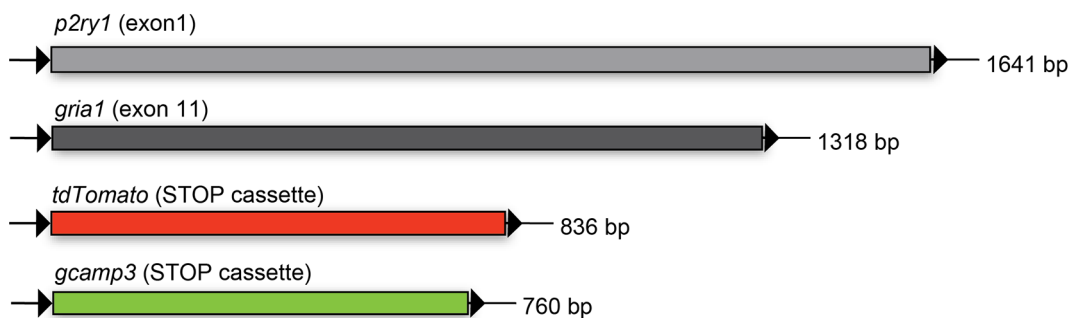


**Figure 39. Length of floxed sequence influences tamoxifen-independent recombination**

The length of floxed alleles differs between receptor knockouts and reporter mice. Floxed exon 1 of the *p2ry1* gene reveals an excision product of 1641 bp. For *gria1* exon 11 is flanked by loxP sites and led to an excision product of 1318 bp. The floxed STOP cassettes of the reporter lines tdTomato (836 bp) and GCaMP3 (760 bp) differ from each other only by 76 bp. The length of the floxed allele can be associated with the degree of non-induced recombination.

The glutamate aspartate transporter (GLAST) is highly expressed by astrocytes (Anderson & Swanson, 2000). As described before, our NGS data revealed high a expression level of GLAST mRNA in astrocytes, thus also Cre<sup>ERT2</sup> is highly expressed in GLAST-Cre<sup>ERT2</sup> mice. This could lead to cytosolic unbound Cre<sup>ERT2</sup> molecules, due to an imbalance of Cre<sup>ERT2</sup> and HSP90 molecules. Higher non-induced cerebellar recombination compared to cortex can be explained by a high GLAST expression in



this region (Mori *et al.*, 2006; NGS data). In NG2-Cre<sup>ERT2</sup> mice, no tamoxifen-independent recombination was detected. NG2 is only weak expressed in adult OPCs (Niehaus *et al.*, 1999), leading to low Cre<sup>ERT2</sup> expression. In the healthy cortex, GFAP expression is also very limited (Middeldorp & Hol, 2011), therefore no tamoxifen-independent recombination in GFAP-Cre<sup>ERT2</sup> mice can be detected, due to less hGFAP promoter controlled Cre<sup>ERT2</sup> expression (Hirrlinger *et al.*, 2006).

We investigated the effect of GFAP upregulation under pathological conditions (SWI or cuprizone model) and observed tamoxifen-independent recombination. Under physiological conditions GFAP-Cre<sup>ERT2</sup> mice without TAM did not recombine. However, after SWI or cuprizone treatment, recombined astrocytes could be observed in GFAP-Cre<sup>ERT2</sup> mice. GFAP is highly upregulated in activated astrocytes (Sofroniew & Vinters, 2010), leading to an upregulation of Cre<sup>ERT2</sup>. Overexpression of Cre<sup>ERT2</sup> causes an imbalance between HSP90 and Cre<sup>ERT2</sup>, resulting in unbound Cre<sup>ERT2</sup> molecules translocating into the nucleus and causing non-induced recombination.

Inducible Cre DNA recombinases (Cre<sup>ER</sup>/Cre<sup>ERT</sup>) can cause recombination in absence of TAM in diverse tested target and reporter mouse lines with different manifestation (Liu *et al.*, 2010, Vooijs *et al.*, 2001). Tamoxifen-independent recombination was observed in three different reporter/target mice, analyzed by IHC of cryosections or western blot. A correlation between promoter activity and extent of ligand-independent recombination was observed. They concluded that due to backcrossing of the mouse line the randomly inserted transgene expression was enhanced, leading to higher independent recombination. Lower non-induced recombination (e.g. in reporter line) was explained by the insertion into a region with less accessible chromatin structure. Taken together, mouse lines with overall lower recombination efficiency also show less tamoxifen-independent recombination (Liu *et al.*, 2010). We could confirm these findings by higher induced and independent recombination of *p2ry1* alleles compared to *gria1*. In addition, tamoxifen-independent recombination is highly variable in different mouse lines and tissues (Vooijs *et al.*, 2001). Cre<sup>ERT2</sup> is known to have a low non-induced Cre activity (Zhong *et al.*, 2015). Here, we report tamoxifen-independent recombination in Cre<sup>ERT2</sup> mice in dependence of the locus activity controlling Cre<sup>ERT2</sup> expression.

Therefore, each new floxed mouse line has to be investigated in combination with the respective Cre<sup>ERT2</sup> driver line to estimate the percentage of tamoxifen-independent recombination. All studies of cKOs, performed in the cortex with GLAST-Cre<sup>ERT2</sup> mice,

are unaffected, while for the cerebellum it is important to observe Cre<sup>ERT2</sup> activity at the chosen floxed loci.

### 7.3. P2Y1 receptor ablation and its impact on astrocytes

As described previously, highest recombination efficiency of the *p2ry1* locus was achieved by three to five TAM injections dependent on the brain region. Recombination efficiency was even increased after an interval injection protocol every eight hours, indicating a favourable accessibility of the locus during injection period. In addition, the locus mainly remained unaffected from tamoxifen-independent recombination. mRNA expression data of total homogenates revealed 50 % to 60 % *p2ry1* mRNA expression by astrocytes in cerebellum and cortex, indicating an important role of the receptor for physiological astrocyte function.

P2Y1R ablation was further analyzed on sorted astrocytic populations of cortex and cerebellum, revealing a reduction of 60 % and 30 % at the DNA level, respectively. It was expected to achieve a total reduction in cKOs compared to controls in purified astrocytes. Based on our mRNA data of total homogenates, which revealed a high expression of *p2ry1* mRNA in cortex and cerebellum, we expected a higher reduction in the pure astrocytic population of cKOs. The percentage of non-recombined alleles indicates that not all astrocytes are recombined. Heterogeneity among astrocytic populations is well known. Therefore, epigenetic modifications (DNA-methylation) of a certain percentage of astrocytes at the *p2ry1* locus could explain the incomplete receptor ablation.

Contamination of the astrocytic population with other cell types was evaluated by mRNA expression of typical cell markers of microglia, neurons, NG2 glia and oligodendrocytes. We found in MACS isolated astrocytes, analyzed by either qRT-PCR or next generation sequencing (NGS), only low expression of other cell type markers. Additionally tested astrocytic markers (Glt1, Aldh1l1, GLAST, GS and Aqp4) were highly enriched in the astrocytic population. *P2ry1* mRNA is highly expressed by neurons and OPCs (Zhang *et al.*, 2014), low contamination with these cell types could therefore increase the amount of non-recombined *p2ry1* alleles. Astrocytic heterogeneity is well known and is also displayed by different expression profiles of astrocytic populations for other markers like GFAP (Sofroniew & Vinters, 2010). The isolation of astrocytes was executed with the Miltenyi ACSA-2 micro bead kit (astrocyte cell surface antigen-2). This antibody is directed against the glycoprotein ATP1B2

(ATPase transporting subunit beta 2), ubiquitously expressed by cortical and cerebellar astrocytes during adulthood (Batiuk *et al.*, 2017). ACSA-2 is a reliable antibody to purify astrocytes (Feldmann *et al.*, 2014), but mRNA sequencing data have shown that ATP1B2 is also highly expressed by neurons and OPCs (Zhang *et al.*, 2014). These findings are well in line with our data after MACS procedure and display the limitations of the system to purify astrocytes.

Next generation sequencing (NGS) analysis of P2Y1R cKO mice confirmed data of the DNA recombination and mRNA expression in total homogenates and MACS isolated astrocytes. In line with previous results, a reduction of about 50 % in the cKO was achieved. Most metabotropic P2Y and ionotropic P2X receptors were not altered. Only the ionotropic P2X6R was upregulated, indicating a compensational mechanism in cKO mice. *P2rx6* mRNA is highly expressed by astrocytes compared to other cell types, leading to  $\text{Ca}^{2+}$  and  $\text{Na}^{+}$  influx upon ATP binding (Zhang *et al.*, 2014). Analysis of astrocytic markers, like GFAP or Glt1, revealed no changes in mRNA expression in cKOs. Molecules of the downstream signaling cascade (PLA, PLC) of P2Y1 receptors were not altered. Volcano plot analysis revealed several differential expressed genes in cKOs. Up- and downregulated genes will help to further characterize changes at the molecular level after P2Y1R ablation.

Astrocytic P2Y1 receptors play an important role for the generation of  $\text{Ca}^{2+}$  signals. Overexpression of the receptor led to larger  $\text{Ca}^{2+}$  signals upon ligand application (Shigetomi *et al.*, 2018). P2Y1R are also involved under pathological conditions like ischemia. Inhibition of the receptor led to a reduction in infarct volume (Kuboyama *et al.*, 2011). Invasive injury models, like SWI, differ from non-invasive models, like ischemia, mainly in their proliferative cell responses, whereas hypertrophy and GFAP-upregulation of astrocytes are comparable (Sirko *et al.*, 2013). The release of glutamate or proinflammatory cytokines (IL-6) and modulation of transcription are well known functions (Sun *et al.*, 2008, Fujita *et al.*, 2009) of astrocytic P2Y1R. Taken together P2Y1R participate in various ways in physiological and pathological mechanisms of astrocytes.

The role of P2Y1R under pathological conditions is controversially discussed in the literature, reaching from beneficial to aggravating effects. Upon traumatic brain injury the first cells that become activated are microglia. ATP released from injured cells is responsible for their activation (Inoue, 2008). Microglia upregulate reactive cytokines

like TNF- $\alpha$ , IL-1 $\beta$  and IL-6 that induce and regulate the activation of astrocytes and therefore trigger astrogliosis. Microglial cells are also responsible for the downregulation of P2Y<sub>1</sub>R expression in astrocytes. This downregulation has many positive effects like facilitation of scar formation, reduction of reactive oxygen species (ROS) production and release, suppression of leukocyte infiltration and repair of the blood brain barrier (BBB). All these effects are beneficial for neuronal survival (Shinozaki *et al.*, 2017, Safiulina *et al.*, 2006). It was also reported that acute injury stimulates P2Y<sub>1</sub>R that directly participate in glutamate-mediated excitotoxicity. Non-selective P2 receptor antagonists reduce the size of the lesion and decrease neuronal and astrocytic cell death (Lämmer *et al.*, 2011).

The stimulation of P2Y<sub>1</sub>R on astrocytes leads to a reduction of cytotoxic edema, necrosis and neuronal cell death after Rose Bengal induced lesions. Activation of astrocytic P2Y<sub>1</sub>R stimulates the mitochondrial metabolism which leads to an increase in ATP production (Zheng *et al.*, 2010). The neuroprotective effect of ATP production after P2Y<sub>1</sub>R activation on astrocytes was also shown after stimulation with the specific agonist 2MeSADP that induces the release of the neuroprotective molecule IL-6 (Fujita *et al.*, 2009). In Alzheimer's disease, astroglial hyperactivity is mainly mediated by P2Y<sub>1</sub>R activity. This effect could be weakened by the non-selective purinergic antagonist PPADS (Pyridoxalphosphate-6-azophenyl-2',4'-disulfonic acid tetrasodium salt) as well as by blocking of intracellular Ins-P<sub>3</sub> receptors. In contrast, an increase in ADP concentration led to an enhancement of astrocytic hyperactivity. Highest P2Y<sub>1</sub>R expression is present in reactive astrocytes surrounding plaques. These are also the areas of astrocytic hyperactivity (Delekate *et al.*, 2014).

Here, we performed SWI experiments on GLAST-Cre<sup>ERT2</sup> x P2Y<sub>1</sub><sup>fl/fl</sup> x Rosa26-tdTomato/ or GCaMP3 mice to investigate the role of P2Y<sub>1</sub>R ablation on astrocytes under an acute injury model. Reporter expression (tdTomato or GCaMP3),  $\alpha$ -GFAP and  $\alpha$ -Iba1 stainings were analyzed for changes in fluorescence intensities at the lesion site. Ipsilaterally and contralaterally, no differences in GFAP or Iba1 fluorescence intensities of cKO and control mice with tdTomato expression were detected. Here, we could not detect any influence of P2Y<sub>1</sub>R ablation on lesion size or on cell types responsible for glial scar formation. In contrast to other publications, P2Y<sub>1</sub>R cKO has in our hands no impact on astroglial and microglial reaction after acute injury.

The same injury model applied to cKOs with Rosa26-GCaMP3 as reporter revealed changes in GFAP and Iba1 expression between cKO and control on the ipsilateral side. GFAP expression of the cKO was upregulated, while Iba1 expression was downregulated. Higher GFAP and GCaMP3 expression was detected on the contralateral side of the cKO. It was shown that GCaMP3 influences gating and signaling of voltage-gated  $\text{Ca}^{2+}$  channels, changes transcription signaling, cell morphogenesis and the global physiology of cells (Yang *et al.*, 2018). Astrocytes seem to be more vulnerable to stress induced by SWI when GCaMP3 is expressed, as a result to lower concentrations of intracellular  $\text{Ca}^{2+}$ . These reactive astrocytes may also act on microglia, leading to a reduction of these cells at the lesion site. The  $\text{Ca}^{2+}$  dependent release of gliotransmitters by astrocytes under pathological conditions, needs the collaboration of activated microglia, reactive astrocytes and inflammatory molecules, released by both cell types (Agulhon *et al.*, 2012). Astrocytic  $\text{Ca}^{2+}$  waves and the release of ATP pass the information of an occurred injury to healthy brain regions. This leads to the activation of microglial purinergic receptors and the release of cytokines, influencing the  $\text{Ca}^{2+}$  wave (Schipke *et al.*, 2002). In P2Y1R cKO mice, less activated microglia were found due to disturbed purinergic signaling.

In summary, these concerted signaling pathways are highly dependent on intracellular astrocytic  $\text{Ca}^{2+}$  levels and intact purinergic signaling, therefore the combination of low intracellular  $\text{Ca}^{2+}$  levels and the loss of P2Y1R could disturb the communication of astrocytes with microglia after brain injury.

#### **7.4. $\text{Ca}^{2+}$ signaling of astrocytes *in vivo***

$\text{Ca}^{2+}$  changes in P2Y1 receptor cKO and control mice were investigated by 2P-LSM. Mice were imaged anesthetized, awake or under influence of exogenous applied ATP. Profound differences in  $\text{Ca}^{2+}$  signaling were found between cKO and control, but also between awake and anesthetized conditions.

##### **7.4.1. Differences in astrocytic $\text{Ca}^{2+}$ signaling after P2Y1 receptor ablation in gliapil and soma**

Anesthetized mice revealed smaller  $\text{Ca}^{2+}$  signals in P2Y1 cKO mice in all classes of  $\text{Ca}^{2+}$  signals in the gliapil. Duration of small and medium sized  $\text{Ca}^{2+}$  signals was shortened, while large signals remained unaffected. Similarly, somatic  $\text{Ca}^{2+}$  signals

were smaller in all signal classes. In contrast, duration was only shortened in large  $\text{Ca}^{2+}$  signals, while small and medium sized signals were not changed.

In awake mice similar results were found, revealing smaller and shorter  $\text{Ca}^{2+}$  signals in gliapil and soma of the cKO. Comparison of anesthetized and awake animals revealed a high influence of isoflurane on amplitude size of  $\text{Ca}^{2+}$  signals in gliapil and soma (Thrane *et al.*, 2012). Signal amplitudes of awake mice were higher in all classes of  $\text{Ca}^{2+}$  signals in gliapil and soma, while duration was shortened or remained unchanged (see Fig. 45, Appendix). The signal composition remained unaffected in anesthetized control and cKO mice in gliapil and soma, with the highest percentage of small signals followed by medium sized and large signals. Under awake conditions the signal composition changed in cKO animals in gliapil and soma, revealing a higher percentage of large signals than small and medium sized signals. Control animals displayed the same signal composition as under anesthetized condition. These findings are well in line with published data. Under anesthesia,  $\text{Ca}^{2+}$  signals were completely different compared to signals of awake mice. Types of  $\text{Ca}^{2+}$  signals like bursts and flares were abolished and also smaller signals like sparkles were significantly reduced as shown before (Nimmerjahn *et al.*, 2009). It was also reported that anesthesia reduces astrocytic network activity,  $\text{Ca}^{2+}$  transients, spontaneous  $\text{Ca}^{2+}$  signals and  $\text{Ca}^{2+}$  responses to external stimuli or agonist application (Thrane *et al.*, 2012). Therefore, the switch to larger  $\text{Ca}^{2+}$  signals in awake mice is reflecting the increased network activity in non-anesthetized mice.

Shortening of signal duration in anesthetized and awake cKOs can be explained by missing metabotropic signaling of P2Y<sub>1</sub>R on astrocytes. Metabotropic signaling induces a second messenger cascade which then leads to the release of  $\text{Ca}^{2+}$  from the endoplasmic reticulum (ER), being more slowly than ionotropic signaling (Burnstock, 2014). The effect of P2Y<sub>1</sub>R ablation was expected to be more pronounced, but based on our mRNA data P2Y<sub>1</sub>R is not completely abolished. It seems probable that a number of astrocytes still expressed *p2ry1* mRNA.

Additionally, the influence of the ligand ATP on a P2Y<sub>1</sub>R control mouse was investigated. Application of the ligand to anesthetized mice induced an increase in amplitude size in all classes of  $\text{Ca}^{2+}$  signals in gliapil and soma. Duration was shortened upon ATP treatment in small, medium sized and large signals of the gliapil, while in the soma only large signals were shorter. ATP is a non-specific ligand for P2Y and P2X receptors, leading to the activation of both receptor types. ATP stimulates

astrocytes via P2 receptors to release ATP that initiates and propagates astroglial  $\text{Ca}^{2+}$  signals either to activate neighboring astrocytes or to influence synaptic transmission (Abbracchio *et al.*, 2009). Therefore, an increase in  $\text{Ca}^{2+}$  signal strength was expected upon ATP application.

In summary, our data revealed differences in  $\text{Ca}^{2+}$  signals of anesthetized and awake animals as well as between controls and P2Y1R cKOs. We could demonstrate the impact of P2Y1R ablation in gliapil and soma by smaller and shorter  $\text{Ca}^{2+}$  signals of the cKO.

## 8. OUTLOOK

In this study we demonstrated the astrocyte specific deletion of the purinergic receptor P2Y<sub>1</sub> at the molecular level. At the DNA level, the loss of floxed *p2ry1* alleles was shown in total tissue homogenates and after purification of astrocytes via MACS. A profound amount of sorted cells still expressed *p2ry1* DNA after tamoxifen-induced recombination, therefore we will further optimize the sorting procedure to exclude contamination with other *p2ry1* expressing cells. In addition, the amount of non-recombined astrocytes has to be evaluated.

The mRNA expression profile of P2Y<sub>1</sub>R cKO and control mice was investigated in the cortex by next generation sequencing (NGS). We observed changes in expression patterns of astrocytic receptors (*p2ry1*, *p2rx6*) in cKO mice but no alterations in the downstream signaling. NGS data will be used to perform pathway enrichment analysis of P2Y<sub>1</sub>R cKOs. In addition, the same comparison of cKO and control will be done for the cerebellum. It will be also possible to elucidate expression differences of cortical and cerebellar astrocytes.

We could demonstrate the influence of P2Y<sub>1</sub>R ablation also *in vivo* by changed Ca<sup>2+</sup> signals. We will extend the characterization of these signals by applying diverse P2Y<sub>1</sub>R agonists and antagonists to cKO and control mice.

Our data demonstrate that each mouse line has to be evaluated for its recombination efficiency and sensitivity to non-induced recombination. To verify, if an increased number of Cre<sup>ERT2</sup> molecules is the reason for tamoxifen-independent recombination in GLAST-Cre<sup>ERT2</sup> mice, RNAscope experiments will be performed.



## 9. REFERENCES

- Abbracchio, M. P., Burnstock, G., Verkhratsky, A. & Zimmermann, H. 2009. Purinergic signalling in the nervous system: an overview. *Trends Neurosci* **32**:19-29.
- Agulhon, C., Petravic, J., McMullen, A. B., Sweger, E. J., Minton, S. K., Taves, S. R., Casper, K. B., Fiacco, T. A. & McCarthy, K. D. 2008. What is the role of astrocyte calcium in neurophysiology? *Neuron* **59**:932-46.
- Agulhon, C., Sun, M. Y., Murphy, T., Myers, T., Lauderdale, K. & Fiacco, T. A. 2012. Calcium Signaling and Gliotransmission in Normal vs. Reactive Astrocytes. *Front Pharmacol* **3**:139.
- Ahmad, A., Ali, S. M., Ahmad, M. U., Sheikh, S. & Ahmad, I. 2010. Orally administered endoxifen is a new therapeutic agent for breast cancer. *Breast Cancer Res Treat* **122**:579-84.
- Alberdi, E., Sánchez-Gómez, M. V. & Matute, C. 2005. Calcium and glial cell death. *Cell Calcium* **38**:417-25.
- Allen, N. D. 2008. Temporal and epigenetic regulation of neurodevelopmental plasticity. *Philos Trans R Soc Lond B Biol Sci* **363**:23-38.
- Anderson, C. M. & Swanson, R. A. 2000. Astrocyte glutamate transport: review of properties, regulation, and physiological functions. *Glia* **32**:1-14.
- Araque, A. 2008. Astrocytes process synaptic information. *Neuron Glia Biol* **4**:3-10.
- Araque, A., Parpura, V., Sanzgiri, R. P. & Haydon, P. G. 1999. Tripartite synapses: glia, the unacknowledged partner. *Trends Neurosci* **22**:208-15.
- Attwell, D., Buchan, A. M., Charpak, S., Lauritzen, M., Macvicar, B. A. & Newman, E. A. 2010. Glial and neuronal control of brain blood flow. *Nature* **468**:232-43.
- Batiuk, M. Y., de Vin, F., Duqué, S. I., Li, C., Saito, T., Saido, T., Fiers, M., Belgard, T. G. & Holt, M. G. 2017. An immunoaffinity-based method for isolating ultrapure adult astrocytes based on ATP1B2 targeting by the ACSA-2 antibody. *J Biol Chem* **292**:8874-91.
- Bazargani, N. & Attwell, D. 2016. Astrocyte calcium signaling: the third wave. *Nat Neurosci* **19**:182-9.
- Becerra-Calixto, A. & Cardona-Gómez, G. P. 2017. The Role of Astrocytes in Neuroprotection after Brain Stroke: Potential in Cell Therapy. *Front Mol Neurosci* **10**:88.
- Benedykowska, A., Ferreira, A., Lau, J., Broni, J., Richard-Loendt, A., Henriquez, N. V. & Brandner, S. 2016. Generation of brain tumours in mice by Cre-mediated recombination of neural progenitors in situ with the tamoxifen metabolite endoxifen. *Dis Model Mech* **9**:211-20.
- Borgna, J. L. & Rochefort, H. 1981. Hydroxylated metabolites of tamoxifen are formed in vivo and bound to estrogen receptor in target tissues. *The Journal of biological chemistry* **256**:859-68.
- Bowie, D. 2012. Redefining the classification of AMPA-selective ionotropic glutamate receptors. *J Physiol* **590**:49-61.
- Browne, L. E., Jiang, L. H. & North, R. A. 2010. New structure enlivens interest in P2X receptors. *Trends Pharmacol Sci* **31**:229-37.
- Burnstock, G. 2014. Purinergic signalling: from discovery to current developments. *Exp Physiol* **99**:16-34.
- Butt, A. M. 2011. ATP: a ubiquitous gliotransmitter integrating neuron-glia networks. *Semin Cell Dev Biol* **22**:205-13.
- Caldas, C. & Tannock, I. F. 2013. Breast cancer: Tamoxifen--when more might be better. *Nat Rev Clin Oncol* **10**:125-6.
- Chang, J. H., Chen, J., Liu, L., Messick, K. & Ly, J. 2016. Rifampin-Mediated Induction of Tamoxifen Metabolism in a Humanized PXR-CAR-CYP3A4/3A7-CYP2D6 Mouse Model. *Drug Metab Dispos* **44**:1736-41.

- Charles, A. C., Merrill, J. E., Dirksen, E. R. & Sanderson, M. J. 1991. Intercellular signaling in glial cells: calcium waves and oscillations in response to mechanical stimulation and glutamate. *Neuron* **6**:983-92.
- Clarke, L. E., Liddel, S. A., Chakraborty, C., Münch, A. E., Heiman, M. & Barres, B. A. 2018. Normal aging induces A1-like astrocyte reactivity. *Proc Natl Acad Sci U S A* **115**:E1896-E905.
- Cornell-Bell, A. H. & Finkbeiner, S. M. 1991. Ca<sup>2+</sup> waves in astrocytes. *Cell Calcium* **12**:185-204.
- Cornell-Bell, A. H., Finkbeiner, S. M., Cooper, M. S. & Smith, S. J. 1990. Glutamate induces calcium waves in cultured astrocytes: long-range glial signaling. *Science* **247**:470-3.
- Cotrina, M. L., Lin, J. H., López-García, J. C., Naus, C. C. & Nedergaard, M. 2000. ATP-mediated glia signaling. *J Neurosci* **20**:2835-44.
- Danbolt, N. C. 2001. Glutamate uptake. *Prog Neurobiol* **65**:1-105.
- Delekate, A., Fächte, M., Schumacher, T., Ulbrich, C., Foddis, M. & Petzold, G. C. 2014. Metabotropic P2Y1 receptor signalling mediates astrocytic hyperactivity in vivo in an Alzheimer's disease mouse model. *Nat Commun* **5**:5422.
- Desta, Z., Ward, B. A., Soukhova, N. V. & Flockhart, D. A. 2004. Comprehensive evaluation of tamoxifen sequential biotransformation by the human cytochrome P450 system in vitro: prominent roles for CYP3A and CYP2D6. *The Journal of pharmacology and experimental therapeutics* **310**:1062-75.
- Ding, F., O'Donnell, J., Thrane, A. S., Zeppenfeld, D., Kang, H., Xie, L., Wang, F. & Nedergaard, M. 2013.  $\alpha(1)$ -Adrenergic receptors mediate coordinated Ca<sup>2+</sup> signaling of cortical astrocytes in awake, behaving mice. *Cell Calcium* **54**:387-94.
- Faulkner, J. R., Herrmann, J. E., Woo, M. J., Tansey, K. E., Doan, N. B. & Sofroniew, M. V. 2004. Reactive astrocytes protect tissue and preserve function after spinal cord injury. *J Neurosci* **24**:2143-55.
- Feil, R., Wagner, J., Metzger, D. & Chambon, P. 1997. Regulation of Cre recombinase activity by mutated estrogen receptor ligand-binding domains. *Biochem Biophys Res Commun* **237**:752-7.
- Feldmann, M., Pathipati, P., Sheldon, R. A., Jiang, X. & Ferriero, D. M. 2014. Isolating astrocytes and neurons sequentially from postnatal murine brains with a magnetic cell separation technique. *JBM Vol 1*.
- Felker, A., Nieuwenhuize, S., Dolbois, A., Blazkova, K., Hess, C., Low, L. W., Burger, S., Samson, N., Carney, T. J., Bartunek, P., Nevado, C. & Mosimann, C. 2016. In Vivo Performance and Properties of Tamoxifen Metabolites for CreERT2 Control. *PLoS One* **11**:e0152989.
- Fields, R. D. & Burnstock, G. 2006. Purinergic signalling in neuron-glia interactions. *Nat Rev Neurosci* **7**:423-36.
- Franke, H., Verkhratsky, A., Burnstock, G. & Illes, P. 2012. Pathophysiology of astroglial purinergic signalling. *Purinergic Signal* **8**:629-57.
- Fuchs, E. C., Zivkovic, A. R., Cunningham, M. O., Middleton, S., Lebeau, F. E., Bannerman, D. M., Rozov, A., Whittington, M. A., Traub, R. D., Rawlins, J. N. & Monyer, H. 2007. Recruitment of parvalbumin-positive interneurons determines hippocampal function and associated behavior. *Neuron* **53**:591-604.
- Fujita, T., Tozaki-Saitoh, H. & Inoue, K. 2009. P2Y1 receptor signaling enhances neuroprotection by astrocytes against oxidative stress via IL-6 release in hippocampal cultures. *Glia* **57**:244-57.
- Goetz, M. P., Kamal, A. & Ames, M. M. 2008. Tamoxifen pharmacogenomics: the role of CYP2D6 as a predictor of drug response. *Clin Pharmacol Ther* **83**:160-6.
- Gordon, G. R. & Bains, J. S. 2006. Can homeostatic circuits learn and remember? *J Physiol* **576**:341-7.
- Gordon, G. R., Howarth, C. & MacVicar, B. A. 2011. Bidirectional control of arteriole diameter by astrocytes. *Exp Physiol* **96**:393-9.

- Grass, D., Pawlowski, P. G., Hirrlinger, J., Papadopoulos, N., Richter, D. W., Kirchhoff, F. & Hülsmann, S. 2004. Diversity of functional astroglial properties in the respiratory network. *J Neurosci* **24**:1358-65.
- Gudi, V., Gingele, S., Skripuletz, T. & Stangel, M. 2014. Glial response during cuprizone-induced de- and remyelination in the CNS: lessons learned. *Front Cell Neurosci* **8**:73.
- Guerra-Gomes, S., Sousa, N., Pinto, L. & Oliveira, J. F. 2017. Functional Roles of Astrocyte Calcium Elevations: From Synapses to Behavior. *Front Cell Neurosci* **11**:427.
- Guo, Z. V., Hires, S. A., Li, N., O'Connor, D. H., Komiyama, T., Ophir, E., Huber, D., Bonardi, C., Morandell, K., Gutnisky, D., Peron, S., Xu, N. L., Cox, J. & Svoboda, K. 2014. Procedures for behavioral experiments in head-fixed mice. *PLoS One* **9**:e88678.
- Harada, K., Kamiya, T. & Tsuboi, T. 2015. Gliotransmitter Release from Astrocytes: Functional, Developmental, and Pathological Implications in the Brain. *Front Neurosci* **9**:499.
- Hattori, M. & Gouaux, E. 2012. Molecular mechanism of ATP binding and ion channel activation in P2X receptors. *Nature* **485**:207-12.
- Helfer, A. G., Michely, J. A., Weber, A. A., Meyer, M. R. & Maurer, H. H. 2017. Liquid chromatography-high resolution-tandem mass spectrometry using Orbitrap technology for comprehensive screening to detect drugs and their metabolites in blood plasma. *Anal Chim Acta* **965**:83-95.
- Hirrlinger, P. G., Scheller, A., Braun, C., Hirrlinger, J. & Kirchhoff, F. 2006. Temporal control of gene recombination in astrocytes by transgenic expression of the tamoxifen-inducible DNA recombinase variant CreERT2. *Glia* **54**:11-20.
- Hollmann, M., Hartley, M. & Heinemann, S. 1991. Ca<sup>2+</sup> permeability of KA-AMPA-gated glutamate receptor channels depends on subunit composition. *Science* **252**:851-3.
- Huang, W., Zhao, N., Bai, X., Karram, K., Trotter, J., Goebbels, S., Scheller, A. & Kirchhoff, F. 2014. Novel NG2-CreERT2 knock-in mice demonstrate heterogeneous differentiation potential of NG2 glia during development. *Glia* **62**:896-913.
- Imamura, T., Uesaka, M. & Nakashima, K. 2014. Epigenetic setting and reprogramming for neural cell fate determination and differentiation. *Philos Trans R Soc Lond B Biol Sci* **369**.
- Inoue, K. 2008. Purinergic systems in microglia. *Cell Mol Life Sci* **65**:3074-80.
- Jahn, H. M., Kasakow, C. V., Helfer, A., Michely, J., Verkhratsky, A., Maurer, H. H., Scheller, A. & Kirchhoff, F. 2018. Refined protocols of tamoxifen injection for inducible DNA recombination in mouse astroglia. *Sci Rep* **8**:5913.
- Jahn, H. M., Scheller, A. & Kirchhoff, F. 2015. Genetic control of astrocyte function in neural circuits. *Front Cell Neurosci* **9**:310.
- Johnson, M. D., Zuo, H., Lee, K. H., Trebley, J. P., Rae, J. M., Weatherman, R. V., Desta, Z., Flockhart, D. A. & Skaar, T. C. 2004. Pharmacological characterization of 4-hydroxy-N-desmethyl tamoxifen, a novel active metabolite of tamoxifen. *Breast Cancer Res Treat* **85**:151-9.
- Jordan, V. C., Collins, M. M., Rowsby, L. & Prestwich, G. 1977. A monohydroxylated metabolite of tamoxifen with potent antioestrogenic activity. *J Endocrinol* **75**:305-16.
- Karakas, E. & Furukawa, H. 2014. Crystal structure of a heterotetrameric NMDA receptor ion channel. *Science* **344**:992-7.
- Katzenellenbogen, B. S., Norman, M. J., Eckert, R. L., Peltz, S. W. & Mangel, W. F. 1984. Bioactivities, estrogen receptor interactions, and plasminogen activator-inducing activities of tamoxifen and hydroxy-tamoxifen isomers in MCF-7 human breast cancer cells. *Cancer Res* **44**:112-9.
- Kirchhoff, F., Dringen, R. & Giaume, C. 2001. Pathways of neuron-astrocyte interactions and their possible role in neuroprotection. *Eur Arch Psychiatry Clin Neurosci* **251**:159-69.
- Kirischuk, S., Möller, T., Voitenko, N., Kettenmann, H. & Verkhratsky, A. 1995. ATP-induced cytoplasmic calcium mobilization in Bergmann glial cells. *J Neurosci* **15**:7861-71.
- Kislin, M., Mugantseva, E., Molotkov, D., Kuleskaya, N., Khirug, S., Kirilkin, I., Pryazhnikov, E., Kolikova, J., Toptunov, D., Yuryev, M., Giniatullin, R., Voikar, V., Rivera, C., Rauvala, H.

- & Khiroug, L. 2014. Flat-floored air-lifted platform: a new method for combining behavior with microscopy or electrophysiology on awake freely moving rodents. *J Vis Exp*:e51869.
- Koizumi, S. 2010. Synchronization of Ca<sup>2+</sup> oscillations: involvement of ATP release in astrocytes. *FEBS J* **277**:286-92.
- Kuboyama, K., Harada, H., Tozaki-Saitoh, H., Tsuda, M., Ushijima, K. & Inoue, K. 2011. Astrocytic P2Y(1) receptor is involved in the regulation of cytokine/chemokine transcription and cerebral damage in a rat model of cerebral ischemia. *J Cereb Blood Flow Metab* **31**:1930-41.
- Lalo, U., Verkhatsky, A. & Pankratov, Y. 2011. Ionotropic ATP receptors in neuronal-glial communication. *Semin Cell Dev Biol* **22**:220-8.
- Leon, C., Hechler, B., Freund, M., Eckly, A., Vial, C., Ohlmann, P., Dierich, A., LeMeur, M., Cazenave, J. P. & Gachet, C. 1999. Defective platelet aggregation and increased resistance to thrombosis in purinergic P2Y(1) receptor-null mice. *J Clin Invest* **104**:1731-7.
- Leone, D. P., Genoud, S., Atanasoski, S., Grausenburger, R., Berger, P., Metzger, D., Macklin, W. B., Chambon, P. & Suter, U. 2003. Tamoxifen-inducible glia-specific Cre mice for somatic mutagenesis in oligodendrocytes and Schwann cells. *Mol Cell Neurosci* **22**:430-40.
- Lewandoski, M. 2001. Conditional control of gene expression in the mouse. *Nat Rev Genet* **2**:743-55.
- Liu, C. Y., Yang, Y., Ju, W. N., Wang, X. & Zhang, H. L. 2018. Emerging Roles of Astrocytes in Neuro-Vascular Unit and the Tripartite Synapse With Emphasis on Reactive Gliosis in the Context of Alzheimer's Disease. *Front Cell Neurosci* **12**:193.
- Liu, Y., Suckale, J., Masjkur, J., Magro, M. G., Steffen, A., Anastassiadis, K. & Solimena, M. 2010. Tamoxifen-independent recombination in the RIP-CreER mouse. *PLoS One* **5**:e13533.
- Luisier, F., Blu, T. & Unser, M. 2010. Fast interscale wavelet denoising of Poisson-corrupted images. *SignalProcessing* **10**:415-27.
- Lämmner, A. B., Beck, A., Grummich, B., Förchler, A., Krügel, T., Kahn, T., Schneider, D., Illes, P., Franke, H. & Krügel, U. 2011. The P2 receptor antagonist PPADS supports recovery from experimental stroke in vivo. *PLoS One* **6**:e19983.
- MacVicar, B. A. & Newman, E. A. 2015. Astrocyte regulation of blood flow in the brain. *Cold Spring Harb Perspect Biol* **7**.
- Madisen, L., Zwingman, T. A., Sunkin, S. M., Oh, S. W., Zariwala, H. A., Gu, H., Ng, L. L., Palmiter, R. D., Hawrylycz, M. J., Jones, A. R., Lein, E. S. & Zeng, H. 2010. A robust and high-throughput Cre reporting and characterization system for the whole mouse brain. *Nat Neurosci* **13**:133-40.
- Matthias, K., Kirchhoff, F., Seifert, G., Hüttmann, K., Matyash, M., Kettenmann, H. & Steinhäuser, C. 2003. Segregated expression of AMPA-type glutamate receptors and glutamate transporters defines distinct astrocyte populations in the mouse hippocampus. *J Neurosci* **23**:1750-8.
- Mayer, M. L. 2005. Glutamate receptor ion channels. *Curr Opin Neurobiol* **15**:282-8.
- Mayer, M. L. & Westbrook, G. L. 1987. Permeation and block of N-methyl-D-aspartic acid receptor channels by divalent cations in mouse cultured central neurones. *J Physiol* **394**:501-27.
- McLaughlin, L. A., Dickmann, L. J., Wolf, C. R. & Henderson, C. J. 2008. Functional expression and comparative characterization of nine murine cytochromes P450 by fluorescent inhibition screening. *Drug Metab Dispos* **36**:1322-31.
- Metzger, D. & Chambon, P. 2001. Site- and time-specific gene targeting in the mouse. *Methods* **24**:71-80.
- Middeldorp, J. & Hol, E. M. 2011. GFAP in health and disease. *Prog Neurobiol* **93**:421-43.

- Mori, T., Tanaka, K., Buffo, A., Wurst, W., Kühn, R. & Götz, M. 2006. Inducible gene deletion in astroglia and radial glia—a valuable tool for functional and lineage analysis. *Glia* **54**:21-34.
- Nagy, A. 2000. Cre recombinase: the universal reagent for genome tailoring. *Genesis* **26**:99-109.
- Namihira, M., Kohyama, J., Abematsu, M. & Nakashima, K. 2008. Epigenetic mechanisms regulating fate specification of neural stem cells. *Philos Trans R Soc Lond B Biol Sci* **363**:2099-109.
- Niehaus, A., Stegmüller, J., Diers-Fenger, M. & Trotter, J. 1999. Cell-surface glycoprotein of oligodendrocyte progenitors involved in migration. *J Neurosci* **19**:4948-61.
- Nimmerjahn, A., Kirchhoff, F., Kerr, J. N. & Helmchen, F. 2004. Sulforhodamine 101 as a specific marker of astroglia in the neocortex in vivo. *Nat Methods* **1**:31-7.
- Nimmerjahn, A., Mukamel, E. A. & Schnitzer, M. J. 2009. Motor behavior activates Bergmann glial networks. *Neuron* **62**:400-12.
- North, R. A. 2016. P2X receptors. *Philos Trans R Soc Lond B Biol Sci* **371**.
- Papouin, T., Dunphy, J., Tolman, M., Foley, J. C. & Haydon, P. G. 2017. Astrocytic control of synaptic function. *Philos Trans R Soc Lond B Biol Sci* **372**.
- Parekh PK, Becker-Krail D, Sundaravelu P, Ishigaki S, Okado H, Sobue G, Huang Y & McClung CA. (2017). Altered GluA1 (Gria1) Function and Accumbal Synaptic Plasticity in the ClockΔ19 Model of Bipolar Mania. *Biol Psychiatry*.
- Pascual, O., Casper, K. B., Kubera, C., Zhang, J., Revilla-Sanchez, R., Sul, J. Y., Takano, H., Moss, S. J., McCarthy, K. & Haydon, P. G. 2005. Astrocytic purinergic signaling coordinates synaptic networks. *Science* **310**:113-6.
- Paukert, M., Agarwal, A., Cha, J., Doze, V. A., Kang, J. U. & Bergles, D. E. 2014. Norepinephrine controls astroglial responsiveness to local circuit activity. *Neuron* **82**:1263-70.
- Perea, G. & Araque, A. 2005. Glial calcium signaling and neuron-glia communication. *Cell Calcium* **38**:375-82.
- Pirttimäki, T. M. & Parri, H. R. 2013. Astrocyte plasticity: implications for synaptic and neuronal activity. *Neuroscientist* **19**:604-15.
- Pologruto, T. A., Sabatini, B. L. & Svoboda, K. 2003. ScanImage: flexible software for operating laser scanning microscopes. *Biomedical engineering online* **2**:13.
- Regan, M. R., Huang, Y. H., Kim, Y. S., Dykes-Hoberg, M. I., Jin, L., Watkins, A. M., Bergles, D. E. & Rothstein, J. D. 2007. Variations in promoter activity reveal a differential expression and physiology of glutamate transporters by glia in the developing and mature CNS. *J Neurosci* **27**:6607-19.
- Reid, J. M., Goetz, M. P., Buhrow, S. A., Walden, C., Safgren, S. L., Kuffel, M. J., Reinicke, K. E., Suman, V., Haluska, P., Hou, X. & Ames, M. M. 2014. Pharmacokinetics of endoxifen and tamoxifen in female mice: implications for comparative in vivo activity studies. *Cancer Chemother Pharmacol* **74**:1271-8.
- Ren, J. Q., Aika, Y., Heizmann, C. W. & Kosaka, T. 1992. Quantitative analysis of neurons and glial cells in the rat somatosensory cortex, with special reference to GABAergic neurons and parvalbumin-containing neurons. *Experimental brain research* **92**:1-14.
- Ricci, G., Volpi, L., Pasquali, L., Petrozzi, L. & Siciliano, G. 2009. Astrocyte-neuron interactions in neurological disorders. *J Biol Phys* **35**:317-36.
- Robertson, D. W., Katzenellenbogen, J. A., Long, D. J., Rorke, E. A. & Katzenellenbogen, B. S. 1982. Tamoxifen antiestrogens. A comparison of the activity, pharmacokinetics, and metabolic activation of the cis and trans isomers of tamoxifen. *J Steroid Biochem* **16**:1-13.
- Rudolph, R., Jahn, H. M., Courjaret, R., Messemer, N., Kirchhoff, F. & Deitmer, J. W. 2016. The inhibitory input to mouse cerebellar Purkinje cells is reciprocally modulated by Bergmann glial P2Y1 and AMPA receptor signaling. *Glia* **64**:1265-80.

- Saab, A. S., Neumeyer, A., Jahn, H. M., Cupido, A., Šimek, A. A., Boele, H. J., Scheller, A., Le Meur, K., Götz, M., Monyer, H., Sprengel, R., Rubio, M. E., Deitmer, J. W., De Zeeuw, C. I. & Kirchhoff, F. 2012. Bergmann glial AMPA receptors are required for fine motor coordination. *Science* **337**:749-53.
- Safiulina, V. F., Afzalov, R., Khiroug, L., Cherubini, E. & Giniatullin, R. 2006. Reactive oxygen species mediate the potentiating effects of ATP on GABAergic synaptic transmission in the immature hippocampus. *J Biol Chem* **281**:23464-70.
- Scemes, E. & Giaume, C. 2006. Astrocyte calcium waves: what they are and what they do. *Glia* **54**:716-25.
- Schipke, C. G., Boucsein, C., Ohlemeyer, C., Kirchhoff, F. & Kettenmann, H. 2002. Astrocyte Ca<sup>2+</sup> waves trigger responses in microglial cells in brain slices. *FASEB J* **16**:255-7.
- Schipke, C. G., Ohlemeyer, C., Matyash, M., Nolte, C., Kettenmann, H. & Kirchhoff, F. 2001. Astrocytes of the mouse neocortex express functional N-methyl-D-aspartate receptors. *FASEB J* **15**:1270-2.
- Seger, S., Stritt, M., Doppler, K., Frank, S., Panaite, A., Kuntzer, T., Steck, A., Pagenstecher, A., Sommer, C. & Stalder, A. K. 2016. A semi-automated method to assess intraepidermal nerve fibre density in human skin biopsies. *Histopathology* **68**:657-65.
- Seger, S., Stritt, M., Vezzali, E., Nayler, O., Hess, P., Groenen, P. M. A. & Stalder, A. K. 2018. A fully automated image analysis method to quantify lung fibrosis in the bleomycin-induced rat model. *PLoS One* **13**:e0193057.
- Seifert, G. & Steinhäuser, C. 2001. Ionotropic glutamate receptors in astrocytes. *Prog Brain Res* **132**:287-99.
- Sheth, S., Brito, R., Mukherjee, D., Rybak, L. P. & Ramkumar, V. 2014. Adenosine receptors: expression, function and regulation. *Int J Mol Sci* **15**:2024-52.
- Shigetomi, E., Hirayama, Y. J., Ikenaka, K., Tanaka, K. F. & Koizumi, S. 2018. Role of Purinergic Receptor P2Y<sub>1</sub> in Spatiotemporal Ca. *J Neurosci* **38**:1383-95.
- Shinozaki, Y., Shibata, K., Yoshida, K., Shigetomi, E., Gachet, C., Ikenaka, K., Tanaka, K. F. & Koizumi, S. 2017. Transformation of Astrocytes to a Neuroprotective Phenotype by Microglia via P2Y. *Cell Rep* **19**:1151-64.
- Sirko, S., Behrendt, G., Johansson, P. A., Tripathi, P., Costa, M., Bek, S., Heinrich, C., Tiedt, S., Colak, D., Dichgans, M., Fischer, I. R., Plesnila, N., Staufenbiel, M., Haass, C., Snapyan, M., Saghatelian, A., Tsai, L. H., Fischer, A., Grobe, K., Dimou, L. & Götz, M. 2013. Reactive glia in the injured brain acquire stem cell properties in response to sonic hedgehog. [corrected]. *Cell Stem Cell* **12**:426-39.
- Sofroniew, M. V. & Vinters, H. V. 2010. Astrocytes: biology and pathology. *Acta Neuropathol* **119**:7-35.
- Stearns, V., Beebe, K. L., Iyengar, M. & Dube, E. 2003. Paroxetine controlled release in the treatment of menopausal hot flashes: a randomized controlled trial. *JAMA* **289**:2827-34.
- Stearns, V. & Rae, J. M. 2008. Pharmacogenetics and breast cancer endocrine therapy: CYP2D6 as a predictive factor for tamoxifen metabolism and drug response? *Expert Rev Mol Med* **10**:e34.
- Sun, J. J., Liu, Y. & Ye, Z. R. 2008. Effects of P2Y<sub>1</sub> receptor on glial fibrillary acidic protein and glial cell line-derived neurotrophic factor production of astrocytes under ischemic condition and the related signaling pathways. *Neurosci Bull* **24**:231-43.
- Takizawa, T. & Meshorer, E. 2008. Chromatin and nuclear architecture in the nervous system. *Trends Neurosci* **31**:343-52.
- Thrane, A. S., Rangroo Thrane, V., Zeppenfeld, D., Lou, N., Xu, Q., Nagelhus, E. A. & Nedergaard, M. 2012. General anesthesia selectively disrupts astrocyte calcium signaling in the awake mouse cortex. *Proc Natl Acad Sci U S A* **109**:18974-9.
- Valny, M., Honsa, P., Kirdajova, D., Kamenik, Z. & Anderova, M. 2016. Tamoxifen in the Mouse Brain: Implications for Fate-Mapping Studies Using the Tamoxifen-Inducible Cre-loxP System. *Front Cell Neurosci* **10**:243.

- Verkhatsky, A. & Kirchhoff, F. 2007. Glutamate-mediated neuronal-glia transmission. *Journal of Anatomy* **210**:651-60.
- Verkhatsky, A., Verkhatsky, A., Krishtal, O. A. & Burnstock, G. 2009. Purinoceptors on neuroglia. *Mol Neurobiol* **39**:190-208.
- Vooijs, M., Jonkers, J. & Berns, A. 2001. A highly efficient ligand-regulated Cre recombinase mouse line shows that LoxP recombination is position dependent. *EMBO Rep* **2**:292-7.
- Wang, X., Lou, N., Xu, Q., Tian, G. F., Peng, W. G., Han, X., Kang, J., Takano, T. & Nedergaard, M. 2006. Astrocytic Ca<sup>2+</sup> signaling evoked by sensory stimulation in vivo. *Nat Neurosci* **9**:816-23.
- Weber, P., Metzger, D. & Chambon, P. 2001. Temporally controlled targeted somatic mutagenesis in the mouse brain. *Eur J Neurosci* **14**:1777-83.
- Wright, A. & Vissel, B. 2012. The essential role of AMPA receptor GluR2 subunit RNA editing in the normal and diseased brain. *Front Mol Neurosci* **5**:34.
- Yang, Y., Liu, N., He, Y., Liu, Y., Ge, L., Zou, L., Song, S., Xiong, W. & Liu, X. 2018. Improved calcium sensor GCaMP-X overcomes the calcium channel perturbations induced by the calmodulin in GCaMP. *Nat Commun* **9**:1504.
- Zhang, Y., Chen, K., Sloan, S. A., Bennett, M. L., Scholze, A. R., O'Keeffe, S., Phatnani, H. P., Guarnieri, P., Caneda, C., Ruderisch, N., Deng, S., Liddelow, S. A., Zhang, C., Daneman, R., Maniatis, T., Barres, B. A. & Wu, J. Q. 2014. An RNA-sequencing transcriptome and splicing database of glia, neurons, and vascular cells of the cerebral cortex. *J Neurosci* **34**:11929-47.
- Zheng, W., Watts, L. T., Holstein, D. M., Prajapati, S. I., Keller, C., Grass, E. H., Walter, C. A. & Lechleiter, J. D. 2010. Purinergic receptor stimulation reduces cytotoxic edema and brain infarcts in mouse induced by photothrombosis by energizing glial mitochondria. *PLoS One* **5**:e14401.
- Zhong, Z. A., Sun, W., Chen, H., Zhang, H., Lay, Y. E., Lane, N. E. & Yao, W. 2015. Optimizing tamoxifen-inducible Cre/loxP system to reduce tamoxifen effect on bone turnover in long bones of young mice. *Bone* **81**:614-19.

## 10. APPENDIX I

### 10.1. No tamoxifen-independent recombination of non-astrocytic Cre<sup>ERT2</sup> driver lines

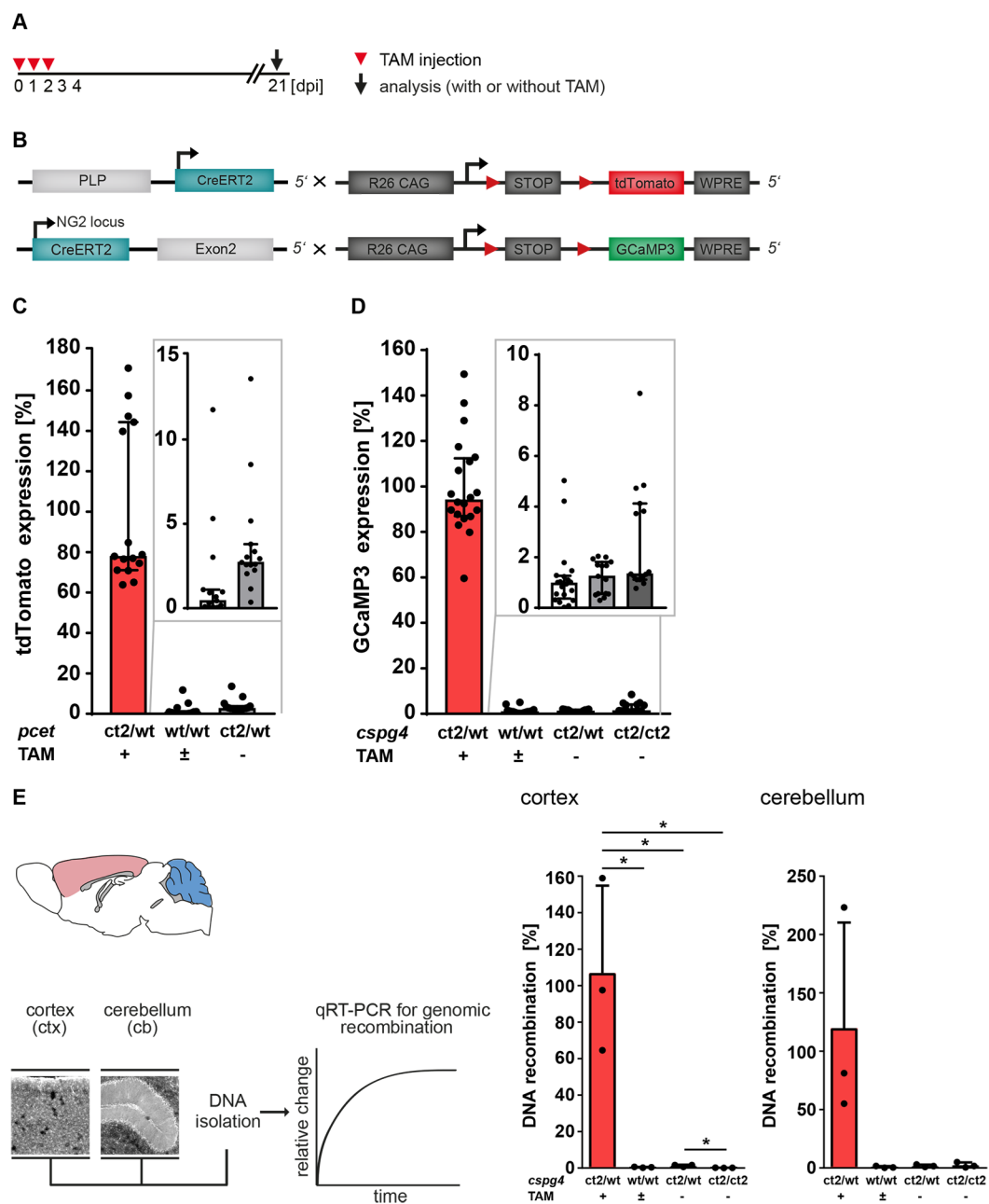
Next to the astrocyte-specific Cre<sup>ERT2</sup> driver lines we investigated the PLP-Cre<sup>ERT2</sup> mouse line, as a non-homologous recombined transgenic line, specific for oligodendroglial recombination, and the NG2-Cre<sup>ERT2</sup> knockin mouse line that recombines oligodendrocyte precursor cells (OPCs; NG2 glia). Non-induced tdTomato ( $\alpha$ -DsRed) or GCaMP3 ( $\alpha$ -GFP) expression were quantified by Orbit image analysis. The PLP-Cre<sup>ERT2</sup> line had less recombined cells compared to GLAST-Cre<sup>ERT2</sup>, but more than NG2-Cre<sup>ERT2</sup> mice, where almost no tamoxifen-independent recombination was detected. Only a few cells were recombined in the homozygous condition (1.3 %). The PLP-Cre<sup>ERT2</sup> mouse line showed less than 3 % reporter expression of heterozygous non-injected animals compared to the negative control (2.7 % to 0.4 %, respectively) (Fig. 40 C, D).

Tamoxifen-independent recombination at the DNA level was determined for cortex and cerebellum of the NG2-Cre<sup>ERT2</sup> line by quantification of recombined *gcamp3* alleles (Fig. 40 E). Highest recombination efficiency for *gcamp3* alleles was found in the positive control, while negative control, heterozygous and homozygous animals remained unaffected for both brain regions.

**Figure 40. Negligible tamoxifen-independent recombination of the PLP- and NG2-Cre<sup>ERT2</sup> driver line**

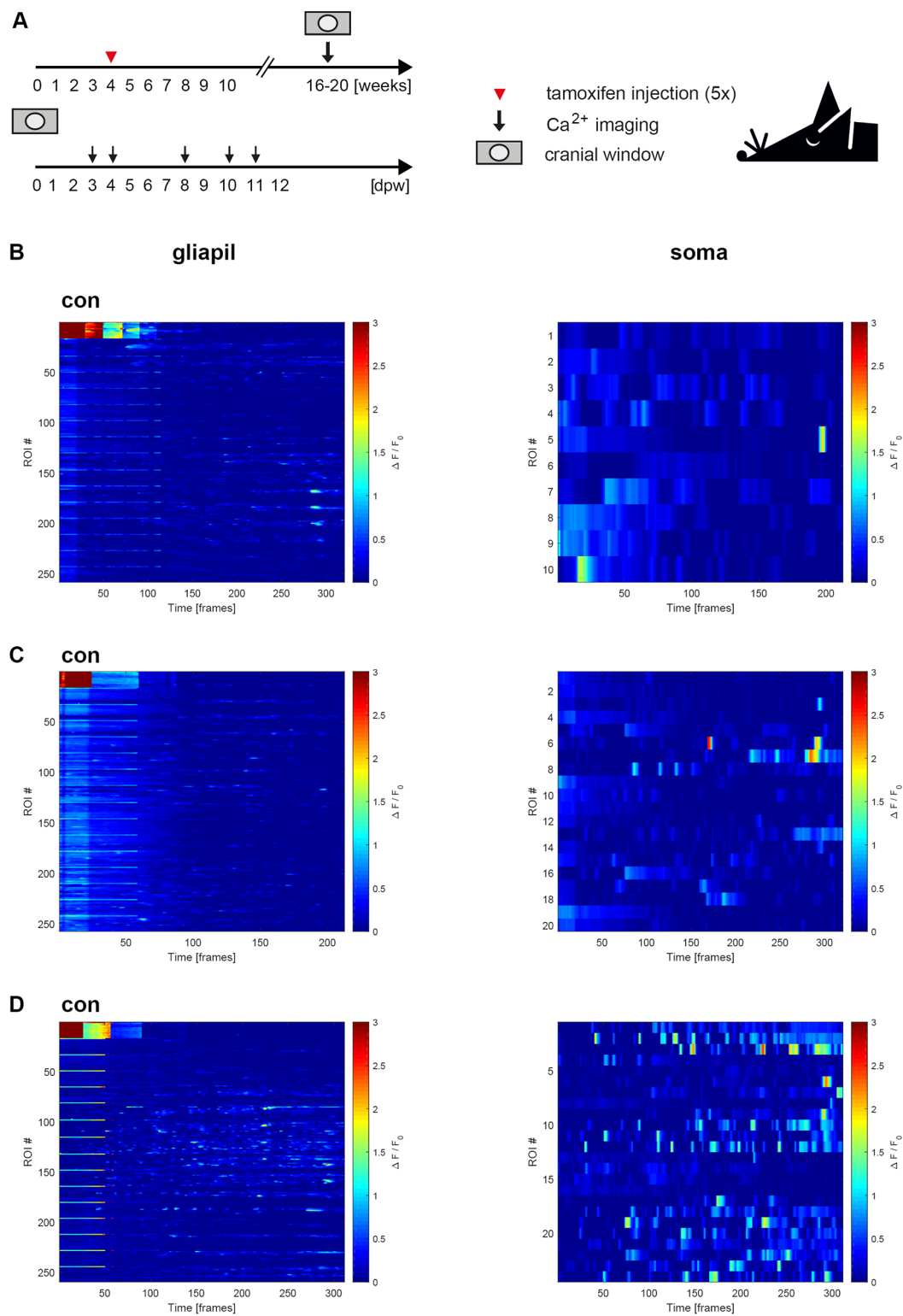
(A) Animals were injected with TAM at an age of four weeks for three consecutive days and analyzed 21 dpi (positive control). (B) PLP-Cre<sup>ERT2</sup> and NG2-Cre<sup>ERT2</sup> driver lines were either crossbred to the reporter line tdTomato or GCaMP3, respectively. (C) PLP-Cre<sup>ERT2</sup> line revealed highest tdTomato ( $\alpha$ -DsRed) expression in the positive control, while no expression could be found for the negative control. Heterozygous animals revealed less than 2.7 % reporter expression. (D) NG2-Cre<sup>ERT2</sup> line revealed highest reporter expression in the positive control, while negative control, heterozygous and homozygous animals were mainly unaffected. (E) DNA recombination of the *gcamp3* locus was determined for cortex and cerebellum of the NG2-Cre<sup>ERT2</sup> line. Highest recombination efficiency for *gcamp3* alleles was found in the positive control, while negative control, heterozygous and homozygous animals remained unaffected. (C, D) The error bars correlate to the median  $\pm$  interquartile range of the biological replicates ( $n = 3$ , \*  $p < 0.01$ -0.05; \*\*  $p < 0.001$ -0.01; \*\*\*  $p < 0.0001$ -0.001; \*\*\*\*  $p > 0.00001$ , Mann-Whitney test). (E) Three animals were analyzed per group and  $\Delta$ CT-values were normalized to the mean value of animals which received 3x TAM. The error bars correlate to the SD of the biological replicates ( $n = 3$ , \*  $p < 0.05$ , \*\*  $p < 0.01$ , \*\*\*  $p < 0.001$ , unpaired t-test).

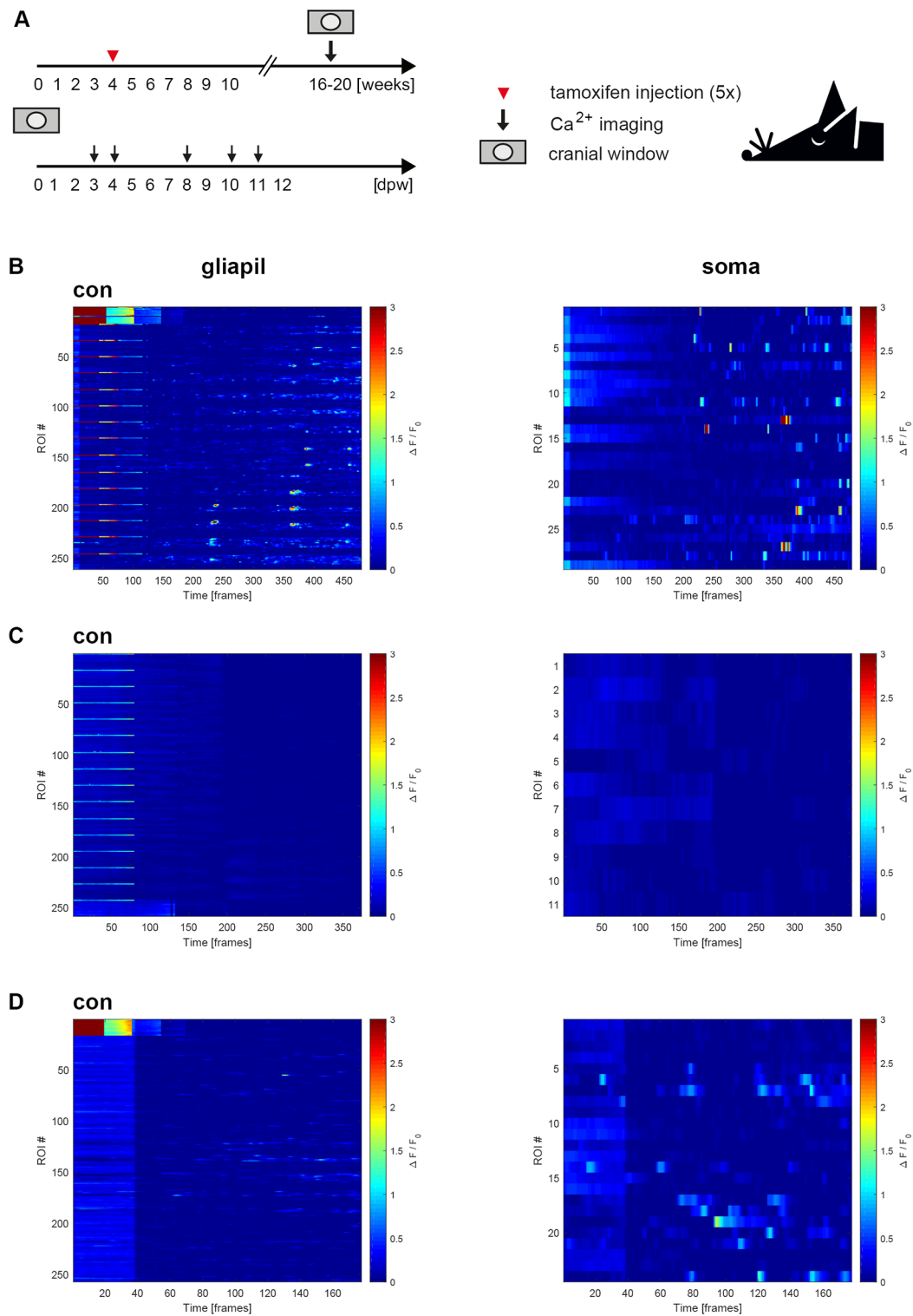


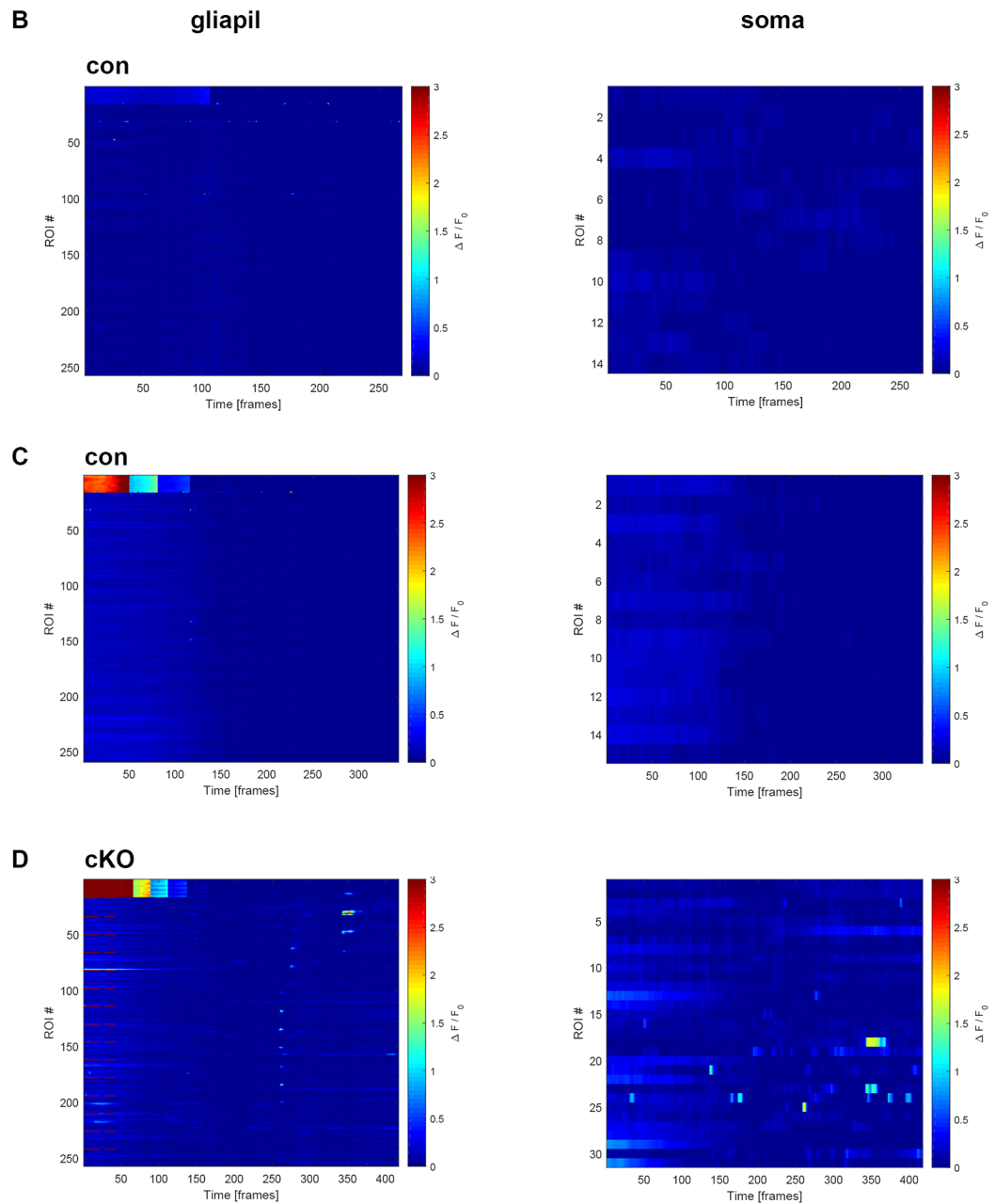
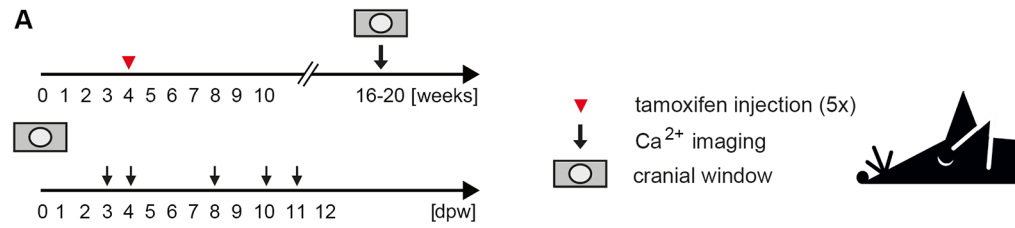


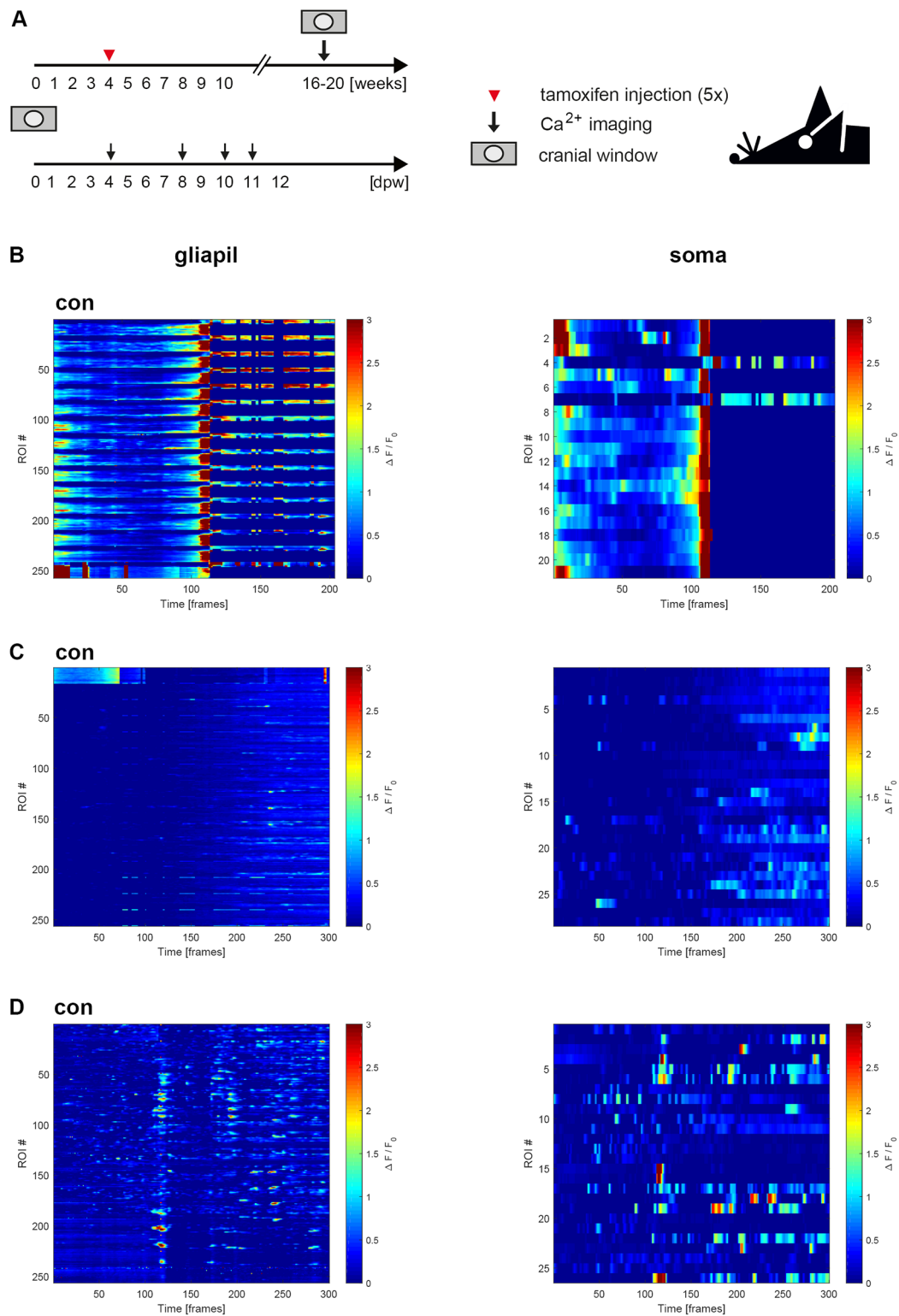
## 10.2. Heatmaps of *in vivo* Ca<sup>2+</sup> imaging

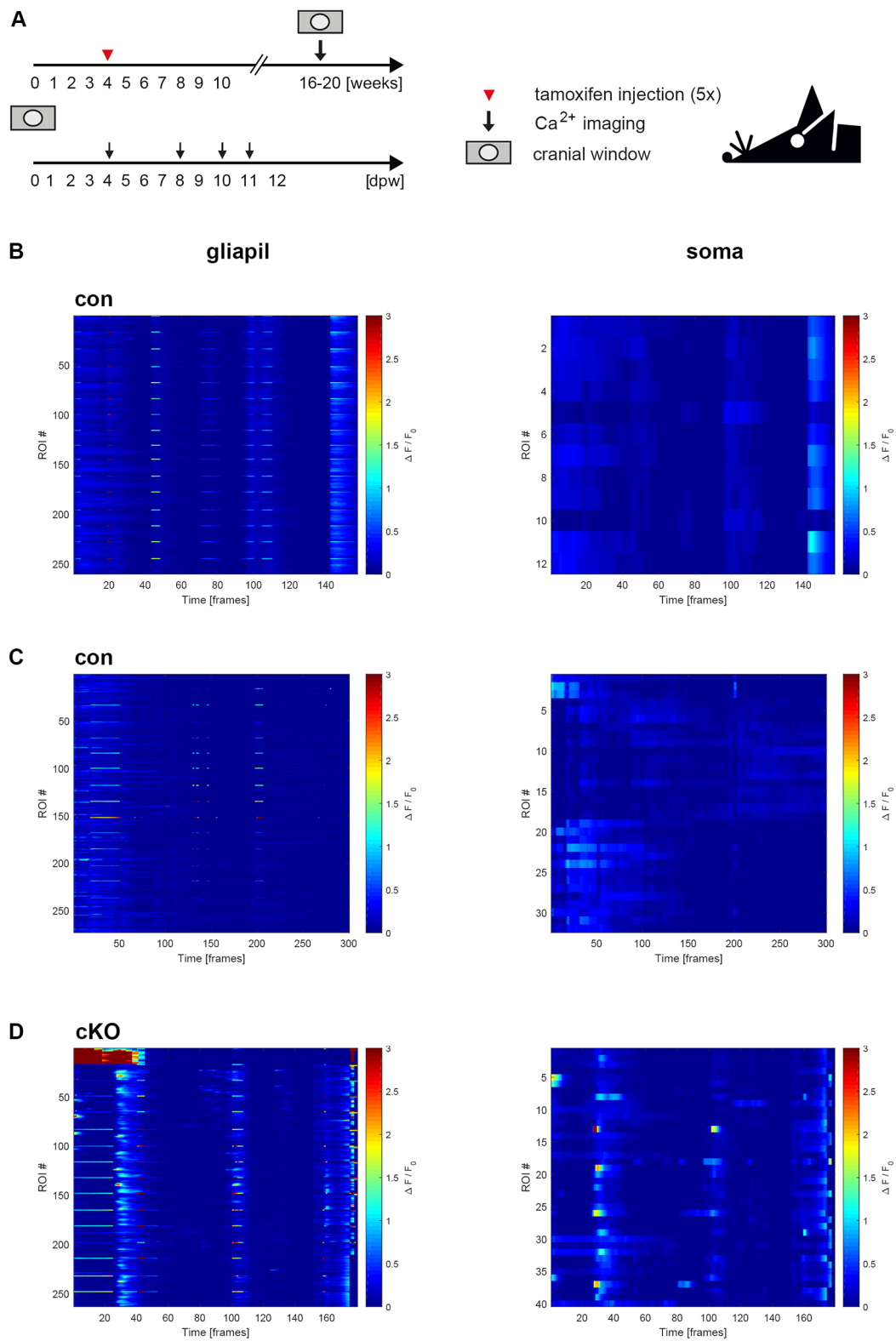
Heatmaps generated by MSparkles for all *in vivo* Ca<sup>2+</sup> data sets (Fig. 35-37) of gliapil and soma. Heatmaps show the magnitude of the signal (y-axis; amplitude or duration) over the time (x-axis). Each single imaging session is depicted in an extra heatmap (Fig. 41).











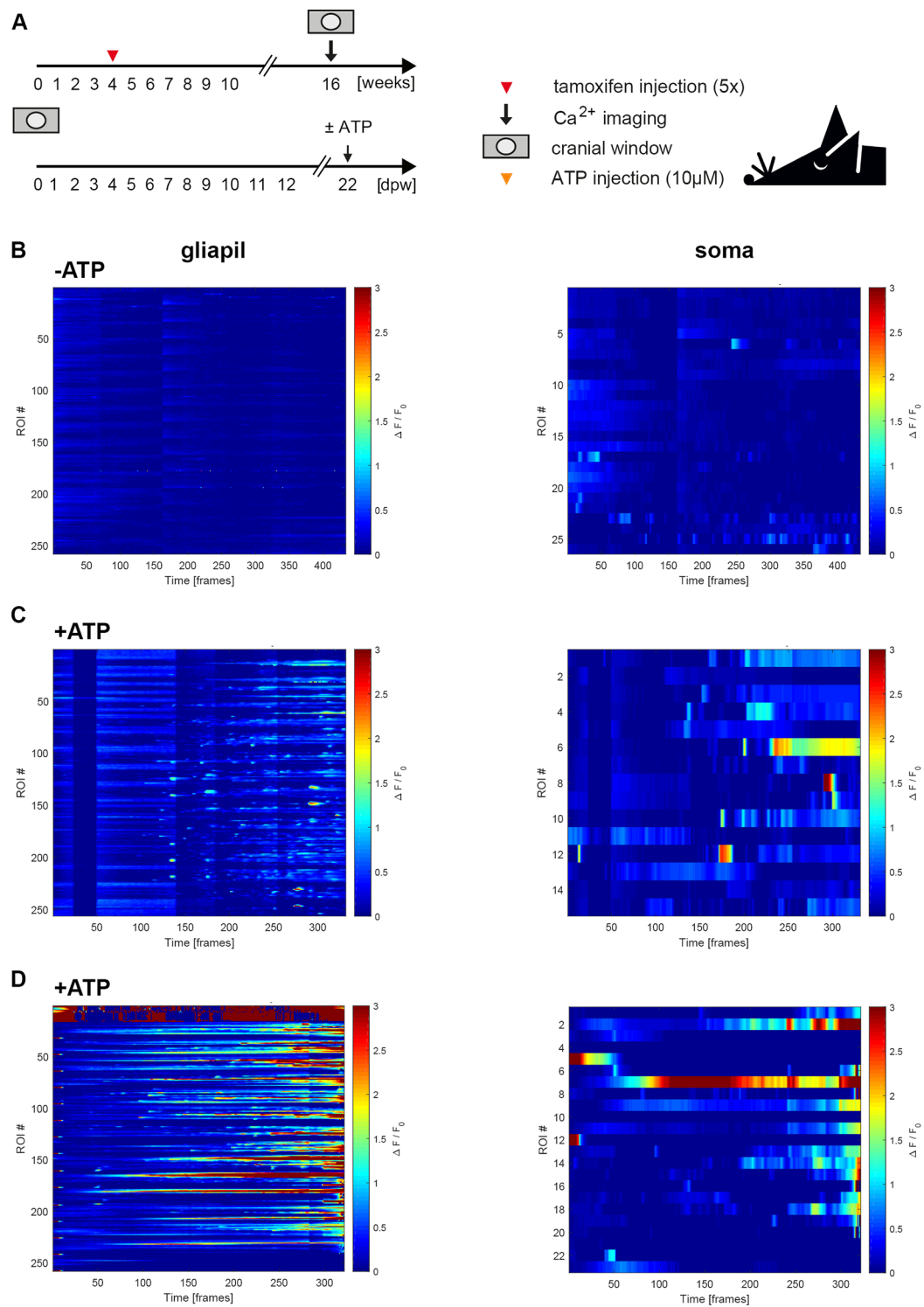


**Figure 41. Heatmaps of *in vivo* Ca<sup>2+</sup> data revealed no pattern changes in Ca<sup>2+</sup> signals**

(A) Heatmaps of Ca<sup>2+</sup> data of five times injected animals either anesthetized, awake or with ATP treatment. (B-D) Heatmaps were separated for gliapil and soma as well as for con and cKOs at different imaging days. All heatmaps indicate the regions of interest (ROIs; left y-axes), timeline (frames) and  $\Delta F/F_0$ . Heatmaps depict randomized Ca<sup>2+</sup> signals with no obvious pattern.

### 10.3. Detailed procedure of Ca<sup>2+</sup> imaging analysis using MSparkles

For clearer understanding of how Ca<sup>2+</sup> data were processed for the results part data of figure 35 were shown in detail (Fig. 42 and 43). Mice were injected and prepared for imaging as described before (Fig. 35). Data are depicted in bar charts with dot plots. Each bar represents a single imaging session on one day and every dot represents a single Ca<sup>2+</sup> signal. Imaging days and investigated animals are indicated beneath x-axes. Colorcode of bars indicate if animals were P2Y1 controls (grey) or cKOs (red). Figures are divided in gliapil (Fig 42) and soma (Fig 43) and in amplitude (Fig. 42 and 43 A) and duration (Fig. 42 and 43 B) of respective Ca<sup>2+</sup> signals. Data are further divided in small, medium sized and large signals (1 SD, 2 SD and 3 SD), respectively. For comparison compressed data (as box plot) of figure 35 are shown on the right side of the figures.



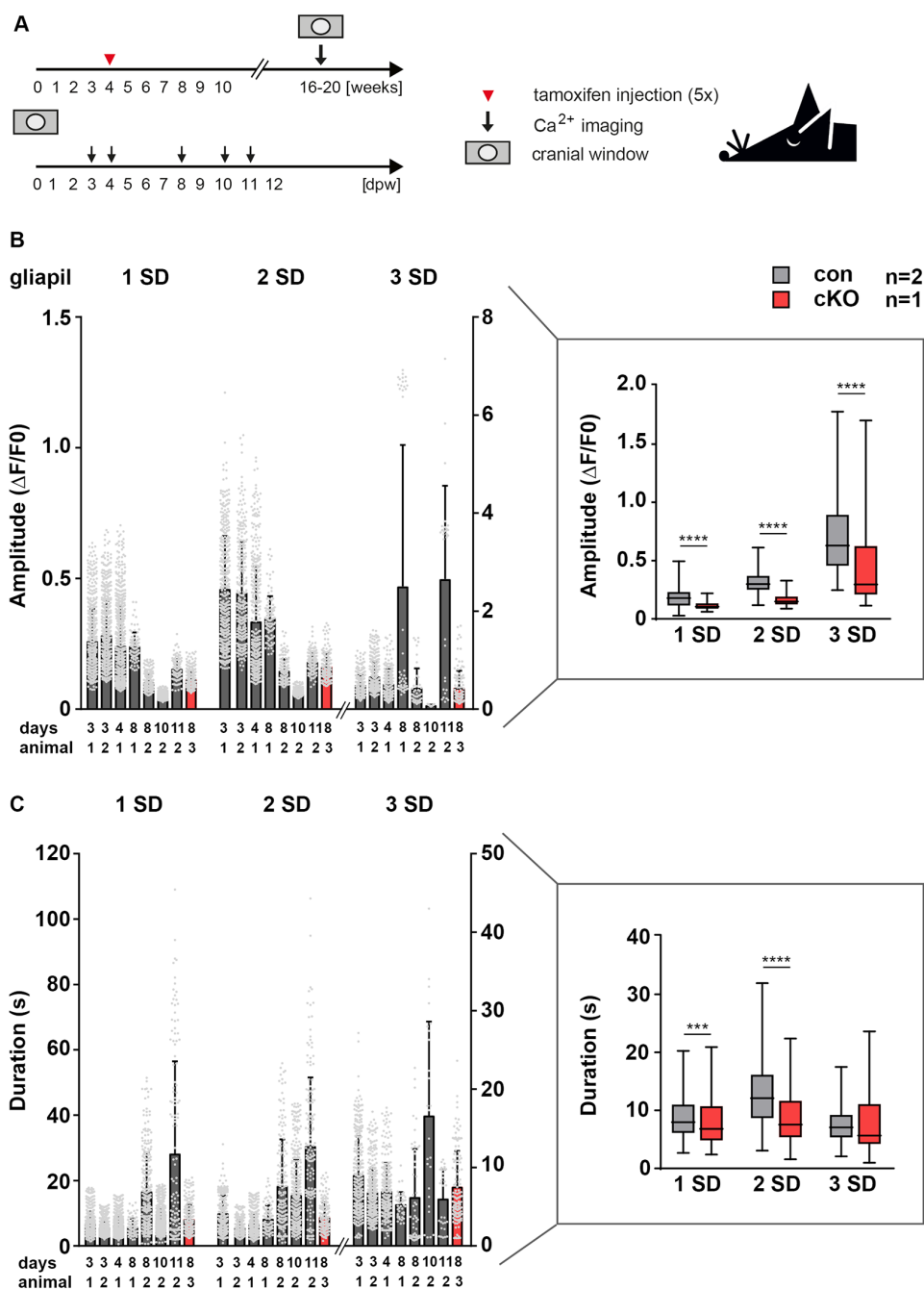


**Figure 42. Composition of Ca<sup>2+</sup> data representing each imaging session, animal and Ca<sup>2+</sup> signal of the gliapil**

(A) Mice were injected and prepared for imaging as described before. (B) Signal amplitudes of the gliapil depicted as bar chart with box plots representing single animals at different imaging days and single measured Ca<sup>2+</sup> signals (dots). On the right side same data are depicted in a compressed version as used in the results part. (C) Signal durations of the gliapil depicted as described before (see B). Con animals and cKOs were indicated by different colors. All data were further divided in small, medium sized and large signals stated as 1 SD, 2 SD and 3 SD, respectively.

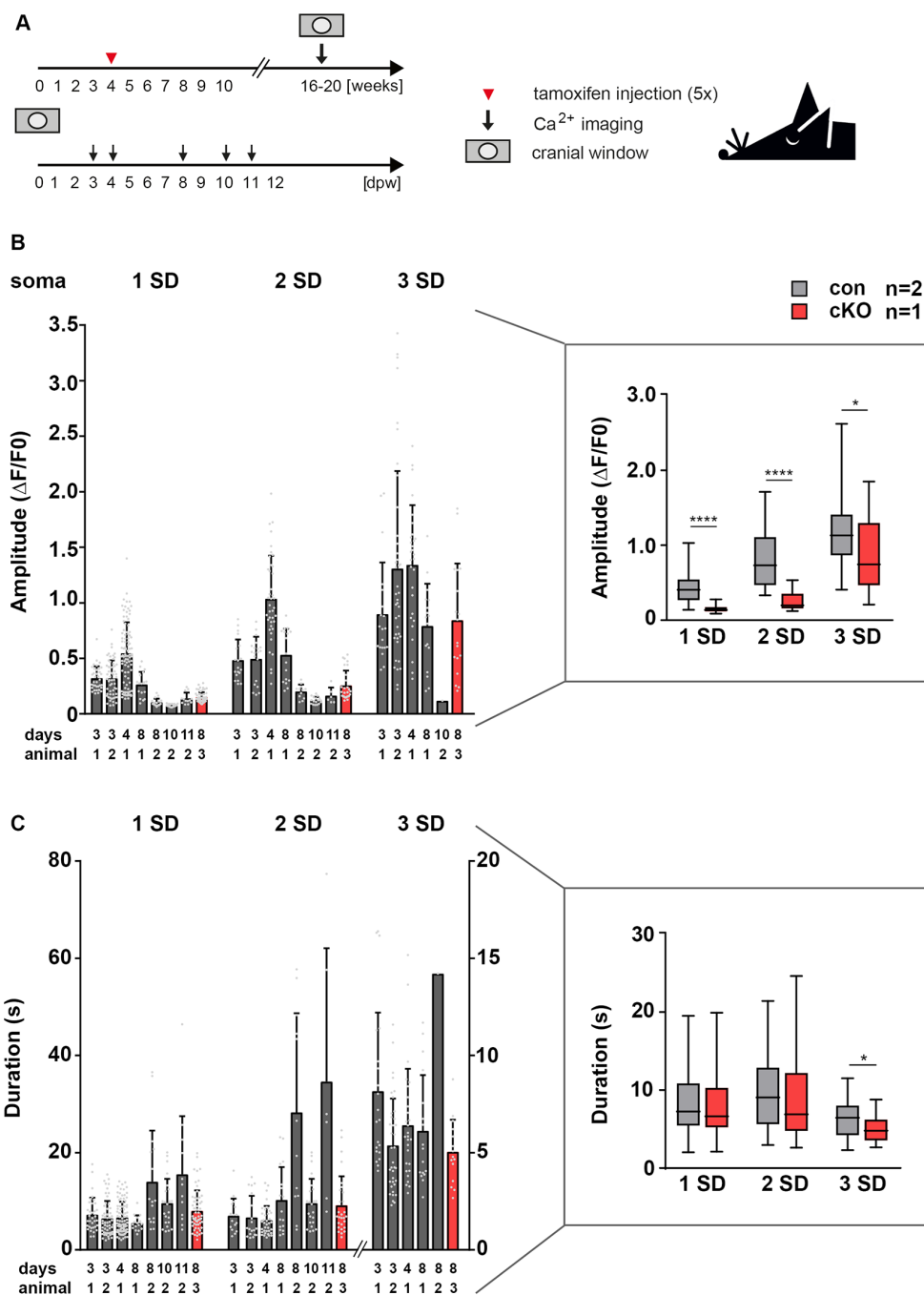


**Figure 43. Composition of Ca<sup>2+</sup> data representig each animal, imaging session and Ca<sup>2+</sup> signal of the soma**

(A) Mice were injected and prepared for imaging as described before. (B) Signal amplitudes of the soma depicted as bar chart with box plots representing single animals at different imaging days and single measured Ca<sup>2+</sup> signals (dots). On the right side same data are depicted in a compressed version as shown in the results part. (C) Somatic signal duration depicted as described before (see B). Con animals and cKOs were indicated by different colors. All data were further divided in small, medium sized and large signals stated as 1 SD, 2 SD and 3 SD, respectively.

#### **10.4. Comparison of anesthetized and awake $\text{Ca}^{2+}$ signals revealed higher signal amplitudes in gliapil and soma**

Comparison of  $\text{Ca}^{2+}$  data of anesthetized (Fig 35) and awake (Fig. 36) P2Y1 control and cKO mice, injected with TAM for five consecutive days at an age of four weeks. Cranial window was performed between 16-20 weeks and mice were imaged at day 3, 4, 8, 10 and 11 after surgery (Fig. 44 A).  $\text{Ca}^{2+}$  signals of the gliapil of anesthetized and awake controls and cKOs revealed higher signal amplitudes in all classes of  $\text{Ca}^{2+}$  signals (1 SD, 2 SD and 3 SD) in awake control and cKO mice. Duration of small signals in awake control animals was shortened, while duration of cKOs was unaltered. Duration of medium sized signals was shortened in awake controls and cKOs compared to anesthetized controls and cKOs. Large signals did not change in duration of the controls under anesthetized and awake conditions, but were reduced in cKOs under awake condition (Fig. 44 B). Somatic signal amplitudes of small (1 SD)  $\text{Ca}^{2+}$  signals were higher in awake controls and cKOs compared to the anesthetized condition. Amplitudes of medium sized signals were only increased in awake cKOs compared to anesthetized cKOs, while amplitudes of large signals were only higher in awake controls. Signal duration was not changed in small and large  $\text{Ca}^{2+}$  signals of anesthetized vs. awake controls and cKOs. Duration of medium sized somatic signals revealed a prolonged duration in controls under awake condition (Fig. 44 C).

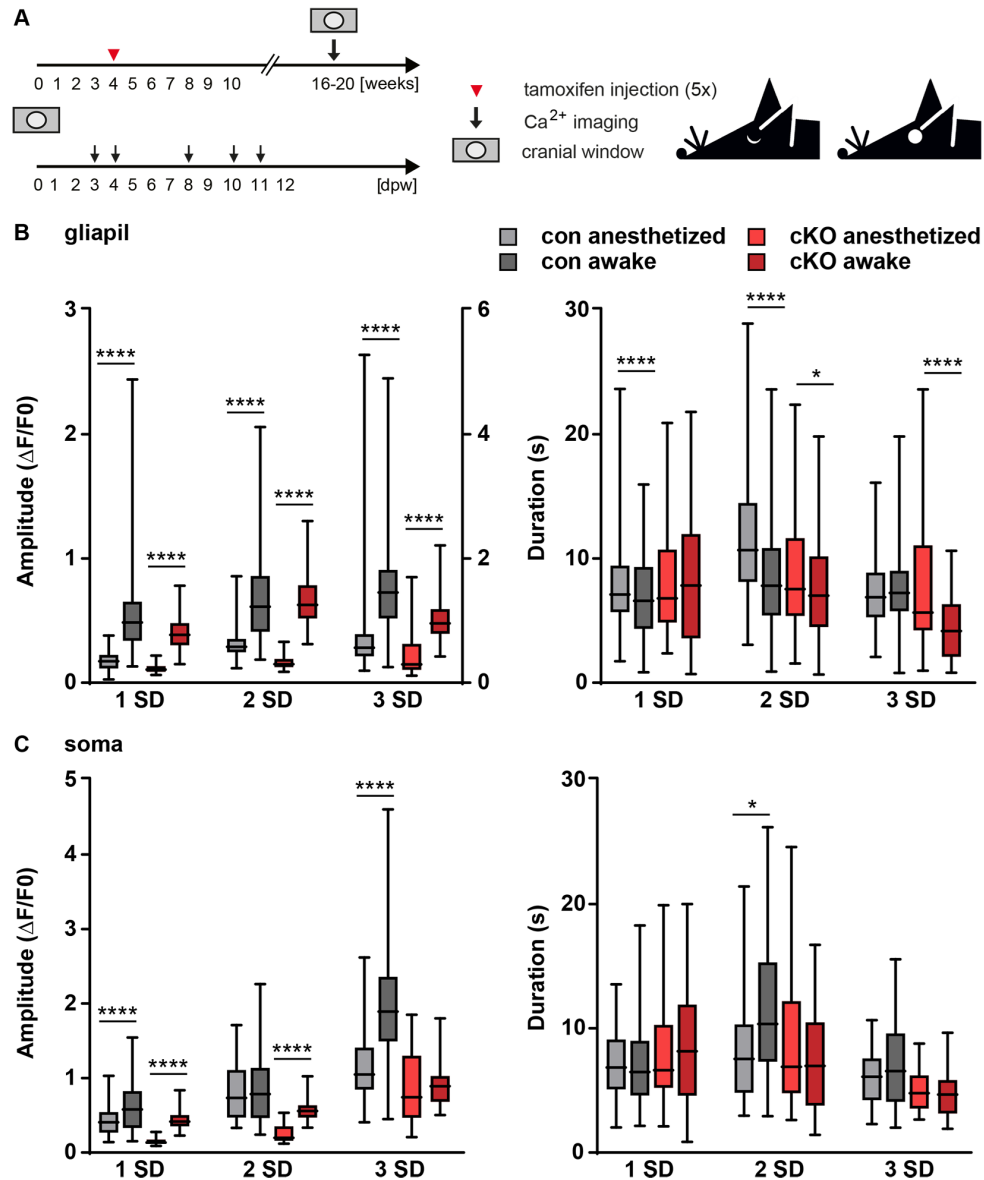


**Figure 44. Differences of Ca<sup>2+</sup> signals in gliapil and soma between anesthetized and awake mice**

(A) Mice were injected with TAM at an age of four weeks for five consecutive days. Cranial window surgery was performed at an age between 16-20 w and mice were imaged at day 3, 4, 8, 10 and 11 after surgery (dpw). Data of anesthetized and awake con and cKO mice were compared. (B) Signal amplitudes of the gliapil revealed higher amplitudes of all classes of Ca<sup>2+</sup> signals under awake condition of con and cKOs. Duration of small signals was shortened in con under awake condition. Medium sized signals revealed shortened duration of awake con and cKOs, while large signals were only shortened in awake cKOs. (C) Somatic signal amplitudes of small signals were enlarged in awake con and cKO animals compared to the respective anesthetized condition. Amplitudes of medium sized signals were only higher in awake cKO animals, while amplitudes of large signals were increased in awake con. Signal duration of small and large signals did not change in con and cKOs under both conditions, while duration of medium sized signals was prolonged in awake con animals.

The error bars correlate to the median  $\pm$  interquartile range of the biological replicates (n = 1-2, \* p 0.01-0.05; \*\* p 0.001-0.01; \*\*\* p 0.0001-0.001; \*\*\*\* p > 0, Mann-Whitney test).

## 10.5. Raw data of *in vivo* Ca<sup>2+</sup> imaging

All raw data of *in vivo* Ca<sup>2+</sup> imaging are listed in tables 19-21. The number of measured Ca<sup>2+</sup> signals (n) of gliapil and soma, respective median  $\pm$  25 % percentile and 75 % percentile are listed.

**Table 19. Data of Figure 35**

gliapil amplitude	1 SD con	1 SD cKO	2 SD con	2 SD cKO	3 SD con	3 SD cKO
n	842	254	408	154	359	116
25 %ile	0.1155	0.08751	0.2499	0.1253	0.4559	0.2098
median	0.1779	0.1053	0.2983	0.1491	0.6284	0.296
75 %ile	0.2305	0.1334	0.3694	0.1919	0.8925	0.6248
gliapil duration						
n	829	235	417	161	415	146
25 %ile	6.112	4.85	8.672	5.387	5.343	4.214
median	7.977	6.804	12.09	7.543	7.084	5.656
75 %ile	10.99	10.72	16.13	11.64	9.216	11.07
soma amplitude						
n	92	57	40	27	40	18
25 %ile	0.2682	0.1165	0.4689	0.1582	0.8679	0.4672
median	0.4061	0.1355	0.7322	0.1985	1.132	0.7439
75 %ile	0.5425	0.1741	1.109	0.3517	1.409	1.298
soma duration						
n	91	57	40	28	39	15
25 %ile	5.448	5.223	5.621	4.784	4.216	3.547
median	7.243	6.629	9.054	6.897	6.445	4.79
75 %ile	10.84	10.29	12.86	12.19	8.015	6.213

**Table 20. Data of Figure 36**

gliapil amplitude	1 SD con	1 SD cKO	2 SD con	2 SD cKO	3 SD con	3 SD cKO
n	731	176	358	161	311	215
25 %ile	0,3446	0,3021	0,4329	0,5176	1,133	0,7893
median	0,4965	0,3858	0,6406	0,6263	1,519	0,9567
75 %ile	0,666	0,4802	0,8755	0,7858	1,986	1,185
gliapil duration						
n	720	195	365	165	342	251
25 %ile	4,467	3,589	5,59	4,484	5,703	2,1

median	6,953	7,84	8,083	7,021	7,234	4,173
75 %ile	10,57	11,97	11,96	10,17	9,3	6,324
<b>soma amplitude</b>						
n	91	31	39	27	31	31
25 %ile	0,3343	0,3512	0,4634	0,4708	1,493	0,6832
median	0,5793	0,4159	0,7843	0,558	1,893	0,8906
75 %ile	0,8237	0,5028	1,135	0,6332	2,358	1,027
<b>soma duration</b>						
n	86	31	39	27	31	34
25 %ile	4,719	4,583	7,32	3,792	4,732	3,155
median	7,607	8,152	10,75	6,977	6,357	4,671
75 %ile	11,17	11,92	15,96	10,48	9,587	5,83

Table 21. Data of Figure 37

gliapil amplitude	1 SD -ATP	1 SD +ATP	2 SD -ATP	2 SD +ATP	3 SD -ATP	3 SD +ATP
n	347	330	189	193	78	106
25 %ile	0.09941	0.3674	0.1581	0.5731	0.2	0.9709
median	0.1179	0.4848	0.1869	0.7402	0.2517	1.384
75 %ile	0.1399	0.6488	0.2308	1.005	0.3154	2.131
<b>gliapil duration</b>						
n	328	307	184	179	87	135
25 %ile	6.985	5.589	8.124	6.277	7.062	4.053
median	13.29	8.638	16.27	8.982	13.13	5.413
75 %ile	20.04	13.7	29.98	13.18	18.61	7.432
<b>soma amplitude</b>						
n	40	21	12	11	10	8
25 %ile	0.1397	0.4743	0.242	0.5346	0.6862	1.937
median	0.2333	0.5554	0.3979	1.003	0.7346	3.312
75 %ile	0.3477	0.9088	0.5648	1.154	0.8587	9.184
<b>soma duration</b>						
n	38	21	12	11	10	9
25 %ile	5.313	7.321	8.36	8.116	6.684	2.71
median	9.296	12.97	18.89	10.43	10.37	4.445
75 %ile	15.26	26.91	40.6	19.56	17.34	7.158

## 11. APPENDIX II

### 11.1. List of Publication

#### 11.1.1. Publication

Published:

Jahn, H. M.<sup>#</sup>, **Kasakow, C. V.<sup>#</sup>**, Helfer, A., Michely, J., Verkhatsky, A., Maurer, H. H., Scheller, A. & Kirchhoff, F. 2018. Refined protocols of tamoxifen injection for inducible DNA recombination in mouse astroglia. *Sci Rep* **8**:5913.

<sup>#</sup> equal authorship

Publications in preparation

**Kasakow, C.V.<sup>#</sup>**, Stopper, L.<sup>#</sup>, Caudal, L. C., Linder, S., Stopper, G., Price, A. M., Guo, Q., Huang, W., Scheller, A., Kirchhoff, F. Comparison of tamoxifen-independent genomic recombination in various Cre<sup>ERT2</sup> transgenic mice.

<sup>#</sup> equal authorship

Welle, A., **Kasakow C.V.**, Nordström, K., Salhab, A., Gasparoni G., Scheller, A., Kirchhoff, F., Walter J. Epigenetic and transcriptional landscape shape astroglial diversity.

**Kasakow, C.V.**, Stopper, L., Linder, S., Stopper, G., Scheller, A., Kirchhoff, F.: The role of P2Y1 receptor ablation for astrocytic Ca<sup>2+</sup> signalling *in vivo*.

#### 11.1.2. Posters/ Oral presentations

International Symposia

**Bohn CV**, Jahn HM, Schlosser L, Stopper G, Scheller A, Kirchhoff F (2017) Analysis of astrocyte-specific P2Y1 receptor gene deletion –gene excision, receptor ablation, Ca<sup>2+</sup> signaling-. Poster presentation at the XIII European Conference on Glial Cells in Health and Disease in Edinburgh, Scotland.

**Bohn CV**, (2016) Analysis of purinergic P2Y1 receptor function in cortical astrocytes and cerebellar Bergmann glia. Oral presentation at the 12<sup>th</sup> Göttingen Meeting of the German Neuroscience Society in Göttingen, Germany.

**Bohn CV**, Jahn HM, Bai X, Scheller A, Kirchhoff F (2016) Impact of the glial P2Y1 receptor under pathological conditions. Role of P2Y1 receptors in cortical astrocytes and cerebellar Bergmann glia. Poster presentation at the 1<sup>st</sup> Young Glia Meeting in Tokio, Japan.

**Bohn CV**, (2015) Analysis of astrocyte-specific gene recombination *in vivo*. Oral presentation at the DAAD-CAPES workshop in Campinas, Brasil.

**Bohn CV**, Jahn HM, Bai X, Scheller A, Kirchhoff F (2015) Analysis of purinergic P2Y1 receptors in cortical astrocytes and cerebellar Bergmann glia. Poster presentation at the XII European Conference on Glial Cells in Health and Disease in Bilbao, Spain.

**Bohn CV**, Jahn HM, Scheller A, Kirchhoff F (2013) Analysis of astrocyte-specific gene recombination *in vivo*. Poster presentation at the XI European Conference on Glial Cells in Health and Disease in Berlin, Germany.

## 12. ACKNOWLEDGEMENT

First, I would like to thank Prof. Dr. Frank Kirchhoff for giving me the opportunity to complete my PhD in his research group. Thank you for five challenging years full of new experiences, interesting projects and intense scientific discussions. Thank you for the possibility to travel the world for international meetings and new collaborations.

I would also like to thank Prof. Dr. Carola Meier for taking over the second referee of my PhD thesis.

My special thank goes to Dr. Anja Scheller for the supervision of my complete scientific career, starting with my Bachelor thesis until now. Thank you for your unrestricted support, helpful project plans, proofreading of all theses and for your friendship beyond the lab work. You always brought light into complicated experimental results.

I am grateful to Dr. Hannah M. Jahn for supervision and support during my Master thesis and the first years of my PhD. Thereby always having a sympathetic ear for experimental problems and challenging results.

Further, I would like to thank all members of the research group of the Molecular Physiology, for an enjoyable working atmosphere and for having a lot of fun at work. I would like to thank Wenhui Huang, Na Zhao, Phillip Rieder, Davide Gobbo, Qilin Guo, Michael Schweigmann, Katrin Bauer and Ute Legler for their accompaniment and support on numerous occasions during my PhD.

Particularly, I would like to thank Frank Rhode for his support and creative ideas in managing daily laboratory work as well as Daniel Rhode and the animal facility members for taking care of my mice. Especially, I would like to thank Svenja Linder for her invaluable help during the last months of my thesis.

I would particularly like to thank my “Glia Girls”: Cai (Xianshu Bai), Laura Stopper and Minime (Laura Caudal). Thank you for giving me the feeling to work with friends and for many unforgettable moments in- and outside of the lab.

A special thank goes to Laura Stopper for helping me with the trials and tribulations of calcium data, for her organizational skills in any situation and for being a friend and a fellow in misery during our PhD. Thank you for your accompany in good times as in bad. I would also like to thank Gebhard Stopper for his time saving software developments and his support with IT problems of all kind.



Ganz besonders möchte ich mich bei meiner gesamten Familie bedanken, die mir immer Rückhalt gibt und mich in jeder Lebenslage unterstützt. Ihr gebt mir die Kraft das zu erreichen, was ich mir in den Kopf gesetzt habe.

Ich danke meinen Eltern für ihr Vertrauen, ihre Liebe und ihre uneingeschränkte Unterstützung seit meines Lebens. Ich danke auch meinem kleinen Bruder für lustige Gespräche und die richtigen Worte, wenn es nötig war.

Ich möchte mich auch bei meinen Freunden für ihre langjährige und aufrichtige Freundschaft bedanken, allen voran Tiffie, Steffi, Michelle, Ralf, Bernhard, Micha und Jochen. Vielen Dank, dass ihr immer für mich da seid.

Besonders möchte ich mich auch noch bei meinem Ehemann Georg bedanken, der seit Jahren mein Anker und Lebensmittelpunkt ist. Vielen Dank, dass du mich unterstützt, erdest, aufbaust und mich so akzeptierst wie ich bin. Ich kann es kaum erwarten mit dir unser neues Projekt zu erleben und zu meistern.